Genetic variants of *LAMC1*, *ATP1B1* as risk factors and transcriptional regulation of *CASP8AP2* in the pathophysiology of Fuchs Endothelial Corneal Dystrophy

By

MAYNAK CHAKRABORTY
LIFE11201504007
NATIONAL INSTITUTE OF SCIENCE EDUCATION AND RESEARCH
BHUBANESWAR

A thesis submitted to the

Board of Studies in Life Sciences

In partial fulfillment of requirements

for the Degree of

DOCTOR OF PHILOSOPHY
of
HOMI BHABHA NATIONAL INSTITUTE

June, 2023

HOMI BHABHA NATIONAL INSTITUTE

RECOMMENDATIONS OF THE VIVA VOCE COMMITTEE

As members of the Viva Voce Committee, we certify that we have read the dissertation prepared by **Maynak Chakraborty** entitled **"Genetic variants of LAMC1, ATP1B1 as risk factors and transcriptional regulation of CASP8AP2 in the pathophysiology of Fuchs Endothelial Corneal Dystrophy"** and recommend that it may be accepted as fulfilling the thesis requirements for the award of Degree of Philosophy.

Chairman – Prof. Chandan Goswami Date: 30/05/2023

Guide / Convener – Dr. Debasmita Pankaj Alone Date: 30/05/2023

Examiner – Prof. P. Sundaresan Date: 30.05.2023

Member 1 – Dr. Srinivas Patnaik Date: 30.05.2023

Member 2 – Dr. Manjusha Dixit Date: 30.05.2023

Member 3 – Dr. Asima Bhattacharyya Date: 30.05.2023

Final approval and acceptance of this thesis is contingent upon the candidate's submission of the final copies of the thesis to HBNI.

I/We hereby certify that I/we have read this thesis prepared under my/our direction and recommend that it may be accepted as fulfilling the thesis requirement.

Date: 30/5/2023

Place: Jodhpur

Dr. Debasmita Pankaj Alone

(Thesis Supervisor)

STATEMENT BY AUTHOR

This dissertation has been submitted in partial fulfilment of requirements for an advanced degree at Homi Bhabha National Institute (HBNI) and is deposited in the library to be made available to borrowers under rules of the HBNI.

Brief quotations from this dissertation are allowable without any special permission, provided that accurate acknowledgement of source is made. Requests for permission for extended quotation from or reproduction of this manuscript in whole or in part may be granted by the Competent Authority of HBNI when in his or her judgment the proposed use of the material is in the interests of the scholarship. In all other instances, however, permission must be obtained from the author.

Maynak Chakraborty

DECLARATION

I, hereby declare that the investigation presented in the thesis has been carried out by me. The work is original and has not been submitted earlier as a whole or in part for a degree/diploma at this or any other Institution / University.

Maynak Chakraborty

List of Publications arising from the thesis

Publications in Refereed Journal:

a) Published:

1. Maynak Chakraborty, Rajesh Kumar Das, Sujata Samal, Sujata Das, Debasmita Pankaj Alone. Fuchs Endothelial Corneal Dystrophy associated risk variant, rs3768617 in *LAMC1* shows allele-specific binding of GFI1B. **Gene**. 2022 Apr 5; 817: 146179. doi: 10.1016/j.gene.2021.146179. Epub 2022 Jan 11. PMID: 35031421.

2. Maynak Chakraborty, Harithalakshmi Jandhyam, Samar Kumar Basak, Sujata Das, Debasmita Pankaj Alone. Intergenic variants, rs1200114 and rs1200108 are genetically associated along with a decrease in *ATP1B1* with Fuchs Endothelial Corneal Dystrophy. Exp Eye Res. 2023 Mar; 228:109403. doi: 10.1016/j.exer.2023.109403. Epub 2023 Feb 1. PMID: 36736852.

c) Under preparation:

1. Maynak Chakraborty, Samar Kumar Basak, Debasmita Pankaj Alone. Identification of SP1 as a transcriptional regulator of *CASP8AP2* and its overexpression in the FECD corneal endothelium.

Conference/Symposium:

1. Role of Monocarboxylate Transporters (MCTs) in the pathophysiology of Fuchs Endothelial Corneal Dystrophy (FECD). **Maynak Chakraborty**. 25th Annual Meeting of Indian Eye Research Group, ARVO India 2018, July 27 – 29 (Poster presentation).

2. Genetic association of rs220057 and rs220060 of *ZEB1* with Fuchs Endothelial Corneal Dystrophy in the Indian population. **Maynak Chakraborty**. 27th Annual Meeting of Indian Eye Research Group, ARVO India 2021, October 7 – 10 (Poster presentation).

Maynak Chakraborty

DEDICATION

This thesis is dedicated to my family for their love, support, and motivation, which inspired me with a positive way of thinking throughout this entire roller coaster ride.

ACKNOWLEDGEMENTS

I would like to express my sincere gratitude to my supervisor **Dr. Debasmita P. Alone** for her invaluable enthusiasm, involvement, and guidance in finishing my doctoral work. Her punctuality, passion for research, and moral integrity helped me to develop a professional attitude during my carrier. I respect her for being patient with me. I also want to thank **Dr. Sudhakar Panda**, Director of NISER, for providing the necessary facilities and the resources in the lab that were required to complete my work. I am grateful to NISER, DAE for providing me the fellowship during my PhD tenure.

I am honor to my doctoral committee members, **Dr. Chandan Goswami**, **Dr. Asima Bhattacharyya**, **Dr. Manjusha Dixit**, and **Dr. Srinivas Patnaik** for their insightful comments and constructive suggestions that significantly improved the quality of my thesis. Additionally, I would like to acknowledge our research collaborators **Dr. Sujata Das**, LV Prasad Eye Hospital, Bhubaneswar, and **Dr. Samar Kumar Basak**, Disha Eye Hospitals, Barrackpore for providing us with the blood and tissue samples to fulfill the specific aims of my research work. Furthermore, I owe my deepest gratitude to all my teachers from school through college for inspiring me with knowledge and enthusiasm to pursue a career in science.

I wholeheartedly appreciate my lab mates for their support, inspiration, and unending help throughout this PhD journey. I am extremely grateful to my seniors **Dr. Gargi**, **Dr. Biswajit,** and **Dr. Bushra** for their love, motivation, and endless guidance; without their cooperation, the completion of my thesis work was unthinkable. I want to thank my junior **Ramani** for her valuable suggestions in the bench work as well as in manuscript writing. I also acknowledge my

past and current labmates- **Vinay**, **Biswa**, **Bhavishya**, **Dibya**, **Rajesh**, **Sushree**, **Senjit, Sushmita, Lipsa, Dr. Harita, Anup**, **Bala**, **Aakash**, **Akhil**, **Om,** and a special thanks to **Bhagyashree** and **Pragnya** for collecting the samples sincerely and for maintaining the record books.

Being away from home and not missing home frequently was only made possible by my exceptionally supportive friends **Rojalin**, **Dipika**, **Satya**, **Himani**, **Pragyesh**, **Dinesh**, **Indrajit**, **Chandan and Tathagata** who always cheered me up on gloomy days.

Last but not the least, without the help of my supportive family, **Ma**, **Baba**, **Kaka,** and **Didisona**, who never stopped believing in me; it is impossible to imagine that I could have finished this thesis. Their encouragement, confidence, and hope always kept my morale up and guided me in overcoming all the barriers to achieving this honor. I would also like to thank my brother-in-law **Tuhinda** and my cute niece **Anushka** for their constant support in my PhD journey.

Maynak Chakraborty

Table of Contents

Abstract

Fuchs Endothelial Corneal dystrophy (FECD, OMIM # 136800) is an age-related, progressive, bilateral and, multifactorial dystrophy. It is marked by the reduction in the number of corneal endothelial cells, the fibroblastic transformation of remaining endothelium cells and deposition of the excess extracellular matrix proteins in the Descemet's membrane (DM). All of these molecular pathomechanism ultimately lead to the cloudiness in the cornea, loss of visual acuity, and formation of the painful tiny blisters on the surface of the cornea. FECD is categorized into two types: early and late, depending on when the symptoms begin to appear. Additionally, cases of FECD occur more frequently in women than in men. Researchers have identified various mutations and polymorphisms that are genetically associated with the pathophysiology of this disease in various populations. Previously we have also identified different polymorphisms associated with the FECD in the Indian population. But the genetic load of these polymorphisms are low compared to the Caucasian population hinting at the association of other new variants with FECD in our population. In the past, researchers observed that caspase 8 associated protein 2 (CASP8AP2) promotes epithelial to mesenchymal (EMT) transition by protecting Zinc finger E-box-binding homeobox 1 (ZEB1) from E3 ubiquitin ligases. Because ZEB1 is also overexpressed in the FECD corneal endothelium, so we hypothesized that upregulation of CASP8AP2 may cause the overexpression of ZEB1 in the FECD condition. Also, the molecular mechanism of the transcriptional regulation of *CASP8AP2* is not yet studied. The focus of this present study is to identify the genetic and functional association of novel polymorphisms associated with FECD in the Indian population and transcriptional regulation of *CASP8AP2* related with the pathophysiology of FECD. The objectives and the major findings of the study are summarized below:

Genetic association and functional role of laminin subunit gamma 1 (*LAMC1*) with late-onset FECD (LO-FECD):

- Variant rs3768617, present in the intronic region of *LAMC1*, is genetically associated with FECD in the Indian population.
- The transcription factor growth factor independent 1B (GFI1B) binds specifically to the risk allele 'C', not protective allele 'T'.

Genetic association of long intergenic non-Protein coding RNA LINC00970/ATPase Na^+/K^+ transporting subunit beta 1 (*LINC00970/ATP1B1*) with LO-FECD and its functional role in disease pathogenesis:

- Polymorphism rs1200114 and its tag variant rs1200108 in the intergenic region of *LINC00970/ATP1B1* are genetically associated with FECD in the Indian population.
- Haplotype 'G-G' of rs1200108-rs1200114 is more prevalent in FECD affected population, indicating that it is a risk haplotype.
- *ATP1B1* is less expressed in the FECD affected endothelium compared with the control endothelium.

Role of CASP8AP2 in the FECD progression:

- CASP8AP2 is overexpressed in the FECD endothelium compared to the control endothelium.
- Transcription factor specificity protein 1 (SP1) binds to the promoter of *CASP8AP2* and regulates its transcription.

List of Tables

List of Figures

List of Abbreviations

AGBL1	ATP/GTP binding protein like 1
AGE	Advanced glycation end products
ARE	Antioxidant response element
ATP1B1	ATPase Na^+/K^+ transporting subunit beta 1
AQP1	Aquaporin-1
BCA	Bicinchoninic acid assay
BMI	Body mass index
BS	Blocking solution
CASP8AP2	Caspase 8 associated protein 2
CCT	Central corneal thickness
CDKN2A	Cyclin-dependent kinase inhibitor 2A
CE	Corneal endothelium
CHED1	Congenital inherited endothelial dystrophy 1
ChIP	Chromatin immunoprecipitation
CHOP	C/EBP homologous protein
CI	Confidence interval
CLU	Clusterin
COL8A2	Collagen type VIII alpha 2
CTG	Cytosine-Thymine-Guanine
DAPI	4′,6-diamidino-2-phenylindole
DISC	Death-inducing signalling complex
DM	Descemet's membrane
DMEK	Descemet membrane endothelial keratoplasty

DSEK	Descemet stripping endothelial keratoplasty
ECM	Extracellular matrix
eIF-2α	Eukaryotic translation initiation factor alpha
EK	Endothelial keratoplasty
EMSA	Electrophoretic mobility shift assay
EMT	Epithelial-mesenchymal transition
ENCODE	Encyclopaedia of DNA elements
EndoMT	Endothelium to mesenchymal transition
EO-FECD	Early-onset FECD
ER	Endoplasmic Reticulum
ETS1	ETS proto-oncogene 1
FAS	Fas cell surface death receptor
FECD	Fuchs endothelial corneal dystrophy
GFI1B	Growth Factor Independent 1B Transcriptional Repressor
GRP78	G protein-coupled receptor 78
GWAS	Genome-wide association study
HEK-293	Human embryonic kidney 293 cells
HG	Human genome
HO-1	Heme oxygenase-1
HRP	Horseradish peroxidase
HSP70	Heat shock protein 70
IC3D	International Committee for Classification of Corneal Dystrophies
IF	Immunofluorescence
IOP	Intraocular pressure
IVCM	In vivo confocal microscopy

KANK4	KN motif and Ankyrin repeat domains 4
LAMC1	Laminin subunit gamma 1
LD	Linkage disequilibrium
LINC00970	Long intergenic non-protein coding RNA 970
LO-FECD	Late-onset FECD
LOXHD1	Lipoxygenase homology PLAT domains 1
MBNL1	Muscleblind like splicing regulator 1
MBNL2	Muscleblind like splicing regulator 2
MCT	Monocarboxylate transporter
MFN2	Mitofusin 2
mRNA	messenger ribonucleic acid
MT3	Metallothionein 3
NRF2	Nuclear factor erythroid 2-related factor 2
NSAID	Non-steroidal anti-inflammatory drugs
OR	Odds ratio
PITX2	Paired like homeodomain 2
PK	Penetrating keratoplasty
PPCD	Posterior polymorphous corneal dystrophy
qRT-PCR	Quantitative reverse transcription PCR
RAD51	RAD51 recombinase
RIPA	Radioimmunoprecipitation assay
RNS	Reactive nitrogen species
ROCK1	Rho associated coiled-coil containing protein kinase 1
ROS	Reactive oxygen species
SAGE	Serial analysis of gene expression

SDS-PAGE	Sodium dodecyl sulphate-polyacrylamide gel electrophoresis
ShRNA	Short hairpin RNA
SLC4A11	Solute carrier family 4 member 11
SNP	Single nucleotide polymorphism
SOD2	Superoxide dismutase 2
SPSS	Statistical package for the social sciences
TCF4	Transcription factor 4
TGFB1	Transforming growth factor beta 1
TNF	Tumour necrosis factor
TSS	Transcription start site
UPR	Unfolded protein response
XRCC1	X-Ray repair cross complementing 1
ZEB1	Zinc finger E-Box binding homeobox 1

CHAPTER 1

A comprehensive overview of Fuchs Endothelial Corneal Dystrophy (FECD)

1.0 A comprehensive overview of Fuchs Endothelial Corneal Dystrophy

1.1 Introduction:

The Corneal endothelium (CE) is the innermost part of the cornea and plays an important role in maintaining the transparency of the cornea. This is a monolayer, composed of hexagonal cells and is connected to the stroma by Descemet's membrane (DM). The essential function of CE is to preserve corneal transparency by maintaining the endothelial barrier and pump functions. Because the endothelium cells are terminally differentiated, the loss of these cells drives the deterioration of the functions of this layer. Corneal endothelial dystrophies includes a category of diseases represented by progressive loss of endothelial cells due to genetic or epigenetic risk factors. They are congenital hereditary endothelial dystrophy 1 (CHED1), congenital hereditary endothelial dystrophy 2 (CHED2), posterior polymorphous corneal dystrophy (PPCD), and Fuchs endothelial corneal dystrophy (FECD).[1] Fuchs endothelial corneal dystrophy (OMIM#136800) is a gradual, multifactorial, bilateral corneal condition first defined by the Austrian ophthalmologist Ernst Fuchs, where patients in their fifth to sixth decade of life experience blurred morning vision that will increase in duration as the disease progresses.[2] Broadly, the key hallmarks of FECD consist of the prominent protrusions (outgrowths) in the DM, named ‘guttae’, a gradual rise in corneal edema, morphological changes of the hexagonal mosaic corneal endothelium, lack of endothelial cell number by time, and last stage is indicated by the formation of painful epithelial bullae because the capacity of the cornea declines to keep stromal dehydrated.[3]

1.2 Clinical staging and inheritance of FECD:

1.2.1 Clinical staging:

In the past, numerous clinical staging methods had been introduced for FECD. One of the methods developed by Laing *et al.* for staging the disease is mentioned below.[4–7]

Stage 1. Corneal biomicroscopy manifests the presence of guttae. These are mountain-shaped protrusions that grow from the DM and are known to be an FECD predictor. Initially the guttae are normally formed within the central cornea and then spread out in the peripheral direction. In this stage, guttae are typically central, nonconfluent, and asymptomatic in patients.

Stage 2. The corneal guttae appear to cluster and outspread into the peripheral region. It lead to the deterioration and enlargement of the endothelial cells with a lack of hexagonal morphology. The endothelial cell density is negatively correlated with the number of the guttae because the fusion of guttae is coupled with the continuous lack of endothelial cells. Patients begin to experience a decline in vision. Glare signs are observed because of excessive swelling of stromal layers.[8]

Stage 3. The lack of endothelial cells causes stromal edema, which gradually builds up in the direction of the epithelial layer and drives the generation of epithelial and subepithelial bullae.[4] The disruption of these bullae triggers painful outbreaks and increases the chance of infection.

Stage 4. The cornea is highly vascularized and opaque. Deposition of subepithelial fibrous tissue occurs due to prolonged and persistent edema. At this point, visual acuity is significantly impaired, but the pain usually attenuates.

This staging system is based on the clinical signs and thus, it contributes very little information for deciding the timing of endothelial keratoplasty in patients. Dr. Jay Krachmer suggested a

clinical grading scale based on the significance of corneal guttae and the appearance of edema for FECD cases to evaluate the advancement of the disease which is widely used and is known as Krachmer grading scale for FECD.[9]

Krachmer Scale:

Grade 0 (G0): No sign of disease.

Grade 1 (G1): 0-12 prominent, dispersed guttae at minimum in one eye; typically asymptomatic.

Grade 2 (G2): more than 12 prominent, non-confluent guttae minimum in one eye.

Grade 3 (G3): 1-2 mm prominent, condensed guttae.

Grade 4 (G4): 2-5 mm of clustered, prominent guttae.

Grade 5 (G5): ≥5 mm condensed, prominent guttae with edema.

1.2.2 The International Committee for Classification of Corneal Dystrophies (IC3D) classification and inheritance:

The latest IC3D category for corneal dystrophies includes four classes.[1] FECD comes into categories one to three. Category four is particular for other corneal dystrophies and does not match the features of FECD. FECD is mostly inherited in an autosomal dominant fashion.[10] The IC3D classification implements most effectively the hereditary examples of FECD and does not follow if no proof of inheritance exist.

1.2.2.1 Category 1 (Early onset FECD):

Category 1 denotes the corneal dystrophy in which the associated gene has been identified and specific mutations have been detected. Early-onset FECD (EO-FECD) includes in this category. EO-FECD generally starts at ten years old and becomes clinically prominent within

the twenty and thirty years. *COL8A2* gene encoding the alpha (α) 2 chain of collagen type VIII, is associated with this category. Mutations of this gene were found in EO-FECD and they are inherited in an autosomal dominant trait.[11–14] In the EO-FECD, each mutation contributes to a unique phenotype characterized by the presence of the minor, circular guttae clustered into cell centres instead of distinctly pointed guttae on the cellular boundaries, as seen in late-onset FECD (LO-FECD). The Gln455Lys and the Leu450Trp *COL8A2* mutations affect the triple helical domain of α2 collagen VIII.[11,12] These mutations could impact the tertiary structure of COL8A2 and the architecture of DM.[15] Because *COL8A2* was noticed to be required in the differentiation of vascular endothelium, an abnormal basement membrane formation may hinder the same process in corneal endothelium.[4,16]

1.2.2.2 Categories 2 & 3 (Late-onset FECD):

Category 2 reflects the corneal dystrophy that has been mapped to one or more chromosomal loci and category 3 includes the corneal dystrophy that has not been not mapped to a specific chromosomal locus. Late-onset FECD (LO-FECD) is grouped in both these two categories. LO-FECD appears after forty years and its frequency is higher than EO-FECD.[9] Several genes such as solute carrier family 4 member 11 (*SLC4A11*), transcription factor 4 (*TCF4*), Zinc finger E-box binding homeobox 1 (*ZEB1*), etc are associated with the LO-FECD. *SLC4A11* codes the NaBC1 protein, which serves as an electrogenic, sodium borate cotransporter.[17] Different mutations of the *SLC4A11* gene on chromosome 20p12 had been recognized.[18,19] Various single nucleotide polymorphisms (SNPs) in the *TCF4* gene were discovered to be associated with sporadic LO-FECD, although no mutation in the coding region or exon-intron boundaries has been identified so far.[20] TCF4 also regulates the transcription of the *ZEB1* gene.[21] An investigation in 2010 identified five LO-FECD related loss of function mutations in the *ZEB1* gene.[22] TCF4 and ZEB1, address crucial parts in epithelial-mesenchymal transition

(EMT) by inhibiting E-cadherin expression, regulating collagen gene transcription, cellular death, etc.[23,24] Because the biological roles are comparable, it's been hypothesized that their mutations affect the similar pathway, resulting in the development of FECD.[20,25,26] But, the exact process, responsible for the pathogenesis is still speculative.

1.3 Prevalence:

According to a global survey in 2016, the majority (39.0%) of the corneal transplantation performed between 2012-2013 were the consequences of the FECD alone.[27] The eye bank association of the United States (EBAA) published a statistical analysis in 2016 that showed FECD was responsible for 93.0% of full corneal transplantations. Various studies reported a high risk of FECD in the Caucasian population. In one study, researchers found that 11.0% of the whole population are FECD affected at Tangier Island, USA and all the affected individuals were above 50 years old.[28] Another cohort research in Reykjavik, Iceland, also showed an similar frequency of incidence; more females than men had widespread corneal guttae.[29] Asian populations exhibit fewer incidences of FECD than Caucasians. In Japan, 4.0% of the people over 40 years had major corneal guttae of grade 1 or above.[30] In an investigation comparing two Asian ethnicities, it was observed that 6.7% of the Chinese Singaporeans (female: male = 2.4:1) and 3.7% of Japanese (female: male = 4.5:1), over the age of 50, had primary corneal guttae.[31] In India, 11.0-16.0% of endothelial keratoplasty had been performed over 5-6 years only for FECD cases and, females were identified to be more susceptible to FECD than males.[32–34] These studies indicated that FECD have late-onset as well as female prevalence, but the cause is not properly known.

1.4 Other complications:

Previously, it was reported that the clearing of the aqueous humour outflow becomes inadequate in the case of FECD patients compared with controls.[35] These researchers

concluded that the function of the trabecular meshwork is affected because of the disease. FECD patients had considerably higher intraocular pressures (IOP) than healthy subjects, as observed by previous researchers.[36] Additionally, the significantly increased central corneal thickness (CCT) noticed in FECD patients may lead to inaccuracies in IOP calculations.[36] Another study reported no impairment of aqueous humour outflow and no association between open-angle glaucoma and FECD.[37] FECD is also associated with a higher frequency of cataract, keratoconus, age-related macular degeneration, and cardiovascular sickness.[38–41] Olsen *et al.* observed increased cardiovascular risk in FECD patients compared with controls; the risk was speculated to be influenced by a common endothelial deformity, even though the corneal endothelium is different from the vascular endothelium. It is anticipated that such pronounced disease interconnections are due to the complicated interactions of other epigenetic factors that result in degenerating alterations, not only in CE but also in other tissues (e.g. retinal and cardiovascular tissues).[8]

1.5 Histopathological changes:

1.5.1 Endothelium:

The hexagonal cells of CE have desmosomes and tight junctions connecting every cell.[42] The endothelium acts like a barricade to access the fluid into the cornea from aqueous humour and also eliminates fluid out of the cornea.[43] In the case of FECD, the cell density is significantly lower and the endothelium is notably narrower than normal, uniquely in areas covering the guttae **(Fig. 1.1)**.[42,44–47] The endothelial cell's thickness is markedly decreased to 0.2 µm adjacent to the cell-to-cell junction and over the guttae in comparison to 2.5 µm thickness of a healthy cornea .[48] In FECD, apoptotic cells are removed, which are replenished by the enlargement of nearby cells followed by the lack of cellular hexagonal architecture (pleomorphism) and alteration in the cell size (polymegathism).[44,49–51] Despite having little

cytoplasm, noticeable vacuolization and melanin pigmentation had been found inside the cells.[42,45,52] Histological examination demonstrated that several endothelial cells have a morphology, similar to fibroblasts. The cells also showed dilated, granular endoplasmic reticulum (ER), enlarged mitochondria, pigment granules, and stretched cytoplasmic filaments.[52–54] Transmission and scanning electron microscopy investigations also explained the presence of ultrastructural characteristics like increased hemi-desmosomes, microvilli, and enhanced immunostaining of cytokeratin-7, and pancytokeratin, commonly found in the epithelial cells.[54] In comparison to a normal corneal thickness of 530 mm, the average thickness of FECD corneas, as estimated by pachymetry, ranges from 580 mm to 690 mm.[49,55] In the initial phases of FECD, the density of Na,K-ATPase was reportedly augmented with a simultaneous increase in transendothelial permeability.[55,56] The density of Na,K-ATPase per cell declines from mild to late phases of FECD, irrespective of the decrease in the number of endothelial cells.[57–59] In a study reported in 2002, the ATPase density in LO-FECD endothelium was found to be identical to that seen in post-cataract corneal surgery.[60] Lower expression of aquaporin was noticed in FECD corneal endothelium which can lead to corneal edema.[61,62] Reports suggested depletion in phospholipid changeover indicated by reduced expression of group 1B phospholipase A2 (PLA2G1B) inferring a lack of endothelial function.[63] Nevertheless, FECD endothelial cells typically undergo endothelial to fibroblastic phenotype, with reduced expression of Na,K-ATPase.[64]

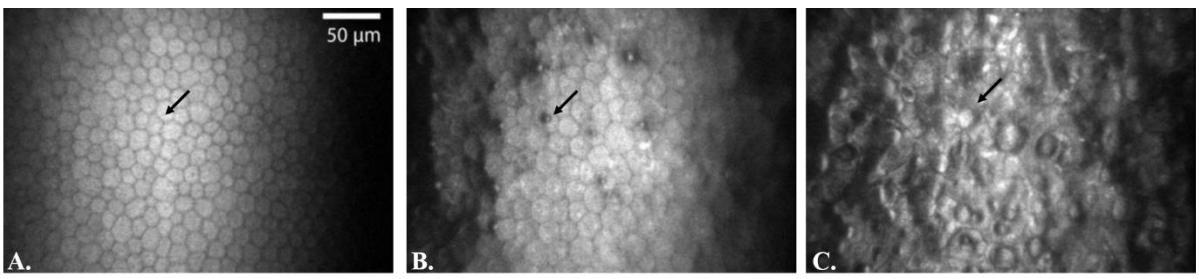

Fig. 1.1: Specular microscopy images of corneal endothelium. Specular microscopy images in **(A)** healthy, **(B)** moderate FECD, and **(C**) acute FECD[47]

1.5.2 Descemet's Membrane (DM):

This acellular layer is located between the endothelium and the posterior stroma. It was noticed to be enlarged in the FECD and guttae seemed like shiny patches, each encircled by dark rounded wheels.[49,51,65] Electron microscopy detected tiny bump-like protrusions throughout the endothelial portion of each FECD subject studied.[45,49,51,66,67] These protrusions are sometimes capsuled by collagenous fibers, making the external of the endothelium flat rather than folded.[49] DM thickens mostly in the central cornea and it eventually spreads into the peripheral cornea as the disease progresses.[49,54,66,67] DM's normal bi-layer structure was disorganized in FECD, wherein although the sublayer lying in the middle of the stroma and layer one was fine in FECD; layer two was either completely absent or was extremely thin (average thickness 1.8 mm to 2.8 mm) in approximately 37.0% of the FECD cases **(Fig. 1.2).**[44,45,52] Two additional DM layers had been confirmed that propose a common response of endothelium in case of the disease; a posterior banded layer and a posterior fibrillar layer comprising of layers three and four, which when merged are named the 'posterior collagen layer' or 'posterior striated layer' **(Fig. 1.2)**.[45] Layer three is evident in every tissue sample of the FECD obtained during keratoplasty and often comprises of irregularly arranged collagen fibres of 110 - 120 nm banding pattern.[44] Layer four is ≥ 0.5 mm in thickness, and this layer was either absent or thinner in corneas with minimal epithelial edema.[45,52] But this layer becomes denser in case of elevated epithelial and stromal edema.[44] Guttae were covered in most of the cases having layer four, resulting in the inconsistent collagenous coating of the guttae.[45,49,66] Corneal decompensation is culpable for swelling of this particular layer, rather than FECD condition itself. Both EO-FECD and LO-FECD patients have disorganized and hyper-reflective fibrous strands of collagen type VIII alpha 1 chain (COL8A1) and collagen type VIII alpha 2 chain (COL8A2); and it has been hypothesized that abnormal expression pattern of COL8A1 and COL8A2 contributes to DM thickening and guttae formation.[12,68] Overexpression of collagen

IV, fibronectin, and laminin was reported in FECD DM.[12] However, other reports showed lower expression of fibronectin and laminin-10 in FECD-affected corneal endothelium samples relative to healthy subjects, with reduced nidogen-1 level.[60] In FECD, transcriptional over-expression of laminin subunit gamma 1 (LAMC1) was observed compared with normal DM samples.[69]

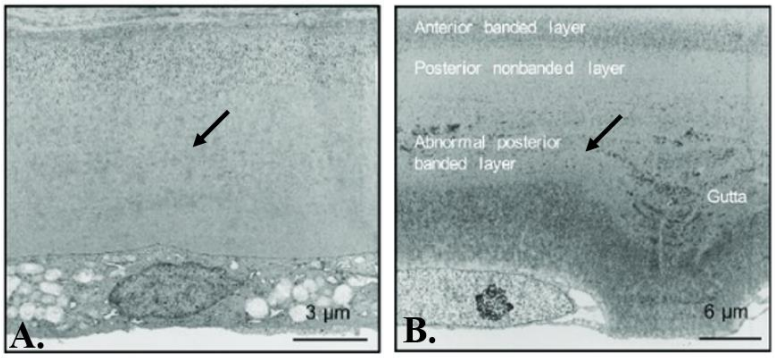

Fig. 1.2: Histological changes of DM in FECD condition. (A) TEM image of a healthy DM bilayer. **(B)** TEM image of a FECD affected DM. In contrast to a healthy DM, one extra layer known as posterior banded layer appears in FECD DM and guttae is visible in this layer.[70]

1.5.3 Corneal stroma:

Corneal edema leads to significant changes in the anterior stroma, causing visual distortions. In vivo confocal microscopy (IVCM) indications of corneal edema are keratocyte hyper-reflectivity with enlarged cell bodies and filaments; the presence of tiny intracellular perinuclear vacuoles, and wide extracellular lacunae between keratocytes. In the late stage of FECD (stages 3 and 4), the density of anterior keratocytes was remarkably lower than healthy controls, as revealed by IVCM and histological examinations **(Fig. 1.3)**.[71,72] Conversely, clinical analysis of mild FECD cases (stages 1 and 2) through IVCM showed increased density of posterior keratocytes relative to controls, but there was no significant variation in the density of anterior keratocytes.[73] The presence of tortuous stromal nerves with loop like structure is often observed in FECD patients by IVCM.[49,74]

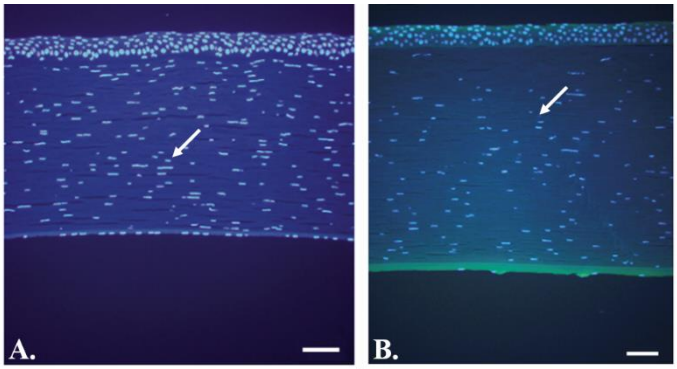

Fig. 1.3: Stromal keratocytes in normal and FECD condition. (A) Sagittal section of a healthy cornea. **(B)** Density of the anterior keratocytes is lower FECD condition.[71]

1.5.4 Corneal sub-basal nerve plexus:

Sub-basal nerve density was identified as notably lower in the early stages of FECD compared to healthy controls.[73] In general, the total count of nerves with primary nerve branches is lower and the overall nerve length is shorter in FECD patients with thicker central corneas. It is possible that sub-basal nerves are fully missing in the late stage of FECD **(Fig. 1.4)**.[49,74] It was shown that central corneal sensitivity is substantially poorer than age-matched controls. The existence of sporadic nerves with abnormal branching forms was found in FECD.[74] Altered signalling pathways between the endothelium and corneal nerves were thought to play an important part in the apoptosis of corneal endothelium.[73] It was presumed that the loss of endothelial cells may contribute to the lower concentration of vasoactive intestinal peptide and different neuropeptides, thereby influencing the number of corneal nerves and their roles.

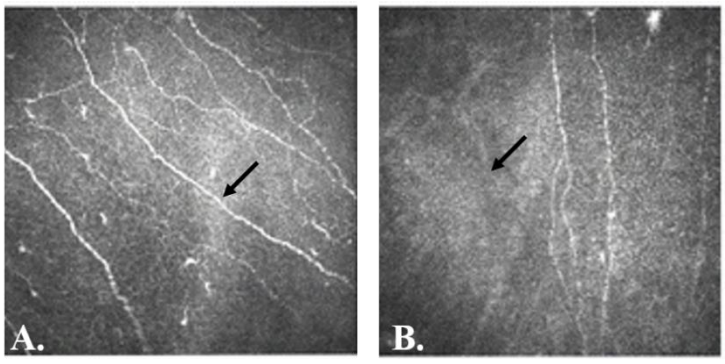

Fig. 1.4: Corneal sub-basal nerves. Images in **(A)** early **(B)** late-stage of FECD corneas.[75]

1.5.5 Corneal epithelium:

Both clinically and with IVCM, LO-FECD cases showed alterations in their corneal epithelium **(Fig. 1.5)**.[49] Bullae are found as dark circles within the epithelium.[49] The existence of sub-epithelial cells distributed randomly between the basal epithelium and Bowman's layer was detected in LO-FECD patients.[49] In LO-FECD, scarring in the sub-epithelium was frequently observed.[49,76] Studies using light and electron microscopy on FECD buttons revealed the presence of fibrous connective tissue between the epithelium and Bowman's layer.[52] Severe corneal edema was correlated with sub-epithelial scarring.

Fig. 1.5: Histological image of a FECD corneal epithelium. Image showing abnormal epithelial basement membrane and intraepithelial cysts.[77]

1.6 Risk Factors:

Although the actual cause of FECD remains unclear, it is associated with both genetic and epigenetic risk factors. Understanding the role of the risk factors would be extremely beneficial in preventing the disease progression.

1.6.1 Genetic factors:

Assessment of the genetic background related to the disease pathogenesis is primarily linked with the identification of different genes having genetic and functional association with the disease. A number of such different genetic factors are associated sporadically or have a familial predisposition. Researchers have used two distinct strategies to classify these genetics factors:

(a) Genetic linkage analysis explores multigenerational families with a minimum of one disease-affected individual to determine the co-inherited chromosomal region among affected persons, and

(b) Genome-wide association study (GWAS) applies information from a wide number of non-related participants, control and disease affected to find different genetic polymorphisms associated with the phenotype of the disease.

The information related to the genes, associated with FECD is presented in **Table 1.1**. All the genetic factors are discussed in the following subsections briefly.

Table1.1: Summary of the genes, associated with FECD pathogenesis

SN	Category of FECD	Gene (Symbol)	Full Name	Location
1	EO-FECD	*COL8A2*	Collagen type VIII alpha 2 chain	1p34.3
2	LO-FECD	*TCF4*	Transcription factor 4	18q21.2
3		*SLC4A11*	Solute carrier family 4 member 1	20p13
4		*ZEB1*	Zinc finger E-Box binding homeobox 1	10p11.22
5		*LOXHD1*	Lipoxygenase homology PLAT domains 1	18q21.1
6		*AGBL1*	ATP/GTP binding protein like 1	15q25.3

7		*KANK4*	KN motif and Ankyrin repeat domains 4	1p31.3
8		*LAMC1*	Laminin subunit gamma 1	1q25.3
9		*ATP1B1*	ATPase Na^+/K^+ transporting subunit beta 1	1q24.2
10		*CLU*	Clusterin	8p21.1
11		*RAD51*	RAD51 recombinase	15q15.1
12		*FAS*	Fas cell surface death receptor	10q23.31
13		*XRCC1*	X-Ray repair cross complementing 1	19q13.31
14		*PITX2*	Paired like homeodomain 2	4q25
15		*TGF-β1*	Transforming growth factor beta 1	19q13.2

1.6.1.1 Collagen type VIII alpha 2 chain (*COL8A2*):

COL8A2 (Gene ID: 1296) codes the α2 chain of collagen VIII. This gene is exclusively associated with the EO-FECD, established in the linkage study. In the UK, genome-wide association search of an EO-FECD family observed the missense mutation Q455K, present in *COL8A2*.[11] After examining 115 unrelated FECD cases, this missense mutation was additionally found in two other EO-FECD families.[11] Another mutation L450W was identified in *COL8A2* in FECD affected people, which was absent in all control individuals.[12] This L450W mutation was also found in a separate UK family having EO-FECD.[78] The DM of the L450W mutant was noticed to have significant deposition of COL8A2, suspected to have started from the time of foetal growth.[79,80] The thermal stability of the L450W mutant *COL8A2* was lesser than the wild type and it gets accumulated in the cytoplasm of CHO-K1 cells.[68] Homozygous knock-in mouse models [*COL8A2* (Q455K/Q455K) and *COL8A2* (L450W/L450W)] exemplify pathology of the EO-FECD like the morphology of the endothelial cells, increased autophagy, and apoptosis by induction of the unfolded protein response (UPR) pathway as evidenced by the dilated ER, and guttae formation.[81,82] The *COL8A2* (L450W/L450W) mice had a less severe phenotype, as confirmed by decreased cell

death and less guttae formation compared with the *COL8A2* (Q455K/ Q455K) mice.[82] The results of these two mutations may be related to abnormal protein folding, resulting in UPR and activation of apoptosis. Another *COL8A2* SNP, rs274754 was identified in one familial EO-FECD case in Australia.[83] In Korea, and India different variants (G495G, A35A, and Q455V) of *COL8A2* were associated with EO-FECD cases.[83,84] The silent variants, c.1485G>A (G495G) and c.112G>A (A35A) of *COL8A2* were associated with LO-FECD cases in India.[85] *COL8A2* mutations might lead to guttae formation in the cornea due to increased deposition and abnormal distribution of collagen proteins in the DM.[12]

1.6.1.2 Transcription factor 4 (*TCF4*):

TCF4 (Gene ID: 6925) recognizes E-box (5′-CANNTG-3′) in many the promoters and enhancers of a number of genes to regulate transcription.[86] Apart from that, it also interact with other transcription factors like oligodendrocyte transcription factor 2 (OLIG2), caudal type homeobox 2 (CDX2) also.[87,88] TCF4 participates in transforming growth factor β (TGF-β) signalling pathways, EMT, apoptosis, etc.[89] The most important genetic contributor to LO-FECD is the increased number of trinucleotide repeats of cytosine-thymine-guanine (CTG) in the third intron of the *TCF4*. The number of people with > 50 CTG repeats was relatively higher in the FECD patients than in the healthy controls.[90] Cases bearing > 40 repeats of the CTG have 15 times increased probability of acquiring the disease than non-repeat carriers.[91,92] Additionally, FECD patients with extended CTG repeats are more prominent to undergo corneal transplantation at a certain age compared with ≤ 50 repeat carriers.[20,92,93] The intensity of the disease's pathophysiology is associated with the occurrence of trinucleotide repeats and the repeat length.[94] Repeat expansion of the monoallelic CTG was seen to result in increased disease severity at repeat numbers > 103, while bi-allelic elongation was enough to initiate diseased phenotype at repeat numbers > 40.[94] FECD is closely related to different trinucleotide

repeat induced diseases for example myotonic dystrophy-1. The extended cytosine-uracil-guanine (CUG)-repeated *TCF4* messenger RNA (mRNA) molecules accumulate as RNA foci in FECD endothelium.[92,95,96] It eventually sequesters and depletes mRNA splicing proteins, such as muscleblind like splicing regulator 1 (MBNL1), muscleblind like splicing regulator 2 (MBNL2) and ultimately leads to RNA mis-splicing and RNA toxicity. Previous study from our laboratory however reported that only 34.0% of the population carrying increased CTG repeat showed pathological symptoms of FECD compared with 79.0% of the Caucasian cohort. It suggested that TCF4-CTG repeat may not be the main causal factor for FECD development in our population.[34] Four variants (rs613872, rs2286812, rs9954153, and rs17595731) of *TCF4*, were genetically associated with the disease in American and Australian ethnic backgrounds.[25,97,98] In Singaporean Chinese, two more polymorphisms, rs17089887 and rs17089925, showed significant association with the disease. In the same study, SNPs rs9954153 and rs17595731 were not checked and the rest of the two SNPs (rs2286812 and rs613872) did not show any association.[26] In addition to the Singaporean Chinese study, rs17089887 showed significant association with the FECD in the East Indian population.[34] Variant rs17595731 and rs613872 were also significantly associated with FECD in the South Indian population.[99]

1.6.1.3 Solute carrier family 4 member 11 (*SLC4A11*):

SLC4A11 (Gene ID: 83959) facilitates Na^+ coupled borate cotransport, which is the primary member of the borate transporter family. Researchers also disclosed the functional involvement of SLC4A11 in water reabsorption across the basolateral surface of the endothelium to preserve deturgescence.[100,101] Fewer than twenty pathogenic variants had been found in *SLC4A11* at a frequency of approximately 4.0% for LO-FECD in South-Asian and Caucasian population.[18] Previously, one deletion mutation (c.99-100delTC) and three missense mutations (E399K,

T754M, and G709E) were found in a case-control study conducted in Singapore. Mutated proteins were also deficient in the localization to the plasma membrane of the cells; co-expression of intracellular wild-type proteins was unable to rectify the deficiency, which highlighted the dominant mode of inheritance of FECD.[102] This particular investigation also reported ten silent non-pathogenic mutations and five missense non-pathogenic mutations. Genetic testing also observed different missense variants (G834S, Y526C, G742R, G583D, R282P, V575M, and E167D) of *SLC4A11* in FECD cases in Baltimore, USA.[18] Proteins with one of the seven variants (E167D) were deficient in post-translational modification, maturation, and cell membrane position.[18] In another study, five new polymorphisms (D886D, N150S, T463T, R158R, and H728H) that existed in the coding region of the *SLC4A11* were also found in African-American FECD cases; all of which were present in controls.[103] Missense variants (W240S, V507I, and T434I) were also found in sporadic LO-FECD individuals in South India. Expression of both wild type and mutant proteins in HEK-293 cell line showed that mutant proteins were dysfunctional in either localization in the plasma membrane of the cells or water pumping rate .[104] In a separate study, the concerned proband of a Korean family with congenital hereditary endothelial dystrophy 2 (CHED2) had a homozygous deletion mutation (C386 *) in the exonic region of *SLC4A11*. The mother of the proband, who had the heterozygous mutation, expressed LO-FECD characteristics. It indicates a similar mechanism for developing FECD and CHED2.[105] A double knock-out cell line of *SLC4A11* showed the reduced ability of cellular proliferation with impaired NH_3:H^+ transport.[106] *SLC4A11* knock-out mice had increased stromal thickness, elevated stromal concentrations of sodium chloride (NaCl), presence of NaCl crystals, and thickening of DM.[107] In a nutshell, these studies confirmed the functional effects of different SLC4A11 mutant proteins and their roles in FECD development.

1.6.1.4 Zinc finger E-box binding homeobox 1 (*ZEB1*):

The *ZEB1* gene (Gene ID: 6935) expresses the transcription factor having two groups of zinc fingers in its DNA binding sites. TCF4 upregulates ZEB1 expression and both were thought to involve identical biological pathways for FECD progression.[21,25] The first silent mutation (D64D) and a missense mutation (N696S) in *ZEB1* were found in a patient with LO-FECD in Singapore in 2008; which was not present in the controls.[108] Five missense mutations (Q840P, Q810P, N78T, P649A, and A905G) were found in FECD cases in Baltimore, USA. Such mutations were absent from controls and revealed the loss of protein function.[22] Screening of LO-FECD patients in northern India reported different mutations (E733K, S234S, Q840P, L947Stop, and A818V) and variants (IVS2 + 276, rs77516068, and rs149166539); not any of these were detected in controls. Significant genetic association of SNP rs220060 was also found with the disease.[109] The expression of mutant proteins of A905G, Q810P, N696S, Q840P, P649A, and N78T did not result in any difference in the abundance of proteins or nuclear localization. But, *in silico* analysis suggested that the mutations might change the regulatory or post-translational modification sites of the protein.[110] So, their effects need to be checked further in future studies.

1.6.1.5 Lipoxygenase homology PLAT domains 1 (*LOXHD1*):

LOXHD1 (Gene ID: 125336) encodes a protein comprising polycystin, lipoxygenase, and alpha-toxin domains that help to regulate directing proteins to the cell membrane. It is the gene originally related to autosomal recessive progressive hearing defect in humans. In a family based study, exon-capture array identified a *LOXHD1* R547C mutation, predicted to be pathogenic in the American population.[111] Antibody staining with LOXHD1 of the concerned proband cornea with R547C mutation, showed enhanced LOXHD1 staining in DM as well as in the endothelium layer in comparison to keratoconus cornea. The enhanced

immunofluorescence signal is not present in either controls or FECD cases without *LOXHD1* mutations. Further analysis of 207 LO-FECD cases detected 14 extra missense mutations. Many of them were suspected to be pathogenic and these mutations were absent in the control population. Two intronic variants (c.1809+155G>A and c.5332-126C>T) in *LOXHD1* were also identified in FECD cases in a multigenerational family study.[112] In a subsequent study, one heterozygous missense variant c.6413G>A; p. (R2138Q) in *LOXHD1* was reported in LO-FECD cases in India.[113] Variant rs450997 in *LOXHD1* was also found to be genetically associated with FECD in the European population.[64]

1.6.1.6 ATP/GTP binding protein like 1 (*AGBL1*):

AGBL1 (Gene ID: 123624) catalyses the deglutamylation of polyglutamylated proteins. Next generation sequencing pinpointed a nonsense mutation (R1028*) present in the *AGBL1* in FECD cases, which leads to protein truncation. This mutation also existed in a very low frequency of 0.26% in controls.[114] The same study also revealed two different unrelated persons having the same mutation and the presence of another missense mutation (C990S) in the FECD cases. Wild type AGBL1 was primarily located in the cytoplasm, whereas the truncated protein displayed a distinct nuclear location and the missense mutant was confined to the cytoplasm. Researchers also proved that AGBL1 interacts with the TCF4 protein, and these particular mutations minimize the interactions.[114] GWAS study of the European population in 2017 reported the genetic association of *AGBL1* with FECD.[64]

1.6.1.7 KN motif and Ankyrin repeat domains 4 (*KANK4*):

KANK4 (Gene ID: 163782) is involved in cytoskeleton formation and tissue integrity. The GWAS study in 2017 found that *KANK4* variant rs79742895, present in chromosome 1, is significantly associated with FECD. Variant rs79742895 resides in the enhancer region of

KANK4 and has the binding probability of allele specific transcription factors.[64] The frequency of the minor allele 'C' is very low in South-Asian (0.8%) and East-Asian population (0.0%) compared with European (3.6%) and American population (1.3%) [rs79742895 (SNP) - Population genetics – Homo sapiens - Ensembl genome browser 108].

1.6.1.8 Laminin subunit gamma 1 (*LAMC1*):

LAMC1 (Gene ID: 3915) serves an important role in the formation of DM. Previous research found that rs3768617 in *LAMC1* is significantly associated with FECD in both discovery (2564 controls and 1404 cases) and replicative set (3342 controls and 2075 cases) also. At this SNP, a gender-specific association was observed, with a higher risk in women, compared to men.[64] Expression study indicated decreased number of cytoplasmic LAMC1 expressed endothelial cells in case of FECD tissue compared with control.

1.6.1.9 ATPase Na^+/K^+ transporting subunit beta 1 (*ATP1B1*):

ATP1B1 (Gene ID: 481) encodes the beta (β) 1 subunit of Na,K-ATPase. The intergenic variant rs1200114, present between *LINC00970* and *ATP1B1* was significantly associated with the FECD. Variant rs1200114 manifested the most significant association in both discovery (2564 controls and 1404 cases) and replicative (3342 controls and 2075 cases) set after *TCF4* variant rs784257. This SNP does not show any important eQTLs in GTEx, but signifies the enrichment of enhancer and promoter features, especially in many brain tissues.[64] The reduction in ATP1B1 expression could increase corneal hypertonicity and lead to the corneal edema seen in FECD cases.

1.6.1.10 Clusterin (*CLU*):

The molecular chaperone *CLU* (Gene ID: 1191) performs an important job in protein folding and is upregulated in the FECD corneal endothelium compared with control.[115] This study also demonstrated increased expression of both secretory as well as nuclear CLU in FECD-DM samples compared with the healthy controls. In South Australian Caucasians, genotyping of the variants observed significant association of rs17466684 with FECD. The differential distribution of CLUs in FECD-affected corneas was also reported. Positive immunolabelling signal of CLU was found only in the anterior surface of the DM in FECD cornea whereas it was visible evenly throughout the DM in healthy cornea. [97] It was indicated that abnormal clusterin secretion could play a major role in the pathogenesis of FECD.

1.6.1.11 RAD51 recombinase (*RAD51*):

RAD51 (Gene ID: 5888) codes for an essential protein involved in the homologous recombination. It rectifies the double-stranded DNA breakage, resulting from reactive oxygen species (ROS). SNP rs1801321 of this gene showed a genetic association with FECD in the Poland population. The allele 'G' showed a protective effect from FECD development with an odds ratio of 0.51. On the other hand, the risk allele 'C' increased the chance of disease causation with an odds ratio of 1.85.[116] The genetic association of this SNP is yet to be replicated in any other population.

1.6.1.12 Fas cell surface death receptor (*FAS*):

This gene (Gene ID: 14102) is a member of tumour necrosis factor (TNF) superfamily. In a study performed with 300 controls and 221 FECD cases, SNP c.671A > G, present in *FAS* showed significant association with FECD in the Poland population.[117] The genetic association of this SNP is yet to be replicated in any other population.

1.6.1.13 X-Ray repair cross complementing 1 (*XRCC1*):

XRCC1 (Gene ID: 7515) repairs the single-strand (ss) DNA breakage induced by different alkylating agents and ionizing radiation. One *XRCC1* SNP (c.1196A > G) was significantly associated with FECD in the Poland population. The risk allele 'A' and risk genotype 'AA' increased the chance of FECD, whereas protective allele 'G' and genotype 'AG' and 'GG' displayed the opposite effect.[118]

1.6.1.14 Paired like homeodomain 2 (*PITX2*):

PITX2 (Gene ID: 18741) encodes essential regulatory factors, involved in the formation of eye tissue. A pedigree study identified a new *PITX2* mutation (G137V) in the Axenfeld–Rieger syndrome affected individuals.[119] Strikingly, most of the affected people also had FECD. This report indicated that this G137V mutation may be associated with FECD but this mutation is yet to be reported with only FECD patients without the Axenfeld–Rieger syndrome.

1.6.1.15 Transforming growth factor beta 1 (*TGF-β1*):

TGF-β1 (Gene ID: 100135628) was overexpressed in FECD condition and also colocalized in guttae with clusterin.[120] Significant haplotype (TAAAT) association of TGF-β1 SNPs (rs756463, rs2073510, rs2302038, rs4572, rs10043360) was found in the Caucasian Australians. This particular haplotype appeared as a risk haplotype with an odds ratio of 2.29.[97]

1.6.2 Epigenetic factors:

Kitigawa *et al.* hypothesized that a higher prevalence of FECD in the Singapore (tropical climate, located 1° N) relative to Japan (temperate climate, located 37° N) is likely due to increased UV exposure due to its proximity to the equator.[31] However, UV exposure studies performed in Reykjavik, Iceland (temperate, 64° 08 ' N) did not distinguish between collateral

increase in the development of corneal guttae and UV exposure.[121] Another study found that twenty packs of smoking per year (P = 0.013) was correlated with a two-fold increase in the development of corneal guttae; higher body weight and BMI were also associated with lower risk but it mechanism is not clear.[121] An independent study, however could replicate that smoking increased their chances of getting FECD by 30.0% in Americans.[122]

MicroRNAs (abbreviated miRNA) are short, endogenous, non-coding RNA molecules that exist in plants, animals, and some viruses. It controls post-transcriptional gene expression**.** Downregulation of eighty-seven miRNAs and a substantial decrease in DICER1 were reported in the FECD endothelium relative to control. Decreased expression of miR-29 was associated with the overexpression of the different ECM proteins like collagen I and collagen IV.[72] Researchers found that DNA hypermethylation in the promoter of miR-199B drives epigenetic silencing of miR-199b-5p expression. It ultimately caused overexpression of its target genes ZEB1 and SNAIL, leading to EndoMT transition and accumulation of ECM deposition in FECD.[123]

DNA methylation in the promoter or within the gene body region epigenetically controls the gene expression. Hypomethylation of the genes associated with the transport of fluids and ions [Aquaporin-1 (AQP1), bicarbonate transporter-related protein-1 (BTR1), and monocarboxylate transporters (MCTs)], was found in the FECD endothelium tissue samples compared with the age matched controls.[124] Significant hypomethylation in the promoter regions of the genes related to the cytoskeletal organization like EMAP like 3 (*EML3*), and zinc finger protein 135 (*ZNF135*) was also found in the FECD samples. Promoter DNA hypermethylation was observed in the genes such as alpha glucosidase (*GAA*), and fatty acid Synthase (*FASN*), associated with the different metabolic pathways. DNA hypermethylation of

the promoter region of *SLC4A11* lead to downregulation of its expression in FECD samples relative to controls.[124]

1.7 Molecular Pathophysiology:

1.7.1 Pump dysfunction:

Endothelial cells have specific receptors that enable the leakage of solutes and nutrients to the cornea from the aqueous humour. Na,K-ATPase which is located on the basolateral surface of CE, pumps the fluid outside of the cornea to keep it in a condition of deturgescence. Functional impairment of these receptors and pumps as noticed in FECD, leads to corneal edema. Researchers found FECD patients with the elevated central corneal thickness (CCT) without any sign of epithelial edema. They noticed increased permeability in FECD CE but no alteration in the pumping rate, implying that the initial problem could be due to the downfall of endothelial barrier function, which led to elevated fluid influx into the cornea but no corresponding improvement in pump function. In the follow up investigation, however, researchers observed no change in the permeability rate of the FECD patients compared with the control group, indicating that the pumping rate is lower and the barrier activity is not compromised in FECD. The difference between the two studies may be due to the possibility that barrier and pump functions may be affected in different ways at various stages of FECD.[125] Other reports showed that the density of the pump site in early FECD is greatly elevated relative to the typical corneal endothelium. As the condition worsens, there tends to be a change from elevated pump density to reduced density of the pump site during the end-stage of the disease. But, when the transition from elevated to reduced pump density occurs and whether this transition is abrupt or gradual is not known till now.[57]

Solute carrier family 4 member 11 (SLC4A11) is a highly clustered sodium coupled borate pump, residing in the membrane of the CE. A reduction in SLC4A11 expression due to its promoter hypermethylation was also found in FECD cases.[124] Due to the diminished expression of SLC4A11 in the membrane, NH3:$2H^+$ cotransport and Na^+ coupled OH^- transport ultimately fails.[100,126] A substantial decrease in the β1 subunit indicated a continuous depletion in the abundance of Na,K-ATPase in the endothelial cells of LO-FECD.[57,127]

1.7.2 Aggregation of extracellular matrix proteins and guttae formation:

Proteomics study reported pronounced upregulation of the molecular chaperone clusterin (CLU) in FECD tissue samples compared with the controls. Both the secretory and the nuclear isoforms of CLU were detected to be overexpressed in the FECD endothelium. Rosette-like aggregation of the FECD endothelial cells was found surrounding the guttae. Studies also showed enhanced CLU staining in the centres of the guttae.[115] The specific role of CLU in FECD causation is yet to be known, but it could be due to is the apoptosis of endothelial cells owing to the overexpression of nuclear clusterin. Transforming growth factor-β-induced protein (TGFβIp) also serves an important role in the development of the guttae.[120] It interacts with fibronectins, collagen, and other ECM proteins.[128–130] It was presumed that interaction between TGFβIp with collagen drives the excess accumulation of collagen fibres in the guttae. Immunofluorescence assay found colocalization of TGFβIp and CLU in the FECD affected endothelium with significantly enhanced intensity in guttae centres.[120] TGFβIp represented positive staining at the DM level, with the most significant staining pointing toward lower guttae sections, whereas CLU immunostaining was located above TGFβIp. TGFβIp overproduction directs the gradual thickening of DM. The interaction between TGFBIp and CLU during guttae formation was thought to drive the aggregation and adhesion of endothelial

cells to the substratum. During guttae formation, the ability of the cells to connect to their substratum is gradually compromised, making them vulnerable to apoptosis.[120]

1.7.3 Mitochondrial pathology:

Because of the constant flow of ions and fluids, corneal endothelial cells are metabolically challenging; hence, they are mostly filled with densely populated mitochondria. FECD is the outcome of elevated oxidative stress with an inadequate mitochondrial network in decompensated corneal endothelial cells. Serial analysis of gene expression (SAGE) in FECD CE showed under-expression of different mitochondrial genes associated with the electron transportation as well as oxidative phosphorylation such as Cytochrome b, Cytochrome c oxidase subunit III, NADH dehydrogenase subunits 1, 2, 4, and ATP synthase F0 subunit 6.[131] The presence of 8-hydroxy-2'-deoxyguanosine, the marker of double-stranded DNA breakage hinted that the mitochondrial genome is the primary site of oxidative damage in FECD.[46] Ultrastructural FECD tissue studies showed significant existence of autophagic vacuoles with internalized and degenerated mitochondria, suggesting engulfment of the degenerated mitochondria by autophagic vesicles. Additionally, increased autophagosomes and autophagolysosomes were also found in the FECD. A simultaneous decrease in Mitofusin 2 (MFN2), indicated the downfall of fusion capacity with concomitant induction of mitophagy caused by fission.[132] The mtDNA genomic variant A10398G was significantly associated with FECD.[133]

1.7.4 Unfolded protein response (UPR):

Several genes involved in the FECD pathophysiology alter the processes of protein folding and may play roles in the UPR. Examination of CE demonstrated markedly enlarged, rough, and granule containing endoplasmic reticulum (ER) in all patients with FECD relative to the

controls. FECD corneas also showed enhanced expression of phospho-eIF2α, G protein-coupled receptor 78 (GRP78), and C/EBP homologous protein (CHOP) engaged in the UPR compared with normal corneas.[53] Colocalization of GRP78 with aggresomes indicated increased rates of misfolded protein accumulation, which subsequently lead to UPR in FECD endothelium.[134] An FECD cell line (iFECD) demonstrated that TGF-β signalling channels the constant influx of ECM proteins into the ER, consequently increasing the deposition of unfolded proteins and triggering the intrinsic apoptotic response.[135]

1.7.5 Endothelium to Mesenchymal transition (EndoMT):

Even if the CE is assumed to be in a condition of terminated growth, the endothelial cells could migrate to mitigate the injury of the surrounded layer, and the presence of stem cell markers in the endothelium and the posterior limbus are also evident. Different proteins engaged in cell proliferation are also expressed in a wounded endothelium. Some other studies suggested significant overexpression of different extracellular matrix (ECM) proteins, like fibronectin, collagen subtypes I, III, and XVI, and agrin on the DM in FECD cornea.[69,136] Researchers hypothesized that genes inducer of endothelial to mesenchymal transition (EndoMT) may be responsible for the excessive deposition of ECM on the DM. Significant overexpression of EndoMT inducing proteins ZEB1 and SNAIL was found in FECD corneal endothelial cells and through the various signalling pathways, they are actively engaged in the uncontrolled development of ECM proteins. Expression levels of ZEB1 and SNAIL were also suppressed after treatment of TGF-β type I ALK receptor inhibitor SB431542 followed by the reduced output of ECM deposition.[137] Evidence suggested that EndoMT also changes the hexagonal corneal endothelium into fibroblastic ones. More studies is required to find a strong relationship between the EndoMT transition and abnormal ECM deposition, which might help in drug design for cure of the disease in the future.

1.7.6 Oxidative stress and apoptosis:

Different mutations, RNA cytotoxicity, UPR, and channelopathy lead to increased aggravation of oxidative damage in FECD. If the cells are unable to remove excessive reactive oxygen species (ROS), the oxidant-antioxidant ratio produces an imbalance that increases oxidative stress. Overproduction of ROS and reactive nitrogen species (RNS) products in FECD corneas has been reported. In addition, FECD corneas displayed an elevated output of nitric oxide synthase relative to the normal corneas, suggesting the increased generation of nitric oxides linked with FECD.[138] The FECD endothelial cells displayed downregulation of antioxidant enzymes like glutathione S-transferase (GST), aldehyde dehydrogenase family 3 member A1 (ALDH3A1), and ferritin.[131] Proteomic analysis showed decreased peroxiredoxin expression in FECD endothelial cells and DM relative to the control.[139] Additionally, heat shock protein 70 (HSP70), involved in the antiapoptotic response, showed lower expression in FECD corneas. The endothelium displayed reduced metallothionein 3 (MT3), superoxide dismutase 2 (SOD2), and thioredoxin reductase 1 (TXNRD1) levels in the mitochondrial matrix.[46] The antioxidant response element (ARE), found in the promoter sequences of numerous antioxidant and xenobiotic-degrading enzymes, controls the expression of several genes related to oxidative stress, including heme oxygenase-1 (HO-1), thioredoxin reductase 1 (TXNRD1), glutathione S-transferases (GSTs) etc.[140,141] This ARE sequence has a high probability of binding nuclear factor erythroid 2-related factor 2 (NRF2) regulatory protein, which may be connected with the transcriptional activation of many antioxidant genes essential for oxidative stress protection.[140] A decrease in the amount of NRF2 and its stabilizer Parkinson disease protein 7 (DJ-1) was found in the FECD endothelium, which in turn manifested oxidant-antioxidant imbalance in the FECD endothelium.[142] It has been hypothesized that in FECD endothelium elevated oxidative stress may result in DNA damage and apoptosis.[46] In the DM and CE of FECD samples, researchers reported high quantities of advanced glycation end

products (AGE) and their receptors (RAGEs), proving evidence of prolonged exposure to oxidative stress in the FECD corneal endothelium.[143]

Cellular apoptotic response and senescence were also reported in the FECD endothelium, suggesting that they may be the reason rather than the outcome, of the disease progression. In FECD samples, endothelial cells showed hallmarks of apoptosis, such as DNA fragmentation, reduction in cellular dimensions, condensed nuclei, and presence of TUNEL positive cells.[144–146] Overexpression of the Fas, Fas ligand, and Bax (apoptotic) was also noticed in the FECD endothelium.[145] Apoptosis induction proteins like caspase 3 and caspase 9 were also increased, pointing out that initiation of the UPR may perform a crucial part in apoptosis activation in FECD. FECD endothelium samples showed altered senescence-related protein expression of p21 and p16.[147-148] Both human FECD endothelium samples and transgenic *COL8A2* (Q455K/Q455K) knock-in mice displayed excessive p21 expression.[147] Previous reports also supported upregulation of the cyclin-dependent kinase inhibitor 2A (CDKN2A) and its transcription activators ETS proto-oncogene 1 (ETS1) and Rho GTPase activating protein 18 (ARHGAP18), along with reduced expression of its transcription repressor inhibitor of DNA binding 1 (ID1) which indicated the sign of senescence and aging in FECD corneal endothelium.[149–151]

1.8 Treatment:

FECD patients are often reported with hazy cornea, scattering of light, wet eyes, and blurred vision. By the 6th or 7th decade of life, as these symptoms intensify, corneal transplantation appears mandatory. Previously, clinicians executed penetrating keratoplasty (PK) to substitute the thickness of the whole cornea. This procedure has limitations such as prolonged visual restoration, chronic epithelial injury, and others. Ophthalmologists have been practising

modifications of endothelial keratoplasty (EK) for the past two decades, where either the endothelium is removed, or descemetorhexis, in which particularly the DM is peeled off.

1.8.1 Surgical techniques:

Currently, corneal transplantation is the sole remedy for the FECD and other corneal endothelial diseases. Penetrating keratoplasty (PK) is an entire-thickness transplantation technique where a trephine of the proper diameter is utilized to prepare a full-thickness resection of the cornea of the patient, followed by a replacement of the full-thickness donor corneal graft. This technique has the maximum failure rate due to the intraoperative and postoperative complexities. Advanced surgical techniques, such as Descemet stripping endothelial keratoplasty (DSEK) and Descemet membrane endothelial keratoplasty (DMEK), particularly transplant the diseased endothelial layer with donor corneal endothelium. The benefits of DSEK over PK include a decreased rate of surgical failure, fewer intraoperative and postoperative problems, astigmatism, and faster visual restoration.[152–154] But, DMEK has drastically reduced the rejection rates and improved the visual recovery over DSEK.[155–157] According to studies, this procedure could mitigate the ocular complications much better than DSEK.[158,159]

1.8.2 Non-surgical techniques:

The advancement of various surgical techniques for corneal transplantation currently allows for the minor invasive procedure with improved therapeutic results, although issues persist. The majority of these are the lack of donor corneas, complex surgical procedures, and the rate of transplantation failure. Such concerns have inspired researchers to design new approaches that can address the existing drawbacks of transplantation.

Eye drops containing the ROCK inhibitor (Y-27632) promoted cellular proliferation and restored endothelium cell density in primates. It prevented the death of corneal endothelial cells and improved cellular regeneration.[160] It also reduced corneal edema in FECD patients.[161] In addition, ROCK inhibitor also improved cellular density, reduced elevated corneal thickness, and thus restored corneal transparency in patients suffering from bullous keratopathy (BK).[162]

Treatment with the antisense oligonucleotide to curtail the extended CTG repeat induced toxic RNA foci formation was shown to effectively inhibit the number and size of RNA foci, mis-splicing of mRNA.[92,96]

Lithium has been utilised as a remedy for neuropsychiatric diseases because it could minimize ER-UPR and oxidative stress. Also, *COL8A2* (Q455K/Q455K) knock-in lithium-treated mice presented enhanced autophagy and improved viability of CE cells, proposing lithium as a therapeutic option.[163] N-acetylcysteine (NAC) enhances the life span of cultured corneal endothelial cells, exposed to ER and oxidative stress. NAC consumption improves the viability of the corneal endothelial cells correlated with the increased antioxidant and reduced ER stress markers in an EO-FECD mouse model.[164]

NSAIDs like Glafenine, Ibuprofen, and Acetylsalicylic acid could restore functional defects of SLC4A11.[165] In a further investigation, combinations of four NSAIDs (Flurbiprofen, Diclofenac, Nepafenac, and Bromfenac) were noticed to drive misfolded SLC4A11-G709E mutant proteins in the plasma membrane of HEK-293 cells.[166]Although both types of treatment improves the complications associated with FECD but these are all cell based and it remains to be explored in human. Thus, the early prediction of the disease and determining the genetic and non-genetic risk factors across in all the populations can help curtail the disease.

1.9 Lacunae and Objectives of the Thesis:

A GWAS of Caucasian population in 2010 reported a significant genetic association between the *TCF4* intronic SNP rs613872 and FECD.[20] Subsequent findings revealed that the expanded CTG trinucleotide repeats (CTG18.1) in the *TCF4* gene has a significant impact on FECD causation. In the Caucasian cohort, 79.0% individuals with CTG repeat lengths > 50 had symptoms of FECD.[90] In contrast, only 34.0% of the FECD cases exhibited this increased repeat length in our population.[34] This would implicate the role of other possible genes apart from *TCF4* as the major genetic candidates in our population. In the latest GWAS in 2017, where three additional variants found in new candidate genes (rs79742895 in *KANK4*, rs3768617 in *LAMC1*, and rs1200114 in *LINC00970/ATP1B1*) were identified as having a significant association with the disease in the European population in addition to the previously reported *TCF4* gene.[64] For the lack of a substantial sample collection, GWAS study in Indian population is yet to be carried out. Replication study of the newly identified genetic variants in the various populations, including Indian population is yet to be carried out and the functional relevance of these genetic variants was also lacking.

In addition to the genetic association of various genes related to FECD, many transcriptional and post-transcriptional regulatory proteins, induce the expression of various genes linked to enhanced apoptosis, ECM production, and cell migration, related to the pathophysiology of the disease.[115,137,167] Caspase 8 associated protein 2 (CASP8AP2, also known as FLASH), was found as a novel post-transcriptional regulator of EMT inducing protein ZEB1 and it was shown that CASP8AP2 protects ZEB1 from proteasomal degradation caused by the activity of the ubiquitin ligases SIAH1 and F-box protein FBXO45.[168] As a result, the lack of CASP8AP2 abruptly affected the ZEB1 expression level in the cells and interrupted the EMT transition. CASP8AP2 is a part of the death-inducing signalling complex (DISC) and participates in

apoptosis by activating caspase 8.[169] ZEB1 is overexpressed in primary FECD corneal endothelium cells, compared with control endothelium cells.[137] But, the expression pattern of CASP8AP2 in control versus FECD endothelium tissues is also not known. Furthermore, the transcriptional regulation of *CASP8AP2* expression is yet to be studied. These two open questions would help to decipher the reasons for ZEB1 overexpression in FECD condition.

Based on these lacunae, we hypothesized that polymorphism rs3768617 in the intronic region of *LAMC1* and rs1200114 in the intergenic region of *LINC00970*/*ATP1B1* might also be the genetically and functionally associated for FECD pathogenesis in the Indian population. We also speculated that transcription factors might bind to the most important regulatory region of the *CASP8AP2* promoter and regulate its expression. To test our hypothesis, the following objectives were designed to accomplish the specific aims related to them:

Objective 1: Genetic association and functional role of *LAMC1* with LO-FECD **(Chapter 3)**

Objective 2: Genetic association of *LINC00970/ATP1B1* with LO-FECD and its functional role in disease pathogenesis **(Chapter 4)**

Objective 3: Role of CASP8AP2 in FECD progression **(Chapter 5)**

CHAPTER 2

Materials and Methods

2.0 Materials and Methods:

2.1 Sample collection:

The Institutional Ethics Committee of the National Institute of Science Education Research, L. V. Prasad Eye Institute, and Disha Eye Hospitals evaluated and approved the present investigation preceding the enlistment of the participants. All the research methods followed the principles of the Declaration of Helsinki. The control and FECD affected people were registered for this examination at L. V. Prasad Eye Institute, a tertiary eye care organization in Bhubaneswar and Disha Eye Hospitals, Barrackpore after obtaining their consent for enlistment in the study. 4 ml of peripheral blood was drawn out by a clinician at the eye care centres and kept at 4°C in EDTA – coated vacutainers to limit blood coagulation. For long time preservation, the blood samples were kept at -80°C. Tissue samples from patients were obtained quickly after post operation in RNAlater (R0901, Sigma-Aldrich, USA), and further used for RNA extraction or immunofluorescence (IF). The inclusion and exclusion criteria for sample collection are discussed below.

2.2. Inclusion-exclusion criteria:

We acquired clinical details of all the candidates after medical screening by using specular microscopy examination. The inclusion criteria for FECD cases are the age range over 40 years and the presence of moderate to confluent central corneal guttae. In a couple of cases, microscopy examination was impossible in either both eyes or one eye because of the progressive stage of FECD and so, we found out the disease status by histopathological examinations including thickened Descemet's membrane (DM) with nodular excrescence and scattered endothelium. FECD cases which showed inconclusive results from specular microscopy or histological examinations, were excluded from the study. Also if the patient had

any other ocular diseases apart from FECD, was not included in the case-control study. The inclusion criteria for control subjects are the absence of corneal guttae and satisfying age range almost similar to cases. Controls who did not match the age range or had inconclusive results from specular microscopy examinations were not considered for the study.

2.3 Genomic DNA Extraction:

The genomic DNA was obtained from the blood leucocytes (by deoxyribonucleic acid salting-out method) of the subjects (both controls and cases) and was kept at 50 ng/µl. First, 500 µl of human blood sample was taken in a microfuge tube from the EDTA coated vacutainer tubes (BD Vacutainer, UK) and was centrifuged at 11000 rpm for 5 minutes to pellet down the leucocytes. The serum-containing supernatant was discarded and 1000 µl RBC (Red-blood cells) lysis buffer was added. Pelleted cells were dislodged for not more than 1 minute by inverting the microfuge tubes several times and then centrifuged for 5 minutes at 11000 rpm. A further 200 µl of RBC lysis buffer was mixed with the retained pellet and re-centrifuged for 5 minutes at 11000 rpm. Subsequently, the lysed RBCs were discarded and only the pellet containing leucocytes was processed. To eliminate the salts and impurities from the previous steps, the pellet was dissolved in 200 µl of ultrapure water by pipetting 2-3 times and centrifuging at 13500 rpm for 6 minutes. The supernatant was thrown away. 80 µl Nuclei lysis buffer and 10 µl of 10% SDS were applied to this pellet. Because of SDS, pipetting this mixture produced saponated froth which assisted to lyse the cell membrane and the nuclear membrane. 100 µl of pre-chilled 5 M NaCl was applied to this solution to coalesce DNA molecules in the presence of high salt concentrations. Furthermore, 200 µl of ultrapure water and 400 µl of PCI solution (P2069, Tris saturated phenol: chloroform: isoamyl alcohol = 25:24:1, Sigma-Aldrich, USA) were applied. The contents were mixed by inverting the tubes until they turned milky

followed by centrifugation for 10 minutes at 12000 rpm. The aqueous layer containing genomic DNA was extracted in fresh tubes and 1000 µl of absolute pre-chilled ethanol was added for precipitation. Mixing was performed carefully by slowly inverting the tubes 20 times which allowed the DNA pool to aggregate. The tube was again centrifuged for 15 minutes at 13500 rpm and the supernatant was removed. The pellet containing the pool of DNA was washed with 200 µl of 70% ethanol and centrifuged for 5 minutes at 13000 rpm. All stages of centrifugation were done at room temperature (RT). The supernatant was discarded by soaking and the pellet was air-dried for at least 3-4 hours. DNA was ultimately resuspended in 30 µl Tris-EDTA buffer (for every 500 µl blood sample as starting material), pH 8.0, and left at 56°C for 1 hour to dissolve the DNA fully. The re-suspended DNA was quantified using NanoDrop 2000 (ThermoFisher Science, USA) and DNA quality was tested with an agarose gel electrophoresis. It was preserved at -20°C at 50 ng/µl until further use. The compositions of all the required buffers for DNA extraction are mentioned in **Table 2.1**.

Table 2.1: Composition of the buffers used for DNA extraction

SN	Buffer	Composition
1	RBC lysis buffer	0.32 M Sucrose, 1 mM $MgCl_2$, 1% Triton X 100, 12 mM Tris-HCl (pH 7.6)
2	Nuclei lysis buffer	20 mM Tris-HCl, 4 mM Na_2EDTA, 100 mM NaCl (pH 7.4)
3	Tris-EDTA buffer	10 mM Tris-HCl (pH 8.0), 1 mM EDTA

2.4 Primer designing:

Primers flanking the polymorphism sites were designed using the NCBI PrimerBLAST online tool [Primer designing tool (nih.gov)] and were manufactured at 25 nmoles, under desalted conditions (GCC Biotech, India). The primer sequences used for the genetic association study are noted in **Table 2.2**.

Table 2.2: Sequences of the primers used for genetic association analysis

SN	SNP ID	Sequence (5′-3′)	Ta	Chapter
1	rs3768617	F: GTTTCCTTACACTCCGTGCTG R: TCCTTTTCCACTTTCCTACCTTGA	58°C	3
2	rs1200114	F: GCACACAACAGAACACGGAA R: CCTTTGCTTGACTGAGCCTG	58°C	4
3	rs4656175 & rs1040506	F: GATGCTCAATGATAGGTGTGCTC R: CAATACTATGGTTTGGGTCTCTC	57°C	4
4	rs10665761	F: ACTGGAACATACAAGAGAACCTT R: GGAGCTTGGCATCTTGAAGG	55°C	4
5	rs1200105	F: ACTGGCTTACCTTGCCACC R: CCTTGAGGCTCCACCTATT	60°C	4
6	rs1200106	F: AATAGGTGGAGCCTCAAGG R: CCTGTGTAATAGAAAACAACAGCC	54°C	4
7	rs1200108	F: TCAAACACAGACAGGGAGTCG R: TGACCTGGCACCATACCTTGT	52°C	4

F: Forward, **R:** Reverse, **Ta:** Annealing temperature

2.5 Tag SNP Selection:

All of the promising tag SNPs were selected within a gene fragment of 7000 base pairs upstream and downstream of the lead SNP rs1200114, according to the International HapMap Project for Han Chinese from Beijing (http://browser.1000genomes.org, http://grch37.ensembl.org/index.html). Using Ensemble software, candidate tag SNPs with minor allele frequencies more than 0.05 were identified. The threshold value of squared correlation between SNPs (r^2) 1.0 and D-prime (D′) value 1.0 was preferred to pick SNPs that are in high linkage disequilibrium (LD) with the reference SNP rs1200114. Six tag SNPs rs4656175, rs1040506, rs10665761, rs1200105, rs1200106, and rs1200108 were ultimately chosen for additional experiments based on the aforementioned criteria.

2.6 Polymerase chain reaction (PCR):

PCR was performed to amplify a particular genomic region. The PCR reaction mix comprised of 100 ng genomic DNA, 0.2 µM flanking primers, 1 mM dNTP mixture (G-4001, GeNet Bio, India), 2.5 µl DMSO (Himedia, India), 1X Reaction Buffer (GeNet Bio, India), 1.0 U ExPrime Taq DNA polymerase (GeNet Bio, India) and nuclease-free water (NFW) to adjust the 25 µl reaction volume. The reaction conditions are mentioned in **Table 2.3**. These amplified products were used directly for elution by the QIAquick Gel Extraction Kit (28706X4, QIAGEN, Germany). The eluted products were then used for Sanger sequencing. The compositions of the PCR reagents are described in **Table 2.4**.

Table 2.3: Thermocycling conditions for the PCR

SN	Steps	Cycle	Temperature	Time
1	Initial denaturation	1	95°C	4 minutes
2	Denaturation Annealing Extension	35	95°C Annealing temperature 72°C	35 seconds 30 seconds 50 seconds
3	Final extension	1	72°C	10 minutes
4	Hold	1	4°C	∞

Table 2.4: Detail composition of the PCR reaction mixture

SN	PCR reagent	Composition
1	10X Reaction Buffer	Tris-HCl (pH 9.0), 20 mM $MgCl_2$, $(NH_4)_2SO_4$, PCR enhancers
2	10 mM dNTP mixture	2.5 mM of each dNTP

2.7 DNA Sequencing using the Sanger sequencing method:

The eluted PCR amplicons were quantified, and sequencing PCR reaction was set up using BigDye Terminator v3.1 Cycle Sequencing Kit (4337455, Applied Biosystems, USA). The components used for each sequencing reaction were 0.25 µl of 2.5X ready reaction mix (0.1 µl

of ready reaction mix was used per 100 bases), 2 µl of dilution buffer (5X), up to 80 ng eluted DNA as a template, 2 µl of primer (2 pmol) and nuclease-free water (NFW) for a total 10 µl reaction volume. The thermocycling conditions for the sequencing PCR reaction is mentioned in **Table 2.5**. Initially, each sequencing reaction product required clean up steps before eventually being sequenced on a Genetic Analyzer 3130xl (Applied Biosystems, USA). 10 µl of NFW with 2 µl of 125 mM EDTA was applied to each sequencing reaction containing 10 µl of sequencing PCR product and the contents were properly mixed. Then 2 µl of 3 M Sodium acetate (NaOAc) (pH 4.6) and 50 µl of absolute ethanol was added to this. The contents were well mixed and incubated for 15 minutes at room temperature. Following incubation, the reaction mixture was centrifuged at room temperature (RT) at a speed of 12000 rpm for 20 minutes. The pelleted sequencing products were washed by adding 250 µl of 70% alcohol and centrifuged at room temperature at 12000 rpm for 10 minutes. The pellets were dried at RT for 2 hours after decantation of the supernatant and solubilized in 12 µl of Hi-Di formamide (4311320, Thermo Scientific, USA). These samples were placed on a 96-well sequencing plate (ABI 1400, Applied Biosystems, USA), coated with septa, denatured at 95°C for 5 minutes, and, snap-chilled on ice for 10 minutes. The sequencing readout was achieved in ABI format and analyzed using BioEdit v7.1 software [(https://bioedit.software.informer.com/7.1/) Tom Hall, Ibis Biosciences, USA]. Sequences acquired from the 1000 genome NCBI Genomes database (https://www.ncbi.nlm.nih.gov/) were used to match either genotype the polymorphic site or to search for nucleotide sequence variations using the local alignment method.

Table 2.5: Thermocycling conditions for the sequencing PCR

SN	Step	Cycles	Temperature	Time
1	Denaturation	25	95°C	10 seconds
	Annealing		50°C	5 seconds
	Synthesis		60°C	4 minutes
2	Hold	1	4°C	∞

2.8 Cell culture:

HEK293 cells (Cell repository facility, NCCS, Pune) were cultured in Dulbecco's Modified Eagle Medium, High Glucose (AL066G, Himedia, India) with 10% fetal bovine serum (11573397, Gibco, USA) and maintained at 37°C and 5% CO_2 under optimum humidity. The cells were routinely checked by a phase-contrast microscope (CKX53, Olympus LS) to avoid any contamination.

2.9 *In silico* analysis:

In silico analysis was performed to check the probability of allele specific transcription factor binding in the encompassing region of rs3768617 and rs1200114 using the JASPAR database (http://jaspar2016.genereg.net/). In JASPAR, the relative profile score threshold was set at 90% to examine the chance of binding transcription factors in the adjoining sequences of both minor and major alleles of all the variants. The transcription factor(s) which showed the differential binding probability of a particular allele was selected for other wet-lab experiments. We also investigate the allele specific transcription factor binding probability in the case of rs1200108 by the Promo 3.0 online tool (http://alggen.lsi.upc.es/cgi-bin/promo_v3/promo/promoinit.cgi?dirDB=TF_8.3) as JASPAR database failed to show any differential allele specific transcription factor for this particular variant. For analysis of the potential promoter region of *CASP8AP2*, we considered the Promoter2 online tool [MatInspector,Genomatix(https://www.genomatix.de/online_help/help_matinspector/matinspector_help.html)] to retrieve the 5′-UTR region of *CASP8AP2*. Lasagna Search 2.0 database (https://biogrid lasagna.engr.uconn.edu/lasagna_search/index.php) was selected to distinguish the different transcription factor binding motifs in the promoter region of *CASP8AP2*.

2.10 Ultra-competent bacterial cell preparation:

A small amount of frozen glycerol stock of DH5-Alpha or Stbl3 was taken by a pipette tip and stroked in an LB plate. The plate was then kept at 37°C for 12 hours for bacterial growth. The next day, an isolated colony was taken from the plate and incubated in 15 ml antibiotic-free SOB growth medium (2% Tryptone, 8.56 mM NaCl, 2.5 mM KCl, 0.5% Yeast extract, 10 mM $MgCl_2$, 10 mM $MgSO_4$) at 37°C with shaking at 220 rpm. Subsequently, from this overnight culture, 4 ml solution was taken and added to 200 ml SOB growth medium in a 500 ml flask. In a second 500 ml flask, 10 ml of the overnight culture was added to 200 ml SOB media. Both the flasks were then placed in a humidified incubator and incubated at 18°C with shaking at 170 rpm. The next day, when the OD_{600} of one of the cultures reached 0.55, that particular flask was immediately transferred to an ice-filled box and it was incubated for 15 minutes in ice to stop the bacterial growth. The bacterial culture of the other flask was discarded. The bacterial cells were harvested by centrifugation at 6000 rpm for 12 minutes at 4°C. The supernatant was discarded and the remaining media was removed by pipetting. The bacterial cells were mixed gently in 70 ml of cold Inoue transformation buffer (10 mM PIPES, 250 mM KCl, 15 mM $CaCl_2$, 55 mM $MnCl_2$). The resuspended cells were centrifuged for a second time at 6000 rpm for 12 minutes at 4°C. The supernatant was removed and the excess Inoue buffer was discarded. The pelleted cells were resuspended again in 15 ml of cold Inoue transformation buffer. 1 ml DMSO was added to this mixture and it was incubated on ice for 15 minutes. The resuspended cells were then aliquoted in chilled 1.5 ml tubes (100 µl cells per tube) and the tubes were snap-frozen and stored at -80°C. To check the efficiency of the transformation, one of the vials was thawed in ice, and in that 100 ng of plasmid DNA was added and mixed well. This DNA-competent cell mixture was then kept on ice for 30 minutes. The tube was then placed in a 42°C water bath for 45 seconds. Then, it was immediately returned to the ice and allowed to cool for 5 minutes. Approximately 600-700 µl of SOC media (SOB medium + 20 mM glucose) was

added to the tube and it was kept in the shaking incubator for 1 hour at 37°C. Next, the tube was again centrifuged at 3000 rpm for 4 minutes and excess SOC medium was poured off. The cells were then suspended in 200 µl of remaining SOC medium and were plated in the LB-agar plate containing the appropriate antibiotic. The transformation efficiency of the ultracompetent cells was checked after 12 hours of incubation in a humidified incubator at 37°C.

2.11 Colony PCR:

Colony PCR was carried out to identify the positive bacterial colony having plasmid DNA with our desired insert. After the transformation of the plasmid DNA in competent cells, we first selected the single colonies and prepared batch cultures of the individual colonies in another LB plate (also known as a patch plate). From the patch plate, we took a small amount of each colony and mixed it with 20 µl of NFW in 0.2 ml PCR tubes individually. They were put in a PCR machine and pre-heated at 95°C for 10 minutes to lysis the cell membrane. After this, the tubes were centrifuged at 13000 rpm for 20 minutes to release the plasmid DNA. 6 µl of the supernatant was removed from each of the tubes as a template for the colony PCR. Insert specific primers were designed for the PCR reactions. After the PCR was completed, the products were electrophoresed in a 1% agarose gel. The positive colonies showed the expected DNA band in the agarose gel and the negative colonies failed to display the expected product. After identifying the positive colony, we again picked up a small amount of colony from the patch pate. It was then added into the 4 ml Luria Bertani (LB)-broth (M1245, Himedia) with the appropriate antibiotic and kept for overnight in the incubator at 37°C with shaking at 220 rpm. Plasmids were isolated from the overnight culture using QIAprep spin miniprep kit (27106X4, Qiagen, Germany) and the plasmid DNA was sequence-verified using vector-specific primers.

2.12 Luciferase reporter assay:

HEK293 cells were seeded into 24-well plates to test the reporter activity. The cells were co-transfected with firefly luciferase constructs (cloned in pGL4.23 vector using double digestion cloning method by KpnI-HF and NheI-HF restriction enzymes) along with the renilla vector (pGL4.74, Promega, USA) at a 100:1 ratio in 70% confluency. Lipofectamine 3000 (L3000015, Invitrogen, USA) was used as the tool for transfection and Opti-MEMI reduced serum media (31985070, Gibco, USA) was preferred as the transfection medium. As a negative control, an empty pGL4.23 vector (E8411, Promega, USA) was used. The transfection efficiency was normalized by the luciferase activity of the renilla reporter vector. Using the Dual-Luciferase Reporter Assay System (E1980, Promega, USA), cell lysates were prepared 48 hours after transfection. Following the instructions of the manufacturer, reporter activities were measured with the Varioskan Flash Multimode Reader (Thermo Scientific, USA). Upon normalization with renilla reporter activity, luciferase activities from the transfected cell lysates were plotted. Each of the experiments with at least three technical replicates was replicated independently for three individual days. The information of the oligos used to prepare the different firefly constructs are mentioned in **Table 2.6**.

Table 2.6: Sequences of the primers/oligos utilized to develop different firefly constructs

SN	Purpose	Sequence (5′-3′)	Chapter
1	rs3768617 ‘A/G’ cloning	F: CGCGGGGTACCGTTATCTCTCACCTGGGATTG R: ATTAAAGCTAGCCATTTTGAAAGGACCATTTTGGC	3
2	rs1200114 ‘G’ cloning	S: CTTCTCAGCCAGCCTCATCTTAG AS: CTAGCTAAGATGAGGCTGGCTGAGAAGGTAC	4
3	rs1200114 ‘A’ cloning	S: CTTCTCAGCCAACCTCATCTTAG AS: CTAGCTAAGATGAGGTTGGCTGAGAAGGTAC	4
4	rs1200108 ‘G’ cloning	S: CGCTAAGGACGCCGTGTAACTGCATAGG AS: CTAGCCTATGCAGTTACACGGCGTCCTTAGCGGTAC	4

5	rs1200108 'A' cloning	S: CGCTAAGGACGCCATGTAACTGCATAGG AS: CTAGCCTATGCAGTTACATGGCGTCCTTAGCGGTAC	4

F: Forward, **R:** Reverse, **S:** Sense, **AS:** Anti-sense

2.13 RNA isolation from the tissue samples:

The endothelium layer plus a thin layer of DM was used to extract RNA. Non-transplant grade control corneal tissues were collected from LV. Prasad Eye Institute, Bhubaneswar and Disha Eye Hospitals, Barrackpore in RNAlater solution and stored at 4°C. The tissues were used within a month for experiments. Post-operative tissues were obtained in RNAlater solution in the case of FECD. All of these tissues were rinsed in NFW to clear the RNAlater solution and followed the manufacturer's RNA extraction protocol (74104, RNeasy Mini Kit, QIAGEN, Germany). Tissues were gently lysed with a 350 µl RLT buffer and mixed with 70% ethanol (in NFW) of equal volume. The solutions were then added to the columns and centrifuged at 13000 rpm for 1 minute at 4°C. The columns were then washed once with a 750 µl RW1 buffer, and twice with a 500 µl RPE buffer to remove membrane DNA, protein, and lipids. RNA was then eluted with 15 µl nuclease-free water from the silica membrane and kept on ice until quantified. Spectrophotometric quantifications of RNA were performed using Nanodrop 2000 (Thermo Scientific, USA).

2.14 Reverse transcription and quantitative real-time PCR:

Extracted and quantified RNA was immediately converted to cDNA using the Verso cDNA Synthesis Kit (AB1453B, Thermo Scientific, USA), and preserved at -20°C until further use. Since the total RNA extracted from FECD or control tissue was of small quantity, the entire eluted RNA was converted to cDNA by mixing it with anchored oligo-dT and random

hexamers in a ratio of 1:3 along with enzyme and buffer mixture into 20 µl reaction volume. The synthesis of cDNA was achieved in a C100 Touch Thermal Cycler (Bio-Rad, USA) at 45°C for 45 minutes, followed by enzyme inactivation for 2 minutes at 95°C. Quantitative real-time PCR (qRT-PCR) was performed in ABI 7500 real-time PCR System (Applied Biosystems, USA), using 8 µM transcript-specific primers (**Table 2.7**, GCC Biotech, India) and FastStart Universal SYBR green mastermix (F-416L, Thermo Scientific, USA). Cycle threshold (Ct) values were exported in Microsoft Excel (MS-Excel) file (https://www.microsoft.com/en-in/microsoft-365/excel) and the fold changes were determined after normalization with internal control, GAPDH values. Each experiment was performed with three experimental replicates. The amplification specificity of the designed primers were verified from melt curve analysis.

Table 2.7: List of primers used for gene expression analysis at mRNA level

SN	Purpose	Sequence (5′-3′)	NCBI Seq. Acc. No.	Chapter
1	ATP1B1 mRNA expression analysis	F: CCCAGTGAACCGAAAGAACGA R: TGAACGGGAAGGACATTTGG	NM_001677.4	4
2	CASP8AP2 mRNA expression analysis	F: GCAGGTGGTGACTCTAAAAGG R:GAGGAGAAGCAGAAAAGACAT CAA	NM_012115.4	5

F: Forward, **R:** Reverse

2.15 Immunofluorescence:

The corneal endothelial buttons were collected in RNAlater and maintained at 4°C. They were washed thrice for 5 minutes in 1X PBS to get rid of any residual storage medium and fixed for 20 minutes in freshly made 4% paraformaldehyde (158127, Sigma-Aldrich, USA). Three

washes were done for 5 minutes each with 1X PBS, followed by PBST (1X PBS + 0.5% Triton-X) washes for 15 minutes each, twice. The blocking solution (BS) was made in PBST with 10% normal horse serum (NHS) (31874, Invitrogen, USA) and the tissue samples were placed in BS for one hour. The primary antibody solutions were then applied to the tissues in BS, held at RT for one hour, followed by 8 hours incubation at 4°C. The tissue samples were washed off to remove unbound primary antibodies with PBST washes followed by incubation with respective secondary antibodies for 2 hours at RT. After washing off the excess secondary antibodies sequentially with PBST and PBS, tissue samples were counter-stained for 10 minutes with 2.5 µg/ml of 4′, 6-diamidino-2-phenylindole (DAPI) (D9542, Sigma-Aldrich, USA) and then washed with 1X PBS again to remove excess DAPI. Subsequently, the tissue samples were placed on a slide that held the endothelial side up (convex side up) and an 20 µl mounting medium (Floromount-G, Southern Biotech, USA) was added before the coverslip was placed. The slides were kept at RT for 12-16 hours and then the prepared slides were checked under Leica SP8 DLS Confocal Microscope (Leica, Germany).

2.16 Electrophoretic Mobility Shift Assay (EMSA):

2.16.1 Oligomer designing and annealing:

20-22-mer oligonucleotides, encompassing the region of interest were designed; both with and without 5′-end biotin labelling [Integrated DNA Technologies (IDT), USA]. Oligomer's sequences are listed in **Table 2.8**. Complementary oligomers were re-dissolved in NEB Buffer 3 and annealed by incubating them at 95°C for 5 minutes, followed by step-cooling to room temperature and storage at -20°C until further use.

Table 2.8: Oligos required for EMSA

SN	oligo	Sequence (5′-3′)
1	rs3768617 (G) labeled/unlabeled	S: GCTCCAATCTCAACATGAAAG AS: CTTTCATGTTGAGATTGGAGC
2	rs3768617 (A) labeled/unlabeled	S: GCTCCAATCTTAACATCAAAG AS: CTTTCATGTTAAGATTGGAGC
3	SP1.1 labeled/unlabeled	S: CACTCAGTCCCGCCTCCATAC AS: GTATGGAGGCGGGACTGAGTG
4	SP1.1 mut labeled/unlabeled	S: CACTCAATCTAGCATCAATAC AS: GTATTGATGCTAGATTGAGTG
5	SP1.2 labeled/unlabeled	S: ACCTTACACCCCGCCCCTCTCT AS: AGAGAGGGGCGGGGTGTAAGGT
6	SP1.2 mut labeled/unlabeled	S: ACCTTAGATTCTGACTTACTCT AS: AGAGTAAGTCAGAATCTAAGGT
7	SP1.3 labeled/unlabeled	S: ATTGAAGCCCCGCCCCATCG AS: CGATGGGGCGGGGCTTCAAT
8	SP1.3 mut labeled/unlabeled	S: ATTGAAATAGCATTGCATCG AS: CGATGCAATGCTATTTCAAT
9	SP1.4 labeled/unlabeled	S: CAGGCCACGCCCCTACCTCC AS: GGAGGTAGGGGCGTGGCCTG
10	SP1.4 mut labeled/unlabeled	S: CAGATTCGGATCGTACCTCC AS: GGAGGTACGATCCGAATCTG

S: Sense, **AS:** Anti-sense

2.16.2 Nuclear extract preparation and quantification:

Nuclear protein lysate was extracted using NE-PER Nuclear and Cytoplasmic extraction reagents (Thermo Scientific, USA). In a 96-well plate, nuclear protein extracts were quantified using Bradford reagent (B6916, Sigma-Aldrich, USA) and bovine serum albumin (BSA) was used to prepare protein standards (2, 4, 8, and 16 mg/ml). Spectrophotometrically, absorbance readings were obtained using Varioskan Flash Multimode Reader (Thermo Scientific, USA) at 595 nm.

2.16.3 Binding reaction for EMSA:

DNA-protein binding reaction was performed using 20 µg of nuclear extract and 100 fmol of biotinylated annealed oligonucleotides per 20 µl total reaction volume. Competitive EMSA was performed using 200-fold excess (20 pmol) of unlabelled double-stranded oligonucleotides, added 20 minutes before the addition of labelled double-stranded oligonucleotides and it was incubated for another 20 minutes. For supershift assays, 4 µg of the antibody was incubated for an additional 15 minutes at RT with the final reaction mixture before mixing with the labelled oligos. A tabulated overview of EMSA binding reactions is mentioned in **Table 2.9**. All ingredients for binding reaction were taken from the LightShift Chemiluminescent EMSA kit (20148, ThermoFisher Scientific, USA) and the reaction was performed according to the manufacturer's instructions.

Table 2.9: Binding reactions formulation for EMSA

SN	**Components**	**Final Conc.**	**Reactions**			
			Free probe	**Probe + NE**	**Probe +NE + Unlabel excess**	**Probe + NE + Antibody**
1	Ultrapure water		11 µl	3 µl	1 µl	1 µl
2	10X Binding buffer	1X	2 µl	2 µl	2 µl	2 µl
3	50% Glycerol	2.5%	1 µl	1 µl	2 µl	1 µl
4	100mM $MgCl_2$	5 mM	1 µl	1 µl	1 µl	1 µl
5	1µg/µl Poly (dI-dC)	50 ng/µl	1 µl	1 µl	1 µl	1 µl
6	1% NP-40	0.05%	1 µl	1 µl	1 µl	1 µl
7	$ZnSO_4$	0.5 mM	1 µl	1 µl	1 µl	1 µl
8	20 pmol Unlabeled oligo	200 pmol			1µl	
9	Nuclear extract	20 µg		8 µl	8 µl	8 µl
10	100 fmol Biotin End-Labelled oligo	100 fmol	2 µl	2 µl	2 µl	2 µl
11	2 µg/µl Antibody	4 µg				2 µl
	Total Volume		20 µl	20 µl	20 µl	20 µl

2.16.4 Electrophoresis of binding reaction:

In a native polyacrylamide gel, the binding reactions were electrophoresed in the 0.5X TBE (Tris-borate EDTA) buffer. 6% or 4.5% polyacrylamide gel was prepared using 0.5X TBE. The casted gel was allowed to flush out unpolymerized polyacrylamide and any residual ammonium persulfate ions with a 60 minutes pre-run at 100 V and 100 mA. With the aid of an ice jacket, the electrophoresis tank was placed at lower temperatures (4-10°C) to minimize overheating. Post pre-run, the binding reactions were loaded onto the wells after mixing with 5 µl of 5X loading buffer. Electrophoresis was conducted at 100 V and 100 mA before the 3/4th migration of the bromophenol blue dye.

2.16.5 Electrophoretic transfer and crosslinking of binding reaction to nylon membrane:

Transfer of the electrophoretic separated DNA-protein complexes from gel to 0.45 µm positively charged biodyne membrane was completed using the mini trans-blot electrophoretic transfer cell (Bio-Rad, USA) for 35 minutes at 380 mA (~100 V). Post-wet-transfer, DNA: protein complexes on the nylon membrane were exposed to UV-light (254 nm, power = 120 mJ/cm^2) for 60 seconds using a UVC 500-crosslinker (Amersham Biosciences, USA). The crosslinked membrane was stored in RT until further use.

2.16.6 Chemiluminescent detection of biotin labelled DNA complexes:

The biodyne membrane was first blocked in 1X blocking buffer and then the crosslinked biotin labelled DNA complexes were conjugated with stabilized streptavidin horseradish peroxidase (HRP), diluted in 1:300 with blocking Buffer (89880, Chemiluminescent nucleic acid detection module Kit , Thermo Scientific, USA). Following this, the membrane was washed 5 times in

1X wash buffer with gentle shaking for 5 minutes each. The membrane was then submerged into the substrate equilibration buffer for 15 minutes. A substrate working solution was prepared by combining a 1:1 amount of luminol and stable peroxide solution and the membrane was filled with this mixture for 5 minutes without shaking. After removing the excess substrate working solution, it was wrapped in the plastic sheet and exposed to high sensitivity chemiluminescent detector (Fusion Solo S Chemi-Doc, Vilber Lourmat, Germany) for visualization.

2.17 Western blotting:

Proteins were extracted from the cells by the use of Radioimmunoprecipitation assay (RIPA) buffer. Briefly, the cell pellet was washed in 1X phosphate buffer solution 2-3 times to remove the cell culture media and after that required amount of ice-cold RIPA buffer was mixed with the cell pellet to homogenize it. It was then incubated on ice for 10 minutes. The cell suspension was then vortexed 5-7 times to break the membrane and solubilize the proteins. Then the cell lysate was sonicated three times for 5 seconds each with a minimum of 2 minutes rest on ice between each pulse. If the lysate was still viscous, then the sonication was again repeated. The sonicated lysate was then incubated for an additional 20 minutes on ice and then centrifuged at 13,000 rpm for 10 minutes at 4°C. The supernatant was aliquoted into new microcentrifuge tubes. Protein concentration was measured using the Pierce BCA protein assay kit (23225, Thermo Fisher Scientific, USA). An equal volume of 2X Laemmli buffer was added to the required amount of protein solution, the cell lysate was boiled in the sample buffer at 95°C for 10 minutes to denature the proteins. The denatured sample was cooled down and loaded into the wells of SDS-PAGE gel along with the molecular marker. The gel was run at 50 V for 2-3 hours. Once electrophoresis was completed, the separated proteins were transferred from the gel into the activated polyvinylidene fluoride (PVDF) membrane (IPVH00010, Merck, USA)

using a semi-dry transfer system (Bio-Rad, USA) at 15 volt for 40 minutes in 1X transfer buffer. If the molecular weight of the required protein was > 150 kDa, we used the wet transfer blotting system at 30 volt for 12 hours in 1X wet transfer buffer. After the transfer was completed, the membrane was placed in the 5% skim milk (GRM1254, Himedia, India) solution for 1 hour to block nonspecific binding. Next, the membrane was incubated in appropriate dilution of primary antibody in blocking buffer overnight at 4°C. The next day, the membrane was washed in TBST three times, each for 10 minutes. It was incubated in horseradish peroxidase (HRP) conjugated secondary antibody solution according to the host of the primary antibody for 1 hour at room temperature. Thereafter, the membrane was washed three times 5 minutes each in TBST. For signal development, we preferred SuperSignal West Femto Maximum Sensitivity Substrate (34094, Thermo Scientific, USA) according to the manufacturer's instructions. Images were captured using Fusion Solo S Chemi-Doc (Vilber Lourmat) and Evolution Capt software was used for densitometry analysis. Expression levels of the target proteins were quantified relative to their endogenous control (GAPDH). The constituents of the required buffers are explained in **Table 2.10**. The list of the primary and secondary antibodies used for the immunoblotting is presented in **Table 2.11**.

Table 2.10: Composition of the buffers essential for protein extraction and western blot

SN	Buffer	Composition
1	RIPA buffer	50 mM Tris-HCl (pH 8.0), 150 mM NaCl, 1% Nonidet P-40 (NP-40) , 0.5% Sodium deoxycholate, 0.1% Sodium dodecyl sulphate (SDS)
2	2X Laemmli Buffer	4% SDS, 10% 2-mercaptoethanol, 20% Glycerol, 0.004% Bromophenol blue, 0.125 M Tris-HCl
3	Running buffer	25 mM Tris, 190 mM Glycine, 0.1% SDS
4	Semi-dry transfer buffer	48 mM Tris-base, 39 mM Glycine, 20% Methanol
5	Wet transfer buffer	25 mM Tris, 190 mM Glycine, 20% Methanol
6	TBST buffer	20 mM Tris, 150 mM NaCl, 0.1% Tween 20
7	Blocking buffer	5% Skim milk in TBST

Table 2.11: List of primary and secondary antibodies

SN	Antibody Name	Type	Host	Source (Catalogue No.)	Dilution
1	Anti-SP1	Primary	Rabbit	Merck (07-645)	1:500
2	Anti-GAPDH	Primary	Mouse	Santa Cruz Biotechnology (sc-365062)	1:1000
3	Anti-CASP8AP2	Primary	Rabbit	Abcam (ab8420)	1:500
4	Goat anti-rabbit IgG-HRP	Secondary	Goat	Geneilabs (HPO3)	1:5000
5	Goat anti-mouse IgG-HRP	Secondary	Goat	Geneilabs (HPO6)	1:5000

2.18 Site-directed Mutagenesis:

Site-directed mutagenesis was performed according to the Inverse PCR approach. In this method, the complete circular plasmid is amplified, and a sequence is deleted, altered, or introduced. On the two opposing DNA strands, the primers are placed end-to-end, in the outside direction. One or both may carry mismatches to induce the required changes and both primers may have phosphorylated 5' ends or a restriction site for further recircularization. The PCR DNA polymerase must have a high degree of fidelity and leave blunt ends for final ligation. After finishing the PCR, the plasmid DNA is gel eluted, the phosphorylated ends are ligated, and the recircularized plasmid is transformed into bacteria. Mutagenesis primers were designed using the NEBaseChanger version 1.3.3 (https://nebasechanger.neb.com/) online designer software. The primers should have minimum non-specific binding sites on the pGL3 basic vector (E1751, Promega, USA) and a very low probability of secondary structure formation. We checked all the criteria of the primers using the IDT OligoAnalyzer tool (https://www.idtdna.com/pages/tools/oligoanalyzer) and picked up the best pair of primers for all mutagenesis reactions. The full length pGL3 plasmid having -381/+68 region of *CASP8AP2* promoter was then amplified using Phusion High-Fidelity DNA polymerase (M0530S, New

England BioLabs, UK) to generate full length, complete, linear mutated plasmid. The primer sequences **(Table 2.12)**, reaction components of the PCR **(Table 2.13),** and the thermocycling conditions **(Table 2.14)** are mentioned below.

Table 2.12: Primers needed for site-directed mutagenesis

SN	Purpose	Sequence (5′-3′)	Ta
1	SP1.1 SDM1	F:CATCAATACCCTGATAGCGCTCTG R:CTAGATTGAGTGCCTACGGCCAAT	65°C
2	SP1.2 SDM2	F:GACTTACTCTCTTAAAGCCCTAGGAAGATTACTG R:AGAATCTAAGGTGGCGGGGAAGGC	68°C
3	SP1.3 SDM3	F:TTGCATCGCCTTCCCCGCCACCTTAC R:TGCTATTTCAATAGGAAGGGGCTGACC	65°C
4	SP1.4 SDM4	F:ATCGTACCTCCACTCAGGTCAGC R:CCGAATCTGAGAGAAGCTTTTTAGTGAAAGAC	62°C

F: Forward, **R:** Reverse, **Ta:** Annealing temperature

Table 2.13: Reaction components and their final concentrations in Phusion PCR

SN	Component	20 µl Reaction	Final concentration
1	Nuclease free water	10.8 µl	
2	5X HF buffer	4 µl	1X
3	10 mM dNTPs	0.4 µl	200 µM
4	10 µM forward primer	1 µl	0.5 µM
5	10 µM reverse primer	1 µl	0.5 µM
6	Template DNA	2 µl	100 ng
7	DMSO	0.6 µl	3%
8	Phusion polymerase	0.2 µl	0.5 units

Table 2.14: Thermocycling conditions for a Phusion PCR

SN	Steps	Cycle	Temperature	Time
1	Initial denaturation	1	98°C	30 seconds
2	Denaturation Annealing Extension	35	98°C Annealing temperature (Ta) 72°C	10 seconds 20 seconds 3 minutes
3	Final extension	1	72°C	10 minutes
4	Hold	1	4°C	∞

The amplified product was then run in 0.7% agarose gel and the specific DNA band was cut from the gel and purified through MinElute Gel Extraction kit (Qiagen, Germany). Next, the purified product was phosphorylated using T4 Polynucleotide Kinase (M0201S, New England BioLabs, UK) at 37°C for 40 minutes. The components of the reaction are discussed in **Table 2.15** below.

Table 2.15: Reaction components for T4 PNK phosphorylated reaction

SN	Reagent	Quantity	Final concentration
1	Eluted PCR product	13 µl	
2	10X T4 PNK buffer	2 µl	1X
3	10 mM ATP	4 µl	2 mM
4	T4 PNK	1 µl	10 units
5	Total	20 µl	

After phosphorylation, we used the Quick Ligation kit (M2200S, New England BioLabs, UK) to ligate the phosphorylated linear product at 25°C for 10 minutes. The materials used for this reaction are the following **(Table 2.16)**.

Table 2.16: Reaction components for Quick ligation reaction

SN	Component	Quantity	Final concentration
1	Phosphorylated product	3 µl	
2	2X Quick ligase reaction buffer	5 µl	1X
3	Quick ligase	1 µl	10 units
4	10 mM ATP	1 µl	1 mM
	Total	10 µl	

One (1.0) µl of DpnI restriction enzyme (R0176S, New England BioLabs, UK) was added to the reaction mixture and incubated at 37°C for 2 hours to remove wild-type plasmid DNA. The

DpnI digested product was combined with 50 µl of E.coli competent cells and incubated on wet ice for 30 minutes. Then the mixture was placed in a 42°C water bath for 30 seconds and immediately returned to the ice for 5 minutes. 1 ml Luria Bertani (LB) broth (Himedia, India) was added to the mixture and placed in a shaking incubator at 37°C for 1 hour. The cells were centrifuged at 5000 rpm for 5 minutes. The excess LB broth was discarded and cells were suspended in 200 µl of remaining LB. Cells were plated on an LB agar (M1151, Himedia, India) plate and incubated at 37°C overnight. After 12 hours, colonies appeared and 10-15 colonies were transferred individually to 4 ml LB broths containing ampicillin (CMS645, Himedia, India). The colonies were allowed to grow at 37°C overnight. The next day, plasmids were isolated from the individual tubes using QIAprep Spin Miniprep Kit (Qiagen, Germany) and they were sequenced using vector specific RVprimer3 (5′ CTAGCAAAATAGGCTGTCCC 3′) for verification.

2.19 Deletional plasmid construction:

Six PCR primer pairs were designed by applying Primer Blast to chop the entire 5′ flanking region of *CASP8AP2* (-1336/+68), and the quality of the primers was checked through the OligoAnalyzer tool (Integrated DNA Technologies USA). All the deletional fragments (-181/+68, -381/+68, -573/+68, -841/+68, -1156/+68, and -1336/+68) have the same reverse primer but their forward primers are different. They were PCR amplified with their respective primer sets, having Kpn1 and Nhe1 restriction sites in forward and reverse primers respectively, by Phusion DNA Polymerase (New England Biolabs, USA) according to the manufacturer's instructions. The amplified products were first electrophoresed in agarose gel and then gel purified using Qiagen Mini elute purification kit (Qiagen, Germany). Subsequently, the eluted products were then digested by the respective enzymes and gel purified again by MinElute Gel extraction kit (Qiagen, Germany). The pGL3 basic vector

(Promega, USA) was also digested using the same enzymes, purified, and concentrated for the ligation reaction. The PCR amplified digested products were then ligated with digested pGL3 basic luciferase vector using Quick ligation kit (M2200S, New England BioLabs, UK). The ligated products were transformed into the competent E.coli DH5-alpha competent cells by the heat shock method. Positive colonies were screened by colony PCR-based method and finally verified by Sanger sequencing. The overall cloning procedure is described below in **Fig. 2.1.** The primers specified for the cloning and sequence verification are mentioned in **Table 2.17**.

Table 2.17: Primers necessary for cloning and screening of the overlapping segments of *CASP8AP2* promoter

SN	Purpose	Sequence (5′-3′)	Ta
1	-181/+68 cloning	F:CTTGAGGGTACCGCCCCTCTCTCTTAAAGCC R:ATTAAAGCTAGCCAACTTACCCGCCCTG	65°C
2	-381/+68 cloning	F: CTTGAGGGTACCTCGTAATCGAGCCCA R: ATTAAAGCTAGCCAACTTACCCGCCCTG	60°C
3	-573/+68 cloning	F: CTTGAGGGTACCTAGACCTACCGGCAC R: ATTAAAGCTAGCCAACTTACCCGCCCTG	62°C
4	-841/+68 cloning	F: TAAATAGGTACCCGCTCGCGTCTATGGT R: ATTAAAGCTAGCCAACTTACCCGCCCTG	60°C
5	-1156/+68 cloning	F: CTTGAGGGTACCGCGTGGGTGGCTCAC R: ATTAAAGCTAGCCAACTTACCCGCCCTG	65°C
6	-1336/+68 cloning	F: GAAAGGGGTACCGGTTGATATGGCAGTTAAGAC R: ATTAAAGCTAGCCAACTTACCCGCCCTG	61°C
7	RV Primer 3 (for sequencing)	CTAGCAAAATAGGCTGTCCC	
8	GL Primer 2 (for sequencing)	CTTTATGTTTTTGGCGTCTTCCA	

F: Forward, **R:** Reverse, **Ta:** Annealing temperature

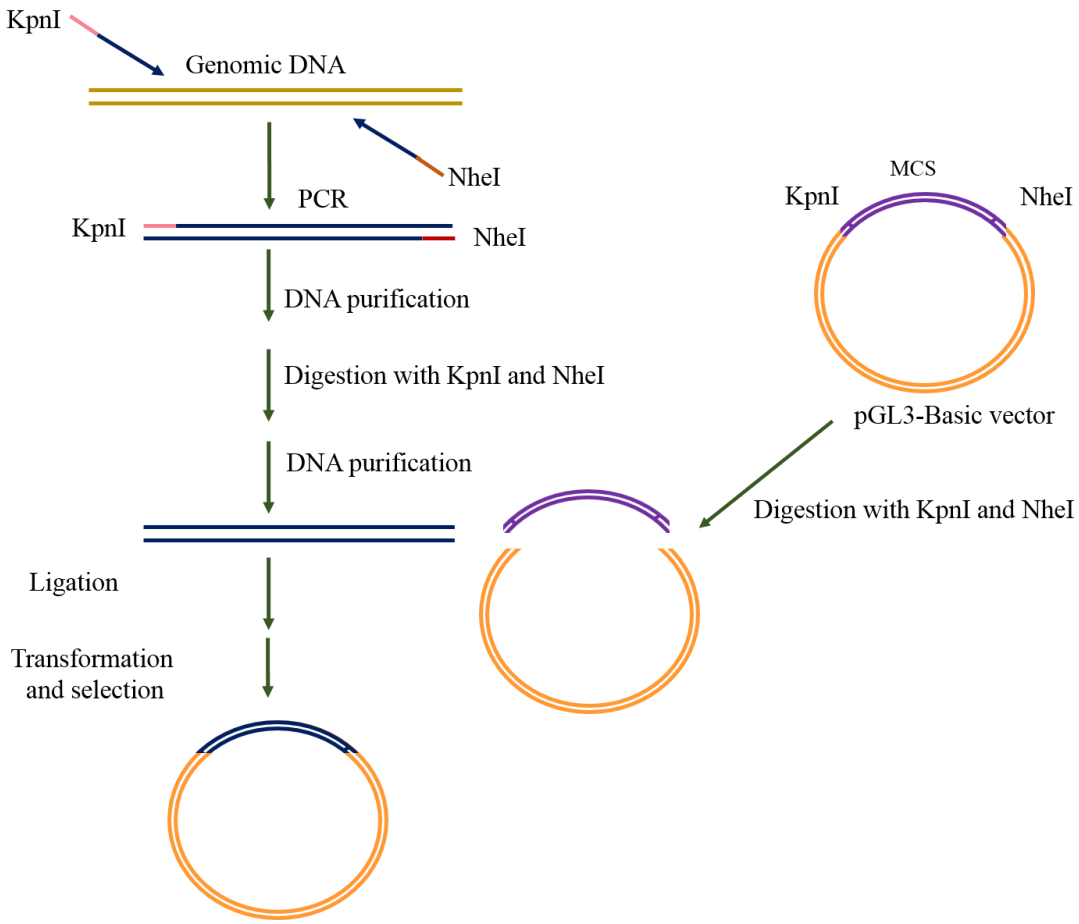

Fig. 2.1: An overall cloning method to prepare different deletional constructs required for luciferase assay.

2.20 Chromatin Immunoprecipitation:

Chromatin Immunoprecipitation (ChIP) was performed using EZ-Magna ChIP A/G (17-10085, Millipore, USA). HEK-293 cells were seeded in a T-75 flask and the experiment was carried out two days after the initial seeding. On the day of the immunoprecipitation assay, the flask should be at least in the 70% confluency stage. Cells were crosslinked by adding 1.0% methanol-free formaldehyde (28906, Thermo Scientific, USA) for 10 minutes at 25°C. The crosslinking reaction was terminated by the presence of glycine solution (56-40-6, Invitrogen, USA) to a final concentration of 250 mM and the flask was allowed to continue rocking for 10 minutes at 25°C. Then, it was washed five times with ice-cold phosphate buffer solution

(Himedia, India) to remove the unreacted formaldehyde and glycine solution. Cells were scrapped into 4 ml of 1X PBS with protease inhibitor cocktail (Roche, USA) and collected in a 15 ml conical tube. Next, the cells were pelleted down by centrifugation at 5000g for 5 minutes. The supernatant was discarded and the pellet was homogenized in 2 ml of cytosolic lysis buffer with protease inhibitor cocktail and incubated on ice for 20 minutes. The efficiency of cell lysis was checked by the trypan blue method. After the incubation, the nuclei were pelleted down by centrifugation at 15,000g for 10 minutes. Thereafter, the pelleted nuclei were resuspended in nuclear lysis buffer with protease inhibitor cocktail and vortexed for 4-6 times. Next, the chromatin was sonicated using a probe sonicator (Qsonica, USA) to an average length of 200-700bp with a 10 seconds ON and 1 minute OFF sonication cycle for 10 minutes. The sonicated DNA was centrifuged at 13,000 rpm for 15 minutes at 4°C to remove the debris and long chromatins. The supernatant was transferred to a new tube and it was diluted 10 fold in ChIP dilution buffer. After this, the sample was precleared with 50 µl of protein A/G agarose beads for 2 hours at 4°C on a rocking platform. Soon after pre-clearing, the beads were pelleted down by centrifugation at 3,000g for 1 minute at 4°C and the supernatant was distributed into individual tubes. 1.0% of the total supernatant was saved and it was used later as input control. In one tube, 4 µg of GFI1B antibody (sc-28356X, Santa Cruz Biotechnology, USA) was added and placed the tube on a rotating mixture at 4°C for overnight to form antigen-antibody complex. As a negative control, normal mouse IgG [5415, Cell Signalling Technology (CST), USA] was added to another tube and this tube was also placed the rotating mixture. The next day, 20 µl of protein A/G mixture was introduced to each tube and the tubes were allowed to rotate at 4°C for 2 hours to collect the antigen-antibody complexes. The beads were pelleted down by brief centrifugation (3000g for 1 minute) and the supernatant fraction was discarded. Beads were then washed sequentially on a rotating platform for 5 minutes each with 1 ml of low salt, high salt, LiCl, and TE buffer. The immune complexes were eluted by adding 250 µl

of elution buffer to each tube with an incubation of 65°C for 30 minutes. 8 µl of 5 M NaCl was added to all the tubes (IPs and input) and placed on a thermomixture at 65°C for 12 hours to reverse the DNA-Protein crosslinks. 8 µl of 1 M Tris-HCl, 4 µl of 0.5 M EDTA, and 1 µl Proteinase K were added to all the tubes and incubated at 50°C for 2 hours. All the DNA samples were then purified using QIAquick PCR purification kit (28104, Qiagen, Germany). The relative enrichment of the specific segment was quantified using the real-time quantitative PCR method and data was normalized using percentage of input method. The compositions of all the buffers are mentioned in **Table 2.18** below. Sequences of the primers used for ChIP-qPCR are mentioned in **Table 2.19**.

Table 2.18: List of buffers and their compositions, needed for ChIP assay

SN	Buffer	Composition
1	Cytosolic lysis buffer	5 mM PIPES (pH 8.0), 85 mM KCl, 0.5% NP-40
2	Nuclear lysis buffer	1% SDS, 10 mM EDTA, 50 mM Tris (pH 8.1)
3	ChIP dilution buffer	0.01% SDS, 1.1% Triton X-100, 1.2 mM EDTA, 16.7 mM Tris-HCl (pH 8.1), 167 mM NaCl.
4	Low salt immune complex wash buffer	0.1% SDS, 1% Triton X-100, 2 mM EDTA, 20 mM Tris-HCl (pH 8.1), 150 mM NaCl
5	High salt immune complex wash buffer	0.1% SDS, 1% Triton X-100, 2 mM EDTA, 20 mM Tris-HCl (pH 8.1), 500 mM NaCl
6	LiCl immune complex wash buffer	0.25 M LiCl, 1% IGEPAL-CA630, 1% Deoxycholic acid (sodium salt), 1 mM EDTA, 10 mM Tris (pH 8.1)
7	TE buffer	10 mM Tris-HCl, 1 mM EDTA (pH 8.0)
8	ChIP elution buffer	100 mM $NaHCO_3$, 1% SDS

Table 2.19: Sequence of the primers used for ChIP-qPCR

SN	Purpose	Sequence (5′-3′)	Chapter
1	rs3768617 ChIP	F: GTTATCTCTCACCTGGGATTG R: CATTTTGAAAGGACCATTTTGGC	3

F: Forward, **R:** Reverse

2.21 Knockdown studies:

HEK-293 cells were seeded in 6 well plate and transfection was performed the next day after ensuring that the cells were growing logarithmically and wells were filled with 60 - 70% confluent cells. First, the growth medium was replaced with Opti-MEM I low serum transfection medium. Two master mix were prepared. In the first, 125 µl of Opti-MEM I medium was aliquoted and 2 µg of pLKO.5 plasmid containing SP1shRNA (TRCN0000285149, Sigma-Aldrich) was added and mixed well. Subsequent to that, 4 µl of P3000 reagent (2 µl/µg of DNA) was supplied to the mixture and combined properly. In the second master mix, 125 µl of Opti-MEM I was taken and 3.75 µl of lipofectamine 3000 was added and mixed well. The mixture was incubated at RT for 6 minutes. Then this second master mix was combined with the first one and mixed very well. The final mixture was incubated for 30 minutes at RT. It was then dispensed to the cells in a dropwise fashion. The transfection medium was changed after 6 hours and the cells were pelleted down 48 hours after the transfection. A nontargeted scramble shRNA (1864, Addgene) was considered as the negative control for the experiment. Western blotting was performed to check the knockdown efficiency.

2.22 Overexpression studies:

Overexpression of the desired protein was performed in HEK-293 cells. First, cells were seeded in a 6-well plate. Transfection was initiated in the next day with 60 - 70% confluent cells. Opti-MEMI reduced serum transfection medium was used for transfection in place of the growth media. There were two master mixes made for the transfection. In the first, 125 µl of Opti-MEM I and 2 µg of pcDNA3.1-CASP8AP2 plasmid were taken and thoroughly mixed. Following that, 4 µl of P3000 reagent (2 µl/µg of DNA) was added to the mixture and mixed

gently. In the second master mix, 125 µl of Opti-MEM I was added to 3.75 µl of lipofectamine 3000 and it was completely mixed. This mixture was incubated at RT for 6 minutes. The second master mix was then blended with the first and mixed perfectly. At room temperature, the resulting combination was incubated for 30 minutes. It was then dropped into the cells. After 6 hours, the transfection medium was changed, and the cells were collected 48 hours after the transfection. The empty pcDNA3.1 vector was preferred as the negative control.

2.23 Statistical analysis:

SPSS 28.0 statistics software for Windows was applied to calculate all of the statistical analysis (IBM SPSS, Inc., Chicago, IL, USA). Both the control and patient samples were selected following a student's t-test to avoid any type of experimental biasness due to the confounding factors age and sex. Pearson's χ^2 test was performed to calculate the significance of allelic and genotypic frequency difference between two experimental groups and Haploview 4.2 (Broad Institute, Cambridge, MA, USA) software was used to conduct the 10,000 permutation test of genetic association. Haplotype association and linkage disequilibrium (LD) plot preparation was accomplished by Haploview 4.2. Based on the idea of three different genetic models- Dominant (DOM), Recessive (REC), and Additive (ADD), the genotypic association and relative risk was computed. Online Sample Size Estimator [OSSE (http://osse.bii.a-star.edu.sg/)] tool was implemented to calculate the statistical power. $P < 0.05$ was considered as statistical significant.

CHAPTER 3

Genetic and functional association of LAMC1 with FECD

3.0 Genetic and functional association of *LAMC1* with FECD

3.1 Introduction:

Fuchs endothelial corneal dystrophy (FECD) affects all the layers of the cornea but the primary site of the disease is the innermost portion of the cornea, the endothelium.[2] The major histological characteristics of FECD include moderate to marked thickening of Descemet's membrane (DM) due to increased accumulation of abnormal extracellular matrix proteins, and the presence of spindle shaped corneal warts associated with the stiffening of the DM.[170–172] Initially it begins within the central membrane and eventually spreads towards the edge.[3] The accumulation of numerous vacuoles inside the cells with the fragmented plasma membrane and the loss of intercellular junctions causes endothelial cells to degenerate, reducing the endothelial pump's capacity to keep the cornea in its usual dehydrated state.[173] The effects are differences in endothelial cell shape, also known as polymagethism and pleomorphism, stromal and epithelial hydration, and corneal edema which causes corneal deformation and loss of vision.[4,174] Based on the population's ethnicity, the disease prevalence ranges from 1.9% to 11.0%. In the United States, around 3.9 – 6.6% of the population over the age of 40 is affected.[175,176] The isolated population of 500 people at Tangier island in the USA, has a higher risk of FECD (21.6%), with a minimum frequency of 11.0 % among those over the age of 50.[28] In Iceland, a major population-based research of Caucasians found that 9.2% of the population over the age of 50 had FECD.[121] Based on the prevalence of corneal guttata in FECD patients, the predominance rate of 3.7% was found in Japan and the frequency of FECD in over the age of 50 was determined to be 6.6% of the Chinese Singaporeans population.[31] Another study reported that 1.9% of total bullous keratopathy (BK) was performed only for Fuchs dystrophy patients between 1999 and 2001 in Japan.[177] In a population-based investigation on the Japanese island of Kumejima, 124 out of 3060 eligible individuals (4.1%) had cornea guttata in at least one eye.[178] The population specific prevalence study is yet to be done in the Indian

population. However, based on the total penetrating keratoplasty performed, approximately 16.6% was only for the FECD cases between January 1995 to March 2001 at a tertiary eye care center in South India.[179] In another study, the total endothelial keratoplasty performed over a period of five years (2007 – 2011) at LV Prasad Eye Institute (LVPEI), Hyderabad in India were 7.5% to 10.4% for FECD affected patients.[180]

Female predominance is reported for all the populations where studies are undertaken to date.

In Texas, USA previous research has identified a notable female majority of FECD at a ratio of 3:1.[175] Subsequently, other studies in the North American population proved the female predominance ranging from 2.5:1 to 3.5:1.[31,121,181] In a multicentre study with 2044 Caucasians, the female sex advanced the probability of FECD by 34%.[182] Corneal transplantation was most commonly carried out for Fuchs dystrophy at Kensington Eye Institute (KEI) throughout for two year studies (2014-2016) and more females were treated in comparison to the male (1.6:1).[183] In a study with 465 Chinese Singaporean and 299 Japanese, corneal guttata was detected at a 2.4:1 (female: male) ratio in the case of Singaporeans and 4.5:1 (female: male) in the case of Japanese.[31] In the southwestern island of Japan, the prevalence of corneal guttata was significantly different between men and women (2.4% versus 5.8%).[30] At Ramathibodi Hospital, Bangkok, Thailand, 81.91% female predominance of FECD was observed between 2007 to 2019.[184] In India, though prevalence studies are lacking, based on the recruited FECD patients in hospital based study, females were noticed more prone to disease in comparison to males at a 1.5:1 ratio.[34]

The first genome-wide association study (GWAS) found risk allele 'G' of rs613872 in the third intron of transcription factor 4 (*TCF4*) on chromosome 18 to be highly associated with FECD in the Caucasian population.[20] The subsequent GWAS study, performed in European ancestry

in 2017 identified a significant association of rs79742895 within the intronic region of *KANK4* gene, rs1022114 residing in the intergenic region between *LINC00970* and the *ATP1B1* gene; and rs3768617 located in the intronic region of *LAMC1* with FECD. They also replicated the previously associated single nucleotide polymorphisms (SNPs) already seen in the *TCF4* gene.[64] Also, a significant linkage disequilibrium (r^2=0.88) was found between rs784257 and earlier published variant rs613872, in the third intron of *TCF4*. Transcriptomic profiling showed that although there are positive expressions of TCF4, ATP1B1, and LAMC1 in corneal endothelium, yet there was no positive expression of the lncRNA LINC00970 has in the endothelium. On the other hand, KANK4 displayed minimal cytoplasmic expression.

Although a link between SNP rs3768617 in 1q25.3 of *LAMC1* and FECD has been shown in the Caucasian population, these finding needs to be confirmed in other populations. Because of the considerable dissimilarities in genetic background and environmental factors between Caucasian and Indian cohorts, genetic markers for FECD should also be explored in the Indian population. In addition, the functional significance of this variant and its role in disease progression is yet to be known. With these gaps in various studies, we aimed at checking for the genetic and functional association of rs3768617 in *LAMC1* with FECD in the Indian population

3.2 Materials and Methods:

Detailed information of all the methodologies are discussed in chapter 2. These includes sample collection, DNA extraction, primer designing, PCR amplification, Sanger sequencing, cell culture, *in silico* analysis, ultracompetent bacterial cell preparation, luciferase reporter assay, EMSA, ChIP, and immunofluorescence. The reverse primer was used for the sequencing PCR of rs3768617 and the data obtained from the Sanger sequencing was categorized as AA, AG

and GG genotypes as mentioned in our published paper. But, in this chapter, we used the standard NCBI nomenclature and have reported the genotypes as CC, CT and TT.

3.3 Results:

3.3.1 rs3768617 residing in the intronic region of *LAMC1* is genetically associated with FECD in the Indian population:

One hundred and twenty (120) FECD affected patients and three hundred and fifty- six (356) controls were recruited for this study after a detailed assessment via Specular Microscopy. The average age of the FECD patients was 60.15 ± 9.1 years; while it was found to be 61.24 ± 7.6 years in the case of control subjects **(Table 3.1)**. Statistical analysis demonstrated that there was no notable age variation between these two comparable groups indicating that the findings of this study were not affected by the influence of uneven age distribution. The male to female ratio of both the groups was 1:2 which also avoided sex biasness. The demographic data is presented below.

Table 3.1: Demographics of samples, used for rs3768617 analysis

Group	Sample size	Mean age ± SD (years)	P value	Gender		P value
				Male	Female	
Control	356	61.24 ± 7.6	0.24	118	238	0.97
Case	120	60.15 ± 9.1		40	80	

Genetic association between the rs3768617 and FECD was tested by comparing the frequency difference of the alleles between controls and cases. The prevalence of allele 'C' was much higher in FECD cases, identifying it as the risk allele for our population. χ^2 test indicated that SNP rs3768617 was significantly associated with FECD with a P value of 2.65×10^{-8} **(Table 3.2)**. Even after performing 10,000 permutation tests the significance of the association remained almost the same ($P = 2.65 \times 10^{-8}$), signifying the potency of the risk allele 'C' for

advancing the disease. The risk of FECD was 2.73 times higher in 'C' allele carriers at rs3768617 than in 'T' allele carriers. The penetrance of the disease, associated with a particular genotype in the population was calculated under different genotypic models of inheritance. We concluded that the 'C' allele of rs3768617 significantly increased the risk of FECD in all the genotypic association models, dominant (P = 0.01, OR = 2.55), recessive (P = 2.99×10^{-8}, OR = 3.43) and the additive (P = 1.95×10^{-4}, OR = 3.86). Based on sample size, allele frequency, and 5.0% desired significance level the statistical power of this association study is 98.3%.

Table 3.2: Allelic and Genotypic association of *LAMC1* rs3768617 with FECD in Indian population

SNP rs3768617	**Type**	**Control Count (freq.)**	**FECD Count (freq.)**	**Model**	χ^2	**P value**	**OR (95%CI)**
Allele	T **C**	266(0.37) 446(0.63)	43 (0.18) 197 (0.82)		30.95	**2.65×10^{-8}** **2.65×10^{-8}***	2.73 (1.90-3.93)
Genotype	TT CT CC	61 (0.17) 144(0.41) 15(0.42)	9(0.08) 25(0.21) 86(0.71)	DOM REC ADD	6.64 30.72 0.15 13.88	**0.01** **2.99×10^{-8}** 0.70 **1.95×10^{-4}**	2.55 (1.22-5.31) 3.43 (2.19–5.38) 1.18 (0.52–2.67) 3.86 (1.83-8.16)

Statistical test = χ^2 (df1), **freq.** = frequency, * = 10,000 permutation test

Since there is a higher prevalence of FECD in females than in males in the Indian population, we segregated the data into specific gender and the genetic association of rs3768617 with FECD was separately checked for each one. In the female group, we noticed significant genetic association in allelic level (P = 3.31×10^{-7}) with an odds ratio of 3.13 **(Table 3.3)**. The 'C' allele of rs3768617 significantly increased the risk of FECD in all the genotypic association models, dominant (P = 7.00×10^{-3}, OR = 3.50), recessive (P = 1.00×10^{-6}, OR = 3.77) and

additive (P = 7.40 × 10^{-4}, OR = 5.96). The statistical power of this genetic association in the case of the female group is 97.1%.

Table 3.3: Allelic and Genotypic association of *LAMC1* rs3768617 with FECD (female only) in Indian population

SNP rs3768617	**Type**	**Control Count (freq.)**	**FECD Count (freq.)**	**Model**	**χ^2**	**P value**	**OR (95%CI)**
Allele	T **C**	185(0.39) 291(0.61)	27 (0.17) 133 (0.83)		26.06	**3.31×10^{-7}**	3.13 (1.99-4.93)
Genotype	TT CT CC	45 (0.19) 95 (0.40) 98 (0.41)	5 (0.06) 17 (0.21) 58 (0.73)	DOM REC ADD	7.24 23.51 0.79 15.70	**7.00×10^{-3}** **1.00×10^{-6}** 0.37 **7.40×10^{-4}**	3.50 (1.34-9.15) 3.77 (2.16-6.56) 1.61 (0.60-4.64) 5.96 (2.26-15.7)

Statistical test = χ^2 (df1), **freq.** = frequency

In the male group, a significant association was found between *LAMC1* rs3768617 risk allele 'C' with FECD (P = 0.02, OR = 2.09). However, we found a significant genetic association only in the recessive model (P = 6 × 10^{-3}, OR= 2.86), while there was no significant association between rs3768617 with FECD based on both dominant (P = 0.56, OR = 1.41) and additive (P = 0.21, OR = 2.11) models **(Table 3.4)** which corroborates to the fact that females are more affected than the males as if seen if many populations.[31,34,121,181,182] The statistical power of genetic association in case of male group is 40.5%.

P.T.O

Table 3.4: Allelic and Genotypic association of *LAMC1* rs3768617 with FECD (male only) in Indian population

SNP rs3768617	Type	Control Count (freq.)	FECD Count (freq.)	Model	χ^2	P value	OR (95%CI)
Allele	T	81 (0.34)	16 (0.20)		5.76	**0.02**	2.09 (1.14-3.85)
	C	155 (0.66)	64 (0.80)				
Genotype	TT	16 (0.13)	4 (0.10)	DOM	0.34	0.56	1.41 (0.44-4.50)
	CT	49 (0.42)	8 (0.20)	REC	7.52	**0.006**	2.86 (1.33-6.16)
	CC	53 (0.45)	28(0.70))	ADD	0.40	0.53	0.65 (0.17-2.46)
					1.57	0.21	2.11 (0.64-6.93)

Statistical test = χ^2 (df1), **freq.** = frequency

3.3.2 Intronic variant rs3768617 is located in a regulatory region of *LAMC1*:

Two different allele specific 100bp constructs surrounding rs3768617 were cloned in luciferase pGL4.23 vector and reporter activities were checked 24 hours after transfection. The luminometric values from the constructs and empty vector were normalized with the values from the respective co-transfected constitutive pGL4.74 [hRluc/TK] vector for each day. The average of the normalized values from the three days was then plotted as relative luciferase activity ± SEM. Significant downregulation of the luciferase activity was observed in the case of plasmids bearing the intronic regions of either rs3768617 allele 'C' (0.26 ± 0.05, $P = 4.02 \times 10^{-5}$) or allele 'T' ($0.002 \pm 2 \times 10^{-4}$, $P = 1 \times 10^{-4}$) compared to the empty pGL4.23 vector (1.0 ± 0.07), suggesting that the intronic region might have a repressor activity **(Fig. 3.1A)**. The luciferase activity of empty vector was considered as 1.0. Also, to show the difference in luciferase activity of 'T' with respect to 'C', the average luciferase activity of 'T' was plotted relative to 'C' whose activity was taken as 1.0 (**Fig. 3.1B)**. Switching of allele 'C' to 'T' also significantly downregulated the luciferase activity ($P = 0.005$).

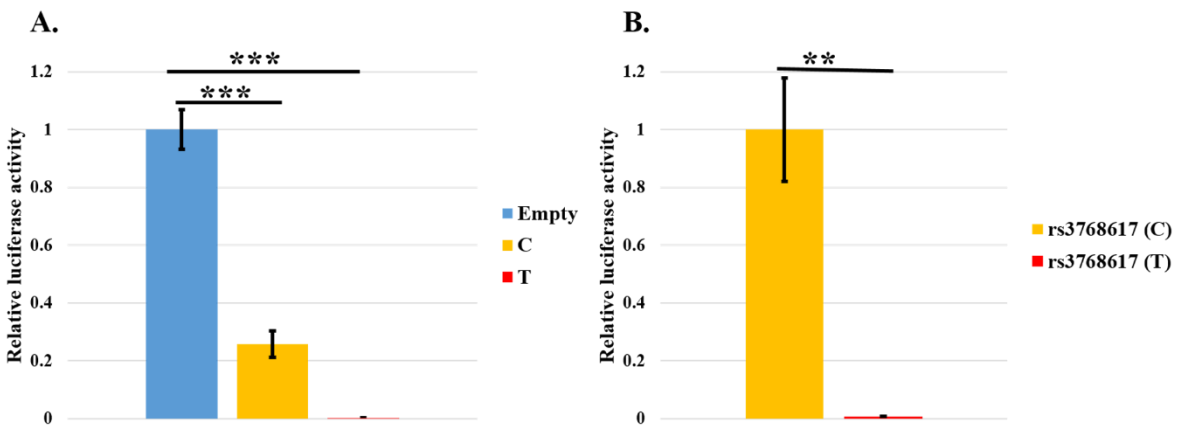

Fig. 3.1: Transcriptional regulatory activity of the genomic region encompassing rs3768617. (A) Luciferase assay was performed to verify the presence of any regulatory activity in the surrounding region of rs3768617. In comparison to the empty pGL4.23 [luc2/minP] vector, there was a significant decrease in luciferase activity in the presence of two different constructs, containing the 100bp of adjoining rs3768617 with either allele 'T' or allele 'C'. Each transfection reaction was conducted at least into three replicates in each single day experiment and the luciferase activity was normalized with co-transfected, constitutive pGL4.74 [hRluc/TK] vector luciferase activity. **(B)** rs3768617 allele specific change in the luciferase activity. Transition from allele 'C' to 'T' diminished reporter gene expression and led to a reduction in luciferase activity. The experiment was performed in triplicate and thrice on separate days and all the biological replicates values obtained is represented as mean ± SEM, relative to the empty vector. Student's t-test was implemented to evaluate the statistical significance (** $P < 0.01$ and *** $P < 0.001$).

3.3.3 Transcription factor GFI1B bind to the risk allele 'C' of rs3768617 but not with 'T' allele:

Furthermore, we checked the probability of binding of various transcription factors (TFs) to this region through the JASPAR database. Keeping the relative profile score threshold at 90%, it was found that out of three (GATA3, GATA1, GFI1B), only one transcription factor, GFI1B has a probability of binding allele 'C' but not allele 'T' of rs3768617. To know the allele specific binding of GFI1B in the intronic region of *LAMC1*, Electrophoretic Mobility Shift Assay (EMSA) assay was performed. Two different biotin labeled 20bp oligos flanking rs3768617 were designed, carrying either allele 'C' or allele 'T', and the experiment was done

using nuclear extract from the HEK-293 cell line. It was noticed that a distinguished DNA–protein complex was formed, noted as a shifted band, in the presence of biotin-labeled C probe of rs3768617 with nuclear extract of HEK-293 cell line but not in the presence of T probe indicating that the complex is specific for 'C' allele of rs3768617 but not allele 'T'. The labeled C probe-protein complex became less intense when the nuclear extract was preincubated with the unlabeled excess probe of 'C' allele **(Fig. 3.2A)**. Competitive EMSA was carried out to confirm the specificity of the shifted band and it was noticed that the formation of DNA-protein complex progressively appeared less intense due to the presence of unlabeled excess probe and it vanished in the presence of 200-fold excess unlabeled rs3768617 C probe, preincubated with nuclear extract **(Fig. 3.2B)**. To make sure that, GFI1B binds in the 'C' allele, supershift EMSA was accomplished. In the presence of the antibody, the protein is unable to bind to the oligos and as a result intensity of the specific shift decreased, reflecting that GFI1B binds to the rs3768617 probe C **(Fig. 3.2C)**. Altogether the EMSA result concluded that GFI1B binds to the 'C' allele of rs3768617 and not the 'T' allele.

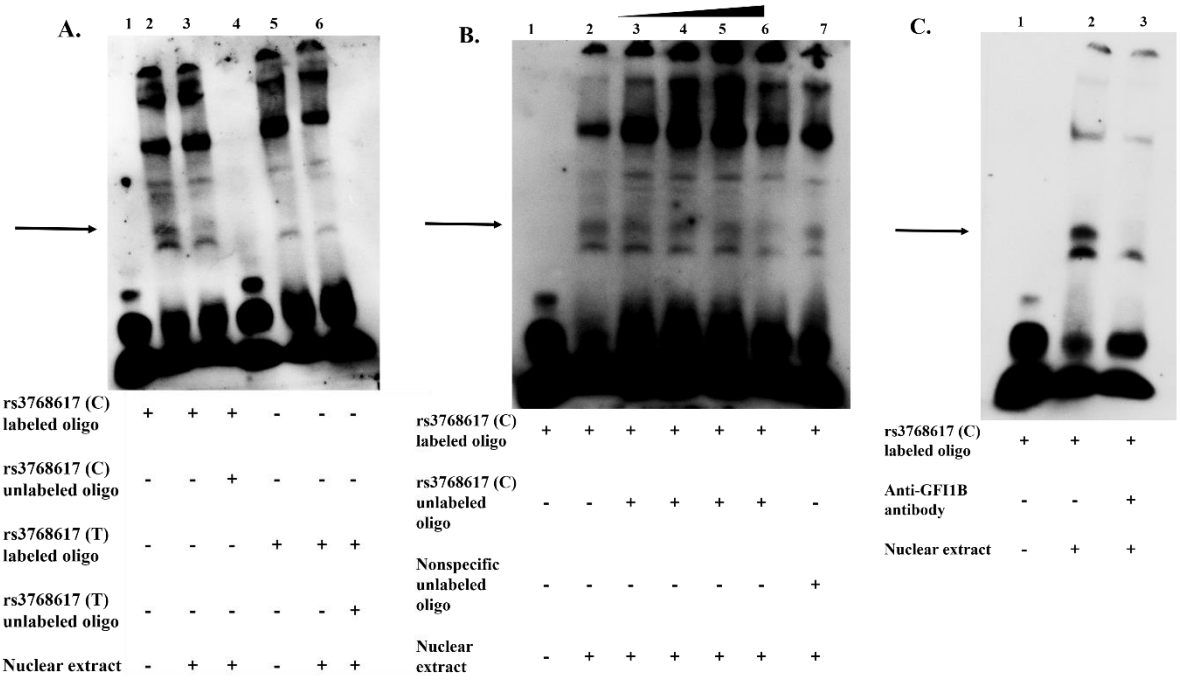

Fig. 3.2: Allele specific transcription factor binding specificity of rs3768617. (A) Electrophoretic Mobility Shift Assay (EMSA) to know the differential ability of DNA-protein complex formation of the probes, having rs3768617 allele 'C' or allele 'T'. Specific band- shift was observed (lane 2, upper band, marked with an arrow) in the presence of biotin labeled allele C probe with nuclear extract of HEK-293 cell line, which did not appear in case of labeled allele T probe (lane 5). Diminution in the intensity of the specific shift in presence of excess (200X) unlabeled C probe denoted its specificity (lane 3). Free biotin-labeled probes without any nuclear extract (lane 1 & lane 4) were considered as the negative control. **(B)** Validation of the specificity of gel shift band, forming in the presence of rs3768617 C probe with the nuclear extract. The intensity of the band gradually got reduced in the presence of the upward gradient (25X, 50X, 100X, 200X) of unlabeled excess rs3768617 C probe (lane 3-6). The shift was reappeared again when the nuclear extract was preincubated with unlabeled excess non-specific probe instead of unlabeled rs3768617 C probe (lane 7). **(C)** Supershift assay to confirm the binding of GFI1B transcription factor in rs3768617 C probe. The specific shift was disappeared when the nuclear extract was preincubated with GFI1B specific antibody suggesting that in presence of antibody the protein cannot able to bind with double-stranded oligonucleotide (lane 3).

To ascertain whether GFI1B binds to the allele 'C' of rs3768617, chromatin immunoprecipitation (ChIP) assay was accomplished with GFI1B specific antibody. It was observed that, in the presence of GFI1B antibody, the amount of immunoprecipitated DNA, surrounding the region of rs3768617 was significantly more than that in the presence of normal mouse IgG which signifies that rs3768617 harbors a potential binding site of the transcription factor GFI1B **(Fig. 3.3)**.

P.T.O

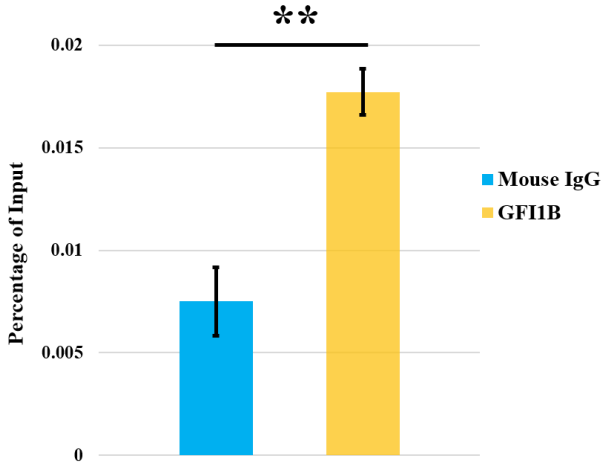

Fig. 3.3: ChIP-qPCR assay using the primers flanking rs3768617. The amount of DNA, pulled down by GFI1B specific antibody was significantly high in comparison to the negative control mouse IgG. The signal was normalized based on the percentage of input and data is represented as mean ± SEM. ** P < 0.01.

3.3.4 No significantly altered expression of GFI1B was observed between control and FECD endothelium samples:

To check if only the binding of GFI1B to rs3768617 is only allele-specific or there is a difference in localisation and expression of GFI1B between control and FECD affected endothelium, immunofluorescence experiments were performed using whole mount of two control and two FECD corneal endothelium tissues. No alteration in localization was observed, and the GFI1B was localized both in the nucleus and plasma membrane **(Fig. 3.4A)**. We found background signal outside the nuclei in both negative controls, showing the specificity of the signal in control and FECD tissues After quantitation of mean fluorescence intensity, we found a decreased expression of GFI1B in the case of FECD affected patients (0.63 fold) which was also not found to be statistically significant (P = 0.4) **(Fig. 3.4B)**. This difference is possible because of decreased number of endothelial cells in patient samples.

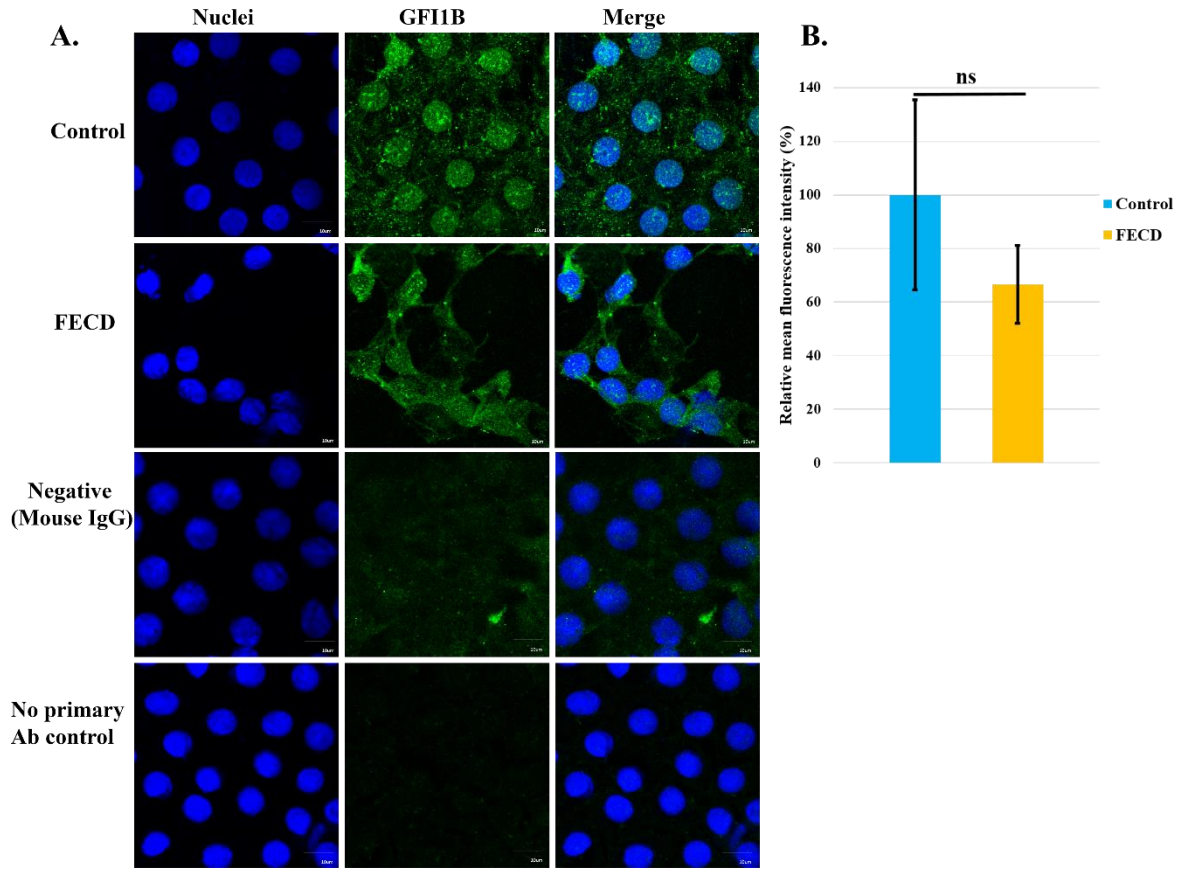

Fig. 3.4: GFI1B expression in age, sex matched control and FECD affected corneal endothelium. (A) Immunofluorescence assay was performed to know the differential expression of GFI1B protein if any. Guttata is visible in FECD endothelium. Background signal was found only outside the nuclei of corneal endothelium in case of both isotype control and no primary antibody control, showing the specificity of nuclear GFI1B signal. **(B)** Quantification of GFI1B immunoreactivity in the endothelium cells using ImageJ. The mean fluorescence intensity signal was calculated after subtracting the background signal and the graph was plotted relative to control. In comparison to control, there is a decrease in fluorescence intensity in FECD cases but failed to be statistically significant. Data defines mean ± SEM of two control and two FECD tissues. Magnification = 630X, zoom factor = 2.5X, scale bar = 10um.

3.4 Discussion:

The heterotrimeric, multidomain family of glycoproteins, laminins are comprised of an alpha (α), a B1 (β) and a B2 (γ) chain and exhibit tissue and cell specific expression with various developmental and pathological stages. They also persist in various genetically distinct isoforms. In mammals, there are five α (LAMA1-5), three β (LAMB1-3), and three γ (LAMC1-

3) chains, which are combined to generate 16 different isoforms that are tissue-specific and developmentally controlled.[185–188] Through various signalling pathways, laminins influence cell specific functions like basement membrane assembly, formation of cellular architecture, cell adhesion, migration, and differentiation, and combat cell death.[189–191] *LAMC1* encodes the laminin γ1 chain which is the most omnipresent subunit in different laminin isoforms. C-16, a peptide derived from the laminin γ1 chain, remarkably promotes cell adhesion, enhances pulmonary metastasis and migration of murine melanoma B-16 cells, most likely by inducing matrix metalloproteinase-9 (MMP-9) secretion.[192] LAMC1 knockout mice failed to produce the proper basement membrane in the embryoid body and as a result, the embryo did not survive.[193]

Previous studies from different populations identified many SNPs, present in the intronic region of the *LAMC1* gene, associated with the severity of different disorders. [194,195] For instance, SNP rs10911241 poses a major risk factor of pelvic organ prolapse in the Chinese population with minor allele 'G' showing an higher chance of the disease.[196] On the other hand, variant rs1062044 G>A present in the 3'UTR of *LAMC1* gene influenced the binding of miR-423-5p and its action in colorectal cancer cases.[194] Another polymorphism rs10911193, found in the promoter of *LAMC1*, builds up the propensity of early-onset pelvic organ prolapse and, the minor allele 'T' significantly affects the binding of the transcription factor NFIL3.[197]

In our present study, we identified the genetic association of intronic SNP rs3768617 (C>T), present in chromosome 1:183123365 with FECD in the Indian population. Apart from the South Asian population (Bangladesh, India, etc.; 0.66), the risk allele 'C' of this variant indicates an increased frequency in European (0.56), African (0.92), and American (0.64) populations in comparison to the protective allele 'T'.

(https://www.ensembl.org/Homo_sapiens/Variation/Population?db=core;r=1:183122865-183123865;v=rs3768617;vdb=variation;vf=2368510). On the other hand, in the East Asian population (Chinese, Japanese, etc.), the frequency of the risk allele 'C' gets decreased (0.48). The FECD prevalence also shows a positive correlation with the frequency of risk allele 'C'. Increased frequency of allele 'C' imparts a significant effect in FECD occurrence in American (3.9 – 6.6%), European (7.0 - 9.2%) and, South Asian population (5.3 – 16.0%), whereas in the case of East Asian population due to the lower frequency allele 'C', the prevalence rate also decreases (1.9 – 4.1%). Genotype tissue expression (GTEx) data presents that rs3768617 has a notable effect on LAMC1 expression in brain cerebellum and frontal cortex tissues **(Fig. 3.5)**.

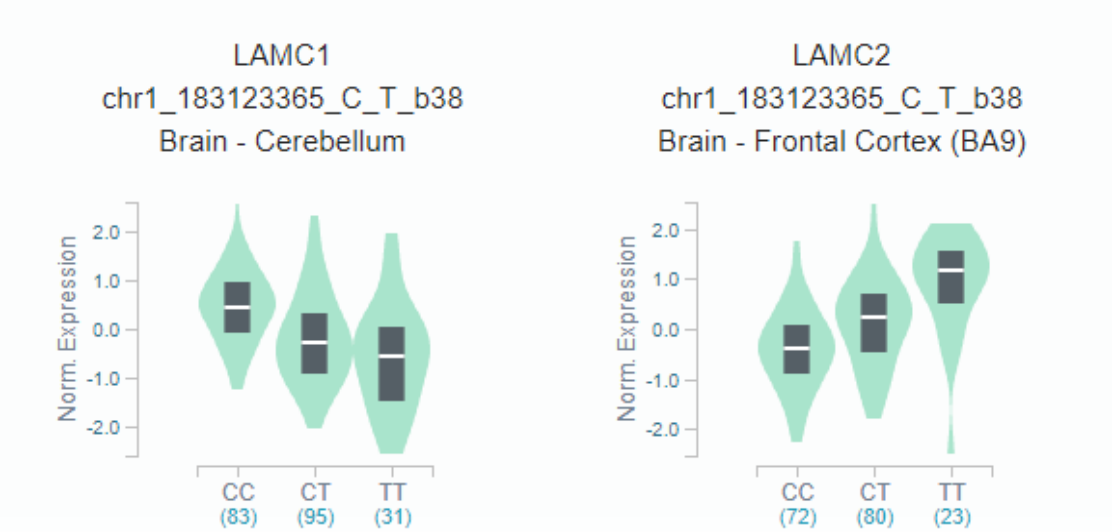

Fig. 3.5: rs3768617 is an expression quantitative trait locus (eQTL) for LAMC1 and LAMC2 expression. eQTL data for rs3768617 were obtained. The eQTL effects of rs3768617 on *LAMC1* and *LAMC2* expression in both brain cerebellum from the GTEx portal (Genotype tissue expression project: https://www.gtexportal.org/home/) and frontal cortex tissue samples are shown respectively.

Previously rs3768617 had appeared as a significant haplotype association with rs12739316 in advanced pelvic organ prolapse, revealing its interaction and outcome with neighboring SNPs

in different diseases.[198] *In silico* analysis through Encyclopedia of DNA elements (ENCODE) suggest that this variant resides in a DNase I hypersensitive site and other epigenetic profiles show the presence of monomethylation of histone H3 (H3K4me1) and acetylation of histone H3 (H3K27ac) modifications in this region **(Fig. 3.6)**. It signifies that the variant rs3768617 resides in an open chromatin region and there is a probability of different transcription factors binding to this region to regulate *LAMC1* and other distal gene regulation.

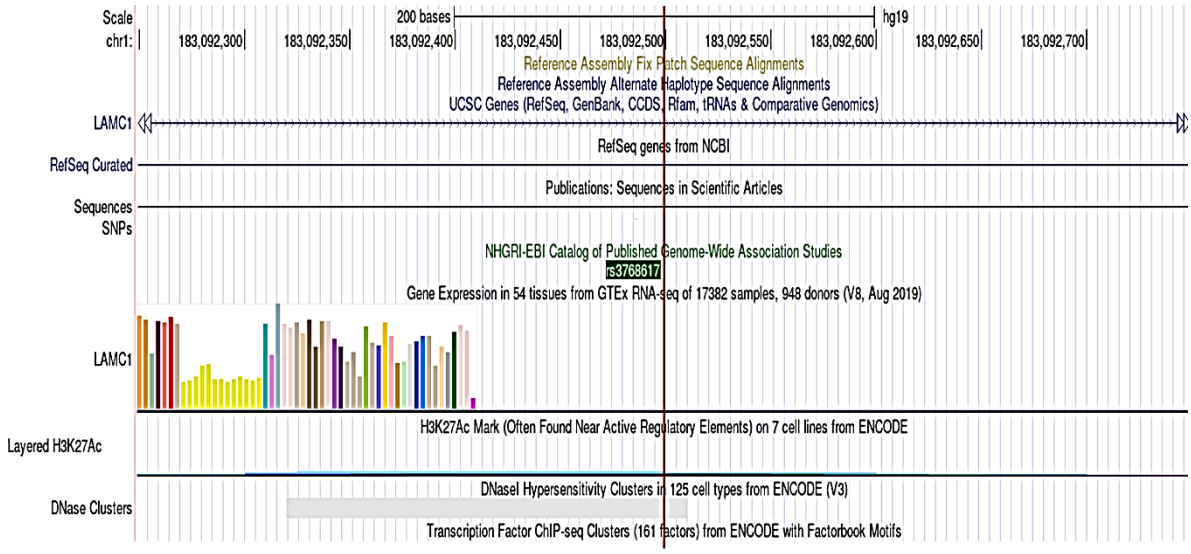

Fig. 3.6: Functional annotation of the region, encompassing rs3768617. Histone modifications (H3K4Me1, H3K4Me3 & H3K27Ac) are shown. DNase clusters are presented in grey bar. The vertical brown line indicates the position of rs3768617 overlapping H3K4Me1, H3K27Ac, DNase hypersensitive site, and transcription factors binding sites. Genomic positions are based on hg19.

Bioinformatic analysis supported that the surrounding region of rs3768617 has a potential binding site for different transcription factors. From our luciferase assay data, we found that the encompassing region displayed decreased regulatory activity in comparison to the empty minimal promoter vector which predicted that this regulatory region may interact with the *LAMC1* promoter or the other regions of the gene to regulate its transcription. One of the important transcription factors which bind around rs3768617 is GFI1B. It is a member of the Gfi family member proteins. GFI1B is made up of three domains: an N-terminal repressor

"SNAG" (SNAIL/ SLUG/ GFI1) domain that engages epigenetic modifiers, a little known middle region, and a C-terminal DNA binding domain with six zinc fingers, with zinc fingers 3–5 binding to the consensus DNA binding site (TAAATCAC(A/T)GCA) and the other zinc fingers interacting with other proteins.[199–201] Furthermore, the SNAG domain is remarkably invariant among orthologs from humans to zebrafish, emphasizing its role and its binding partners' importance. The SNAG domain is required and sufficient for GFI1 and GFI1B to bind lysine-specific demethylase 1 (LSD1).[202] LSD1 is a Flavin-dependent monoamine oxidase that affects chromatin structure and gene expression by demethylating mono- and dimethylated histone 3 lysine 4 and 9 (H3K4me1/2 and H3K9me1/2).[203,204] In this study, we report that rs3768617 transcription factor GFI1B binds to the risk allele 'C' and enhances the luciferase activity in contrast to protective allele 'T'. Chromatin Immunoprecipitation assay suggests that not only *in vitro* but GFI1B binds to the rs3768617 specific 'C' allele *in vivo*. As revealed by immunofluorescence data, GFI1B expresses in the nucleus and membrane at a lower level in FECD cases. Because the frequency of the risk allele 'C' was very high in the FECD cases, so it may be possible that GFI1B binds to the rs3768617 'C' allele in the FECD corneal endothelium to regulate its expression. In the future, genotype specific studies involving more human tissue samples will help us understand the effect of decreased expression of GFI1B if any for FECD progression in a better way. The previous study detected decreased LAMC1 signal in FECD endothelium due to the presence of a low number of endothelium cells.[64] On the contrary Matthaei *et al.*, reported a trend of the upregulation of LAMC1 expression in corneal endothelium samples.[72] The major weakness of the study is the limited number of tissue samples. In the future, *LAMC1* polymorphism with its genotype based expression may help to identify cases, who are more prone to FECD. This present study explains the significant genetic association of *LAMC1* rs3768617 with FECD, replicating the previous reports involving the Caucasian population. From this study, we conclude that *LAMC1* rs3768617 is both genetically

and functionally associated with FECD through differential allele-specific binding to GFI1B. Altogether this study emphasizes the contribution of rs3768617 for FECD pathogenesis globally.

CHAPTER 4

Genetic association of *LINC00970/ATP1B1* and its functional role in disease pathogenesis

4.0 Genetic association of *LINC00970/ATP1B1* and its functional role in disease pathogenesis

4.1 Introduction:

In Fuchs Endothelial Corneal Dystrophy (FECD), the primary problem is believed to be in the functioning of the endothelial cell layer, as affirmed by ultrastructural examination.[47].[8] Patients in the fifth to sixth decade of their life experience hazy morning vision that increases with time as the condition progresses, ultimately leading to visual impairment [205,206].[144,145,206] The more prevalent late onset FECD normally occurs after the age of 40 years, and genetic studies showed that a number of mutations and single nucleotide polymorphisms in genes encoding different proteins that regulate endothelium barrier function, pump activity, etc. are significantly associated with the pathophysiology of the disease across various populations.[207,208] In a genome-wide association analysis among Caucasian population in 2010, researchers found a significant association ($P = 2.3 \times 10^{-26}$) of *TCF4* intronic SNP, rs613872 with FECD, with follow-up studies reporting an expanded CTG trinucleotide repeats (CTG18.1) in the *TCF4* gene exhibiting major effects on disease causation.[20,90] A previous study revealed population-specific effect of the *TCF4* variant CTG18.1 allele in the Indian population (only 34% in contrast to 79% in the Caucasian population), indicating the scope of new genes rather than TCF4 as a major candidate in this population [34] Another GWAS in 2017 identified three novel candidate genes having a significant association with the disease in the European population along with the previously reported *TCF4* gene. These variants are rs3768617 in laminin subunit gamma 1 (*LAMC1*), rs1200114 in long intergenic non-Protein coding RNA LINC00970/ATPase Na^+/K^+ transporting subunit beta 1(*LINC00970/ATP1B1*), and rs79742895 in KN motif and Ankyrin repeat domains 4 (*KANK4*).[64].[209] But, to date, no replication study has been reported for the genetic association of rs1200114 with FECD in different ethnic backgrounds. To address these lacunae, we aimed at finding the genetic and

functional association of rs1200114 and other associated tag SNPs, through case-control assessment in the Indian population. We also wanted to check the differential expression pattern of ATP1B1 between controls and FECD cases.

4.2 Materials and Methods:

The methods, implemented to execute the specific aims of this chapter are discussed in chapter 2 in detail. These are sample collection, DNA extraction, PCR amplification, Sanger sequencing, cell culture, *In silico* analysis, ultracompetent bacterial cell preparation, luciferase reporter assay, tag SNP selection, RNA isolation from tissue samples, quantitative real time PCR.

4.3. Results:

4.3.1 rs1200114 residing in the intergenic region of *LINC00970/ATP1B1* is genetically associated with FECD in the Indian population:

A total of three hundred and eighty (380) controls and one hundred fifty-five (155) FECD patients were selected from the samples collected at LV Prasad Eye Hospital, Bhubaneswar, and Disha Eye Hospitals, Kolkata after obtaining the written consent from the subjects for participation in this study. All control and patient individuals underwent a detailed assessment of specular microscopy before the enrolment into this study. The demographical data of the samples indicates that this study's findings are not affected by the uneven distribution of age and sex **(Table 4.1)**.

Table 4.1: Demographics of samples, used for rs1200114 analysis

Group	Sample size	Mean age ± SD (years)	P value	Sex		P value
				Male	Female	
Control	380	60.54 ± 8.56	0.45	153	227	0.96

Case	155	59.88 ± 9.47		62	93	

The genetic association study of rs1200114 with FECD was evaluated as presented in **Table 4.2**. It was found that the minor allele 'G' of rs1200114 is significantly associated with the risk of FECD in the Indian population [P = 0.01; OR (95%CI) = 1.64 (1.12 - 2.39)]. 30.0% of the FECD affected individuals have a single copy of the risk allele 'G' for rs1200114 whereas only 1.0% have double copies of the minor allele 'G'. We performed a 10,000 permutation test of the allelic association based on 380 controls and 155 FECD cases and observed that the genetic association remains significant even at a higher sample size (P = 0.02). Genotypic association study indicated that allele 'G' increases the disease risk under the dominant [AA versus AG+GG: P = 0.001, OR (95%CI) = 2.02 (1.32 – 3.10)] and additive model [AA versus AG: P = 0.0002, OR (95%CI) = 2.30 (1.48 – 3.60)] only. Our results draw a similar inference to what was found previously in the Caucasian population, indicating that SNP rs1200114 is genetically associated with FECD in both the ethnicities studied to date. The statistical power of this study is 49.1%.

Table 4.2: Representation of the allelic and genotypic frequency distribution of rs1200114 in *LINC00970/ATP1B1*

SNP rs1200114	**Type**	**Control Count (freq.)**	**FECD Count (freq.)**	**Model**	χ^2	**P value**	**OR (95%CI)**
Allele	A G	680 (0.89) 80 (0.11)	260 (0.84) 50 (0.16)		6.48	**0.01** **0.02***	**1.64 (1.12-2.39)**
Genotype	AA AG GG	311 (0.82) 58 (0.15) 11 (0.03)	107 (0.69) 46 (0.30) 2 (0.01)	DOM REC ADD	10.57 1.20 13.95 0.70	**0.001** 0.27 **0.0002** 0.40	**2.02 (1.32-3.10)** 0.44 (0.10-2.00) **2.30 (1.48-3.60)** 0.53 (0.12-2.42)

Statistical test = Pearson Chi-Square (χ^2, df1), **freq.** = frequency, **DOM** = Dominant, **REC** = Recessive, **ADD** = Additive, * =10,000 permutation test

4.3.2 Switching of allele 'G' to 'A' of rs1200114 showed no significant change in regulatory activity of the intergenic region between *LINC00970/ATP1B1*:

In silico analysis of the intergenic region between *LINC00970* and *ATP1B1* (200bp surrounding the rs1200114) using the UCSC genome browser revealed that rs1200114 is located within the DNaseI cluster region and it harbours the binding sites for various transcription factors. We checked the possibility of different transcription factors binding through the JASPAR database and found that only one transcription factor, Nuclear Factor I C (NFIC) has a very low probability of allele specific binding (Score for allele 'A' = 8.52, the score for allele 'G' = 7.219) in the surrounding region of rs1200114. To determine the presence of any regulatory activity in the encompassing region of rs1200114 and to find out the presence of any allele specific transcription factor activity, we performed luciferase assay using a 21bp construct carrying either the rs1200114 'G' allele or the 'A' allele. The result indicated that compared with the minimal promoter pGL4.23 vector (1.00 ± 0.23), there is no significant difference in luciferase activities in the plasmids having either rs1200114 allele 'G' (1.09 ± 0.03, P = 0.74) or rs1200114 allele 'A' (1.04 ± 0.06, P = 0.89, unpaired t-test) **(Fig. 4.1).** These results hinted at the possibility that another nearby locus in this region might confer the regulatory activity rather than rs1200114 itself.

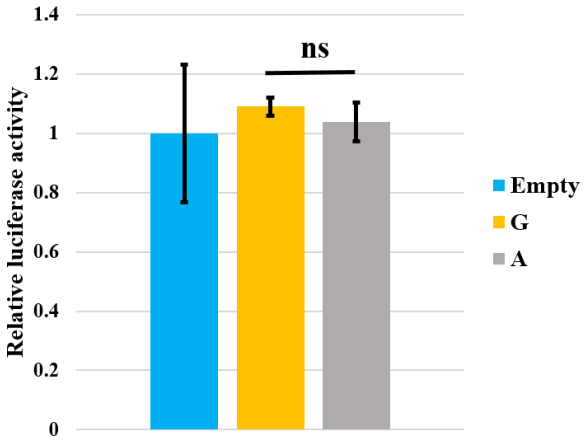

Fig. 4.1: Allele specific regulatory activity of rs120114. Luciferase activity was performed to check for any change in reporter activity in the case of shifting from rs120114 'G' to rs120114 'A'

allele. In comparison to the empty vector, no significant change in luciferase activity was observed between constructs containing allele 'G' or allele 'A'. The experiment was performed at least for three separate days with triplicates of each individual on a single day, and the data is represented relative to the empty vector. Student's t-test was applied to calculate the statistical significance (ns = non-significant).

4.3.3 Decreased expression of *ATP1B1* was observed in the FECD endothelium compared with control endothelium:

rs1200114 resides in the intergenic region of *LINC00970* and *ATP1B1* genes. Previous studies reported decreased expression of *ATP1B1* in the FECD endothelium.[64,127] However, Mathieu et al. reported no significant difference in *ATP1B1* expression between control and FECD endothelium samples at both mRNA and protein levels.[167] Because of these discrepancies in its expression profile across various reports, we checked the expression status of *ATP1B1* in control and FECD individuals in the Indian population. Quantitative real time PCR was performed with age and gender matched eight (8) control and nine (9) FECD endothelium samples and the result showed that there is 0.82 fold decreased expression of *ATP1B1* in FECD corneal endothelium samples (0.18 ± 0.17) with respect to control (1.00 ± 0.24, P = 0.007, unpaired t-test) **(Fig. 4.2).**

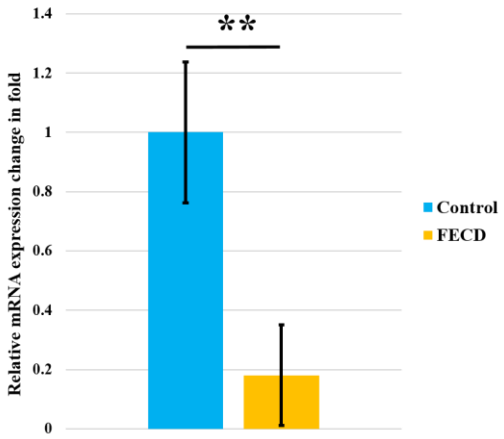

Fig. 4.2: Differential expression of *ATP1B1* between control and FECD affected corneal endothelium samples. qRT-PCR was performed to evaluate the mRNA level expression status of *ATP1B1* in eight (8) control and nine (9) FECD subjects. A significant decrease (P = 0.007) in *ATP1B1*

expression was noticed in FECD individuals with respect to controls. Each experiment was repeated at least three times. Data is represented as mean ± SEM and the student's t-test was carried out to compute the significance level. **P < 0.01.

4.3.4 Analysis of genetic association of rs1200114 tag SNPs with FECD:

Despite displaying a strong genetic association, no change was seen in allele specific luciferase activity of rs1200114. Therefore, we hypothesized that the neighbouring SNPs which are in high linkage disequilibrium (LD) with rs1200114, might be the contributing factors for this genetic association. Six tag SNPs within a gene fragment 7000 base pairs upstream and downstream of the lead SNP rs1200114, were selected using the Ensembl genome browser 105, based on their r^2 and D′ values with rs120014 ($r^2 = 1$ and D′ = 1) for subsequent genetic association studies. The representative genomic positions of the tag SNPs are shown in the supplementary section **(Fig. 4.3)**. The genomic position and the alleles (Major/Minor) of the tag SNPs are presented in **Table 4.3**.

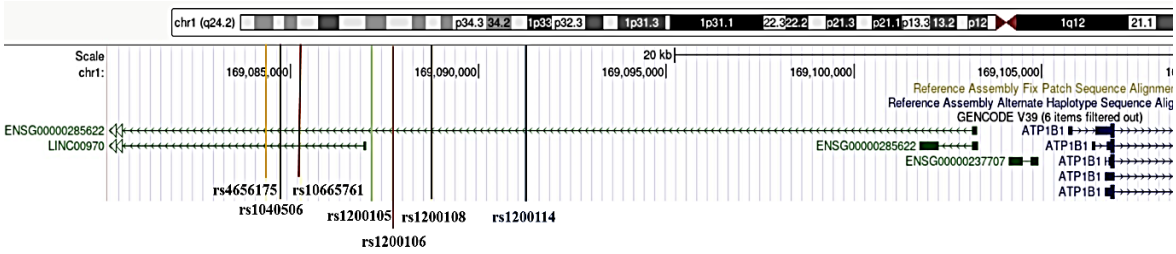

Fig. 4.3: Genomic positions of the reference and Tag SNPs based on hg38 (Human hg38 chr1:169085000-169110000 UCSC Genome Browser v436). The front lines indicate the location of the reference SNP rs1200114 and its tag SNPs in chromosome 1 in different colours. Four variants rs1200114, rs1200108, rs1200106 and rs1200105 are situated in the intergenic region between *LINC00970* and *ATP1B1* whereas the other three rs10665761, rs1040506 and rs4656175 are located in the *LINC00970*.

P.T.O

Table 4.3: Overview of the selected Tag SNPs

SNP	Position (hg 38)	Allele (Major/Minor)	Region
rs4656175	169084322	C/G	Intronic
rs1040506	169084687	A/G	Intronic
rs10665761	169085259-169085263	TAAAATAAAA/TAAAA	Intronic
rs1200105	169087160	C/T	Intergenic
rs1200106	169087708	G/A	Intergenic
rs1200108	169088731	A/G	Intergenic

The genetic association of six tag SNPs with FECD was tested with 100 controls and 100 FECD affected individuals. The age range of the control group was 62.64 ± 6.46, while it was 62.74 ± 7.84 in the case of FECD. There was no significant difference in either age (P = 0.93) or sex (P = 0.92) between these two comparable selected groups. It was found that except for dominant [CC versus GG+CG: P = 0.04, OR (95%CI) = 2.19 (1.02 – 4.69)] and additive models [CC versus CG: P = 0.002, OR (95%CI) = 4.19 (1.62 – 10.87)] of genotypic association, there was no significant difference in minor allele 'G' frequency between controls and cases in rs4656175 **(Table 4.4)**. Minor allele 'G' of rs1040506 was not associated with FECD in both allelic and different genotypic models **(Table 4.4)**. Previous reports suggested that trinucleotide repeats present in the third intron of the *TCF4* gene is significantly associated with the FECD pathophysiology. Approximately 79.0% of the Caucasians and 34.0% of the Indians suffering from FECD, have this unstable repeat. [34,90] It is possible that apart from trinucleotide repeats, other insertions deletions might have a role in FECD pathogenesis. We checked for a genetic association between DELINS variant rs10665761 and FECD in this study, but did not find any significant genetic association **(Table 4.4)**. Also, no notable difference in allelic frequency was found between the control and case population [P = 0.63, OR (95%CI) = 1.12 (0.70 - 1.82)] for rs1200105 **(Table 4.4)**. No significant genotypic association was noted in the dominant, recessive, or additive models. Similarly, no statistically

significant [P = 0.43, OR (95%CI) =1.29 (0.69 – 2.40)] **(Table 4.4)** genetic association of rs1200106 was observed with FECD. A very weak association was also observed in the additive model only for rs1200106 [P = 0.05, OR (95%CI) = 2.12 (0.99 – 4.55)]. It was noticed that the minor allele 'G' of rs1200108 was present at higher frequency in FECD cases, implying it is a risk allele for the population [P = 0.03, OR (95%CI) = 2.15 (1.07 - 4.32)]. A significant association was also found in the dominant model [AA versus GG+AG: P = 0.02, OR (95%CI) = 2.44 (1.15 – 5.20)] and additive model [AA versus AG: P = 0.02, OR (95%CI) = 2.56 (1.18 – 5.57)] **(Table 4.4)**.

Table 4.4: Categorization of alleles and genotypes of enlisted tag SNPs and their genetic association with FECD with discovery set

SNP	Type Allele / Genotype	Control Count (freq.)	FECD Count (freq.)	Model	$\chi 2$	P value	OR (95%CI)
rs4656175	C	182(0.91)	176(0.88)		0.96	0.33	1.38 (0.72 – 2.63)
	G	18 (0.09)	24 (0.12)				
	CC	88 (0.88)	77 (0.77)	DOM	4.19	**0.04**	**2.19 (1.02 – 4.69)**
	CG	6 (0.06)	22 (0.22)	REC	3.70	0.05	0.16 (0.02 – 1.34)
	GG	6 (0.06)	1 (0.01)	ADD	9.75	**0.002**	**4.19 (1.62 –10.87)**
					2.84	0.09	0.19 (0.02 – 1.62)
rs1040506	A	184(0.92)	172(0.86)		3.68	0.06	1.87 (0.98 – 3.58)
	G	16 (0.08)	28 (0.14)				
	AA	87 (0.87)	77 (0.77)	DOM	3.38	0.07	2.00 (0.95 – 4.22)
	AG	10 (0.10)	18 (0.18)	REC	0.52	0.47	1.70 (0.40 – 7.32)
	GG	3 (0.03)	5 (0.05)	ADD	2.88	0.09	2.03 (0.89 – 4.67)
					0.74	0.39	1.88 (0.44 – 8.14)
rs10665761	I	182(0.91)	177(0.88)		0.68	0.41	1.31 (0.69 – 2.52)
	D	18 (0.09)	23 (0.12)				
	II	84 (0.84)	77 (0.77)	DOM	1.25	0.26	1.50 (0.73 – 3.06)
	ID	14 (0.14)	23 (0.23)	REC	2.02	0.16	1.02 (0.99 – 1.05)
	DD	2 (0.02)	0 (0.00)	ADD	3.03	0.08	1.14 (0.95 – 1.38)
					1.81	0.18	1.02 (0.99 – 1.06)

rs1200105	C	159(0.79)	155(0.77)		0.24	0.63	1.12 (0.70 - 1.82)
	T	41 (0.21)	45 (0.23)				
	CC	62 (0.62)	58 (0.58)	DOM	0.33	0.56	1.18 (0.67 – 2.08)
	CT	35 (0.35)	39 (0.39)	REC	0.00	1.00	1.00 (0.20 – 5.08)
	TT	3 (0.03)	3 (0.03)	ADD	0.35	0.55	1.19 (0.67 – 2.13)
					0.01	0.94	0.94 (0.18 – 4.82)
rs1200106	A	20 (0.1)	25 (0.12)		0.63	0.43	1.29 (0.69 – 2.40)
	G	180 (0.9)	175(0.88)				
	AA	4 (0.04)	1 (0.01)	DOM	2.00	0.16	1.66 (0.82 – 3.35)
	AG	12 (0.12)	23 (0.23)	REC	1.85	0.17	0.24 (0.03 – 2.21)
	GG	84 (0.84)	76 (0.76)	ADD	3.81	0.05	2.12 (0.99 – 4.55)
					1.47	0.22	0.28 (0.03 – 2.53)
rs1200108	A	187(0.94)	174(0.87)		4.80	**0.03**	**2.15 (1.07 - 4.32)**
	G	13 (0.06)	26 (0.13)				
	AA	88 (0.88)	75 (0.75)	DOM	5.60	**0.02**	**2.44 (1.15 – 5.20)**
	AG	11 (0.11)	24 (0.24)	REC	0.00	1.00	1.00 (0.06 –16.21)
	GG	1 (0.01)	1 (0.01)	ADD	5.86	**0.02**	**2.56 (1.18 – 5.57)**
					0.01	0.91	1.17 (0.07 –19.08)

Statistical test = Pearson Chi-Square (χ^2, df1), **freq.** = frequency, **I** = Insertion and **D** = Deletion, **DOM** = Dominant, **REC** = Recessive, **ADD** = Additive

Haplotype analysis of these six tag SNPs with rs1200114 showed that the frequency of the risk haplotype "G-G-D-C-A-G-G" (rs4656175 – rs1040506 – rs10665761 – rs1200105 - rs1200106 – rs1200108 - rs1200114) is slightly higher in FECD cases (0.02, P = 0.05) compared with the control group (0.001) with a sample size of 100 per study group **(Table 4.5)**. All the computed haplotypes based on our study subjects are represented in **Fig. 4.4** for a better comparison.

Table 4.5: Haplotype association analysis of rs1200114 with tag SNPs (rs4656175 – rs1040506 – rs10665761 – rs1200105 - rs1200106 – rs1200108 - rs1200114) in the Indian population

Haplotype	Haplotype frequency		χ^2	P value
	Control	Case		
C-A-I-C-G-A-A	0.73	0.68	1.59	0.20
C-A-I-T-G-A-A	0.11	0.13	0.45	0.50
G-G-D-T-A-G-G	0.03	0.05	0.89	0.35
C-A-I-C-A-A-A	0.03	0.01	0.88	0.35
G-G-D-C-A-G-G	0.001	0.02	3.73	**0.05**
C-A-I-C-G-A-G	0.01	0.007	0.42	0.52
C-G-I-C-G-A-A	0.005	0.02	0.96	0.33

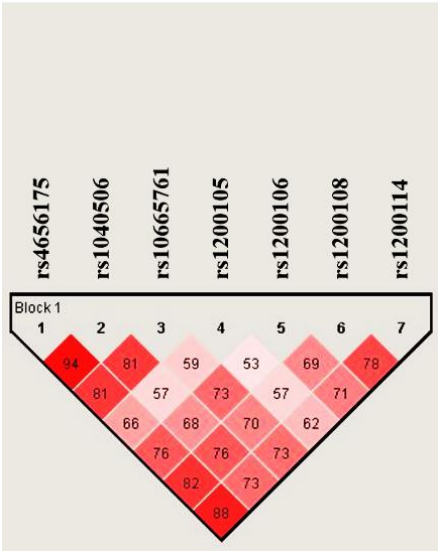

Fig. 4.4: Linkage disequilibrium plot of all the intergenic SNPs. LD plot of the intergenic variants based on the sample size of 100 per group. The Diamond-shaped box represents the D′ value.

Because we noticed genotypic association in the dominant and additive model in the case of rs4656175 and both allelic and genotypic association of rs1200108 at discovery set, so we increased the sample size to three hundred and eighty (380) controls and one hundred fifty-five (155) FECD cases to analyze the genetic association of these two variants with FECD in the replicative set. In the case of rs4656175, we did not find any significant difference in allelic and genotypic frequency between controls and cases **(Table 4.6)**. On the otherhand, we noticed

a significant difference in risk allele ('G') frequency between controls and cases [P = 0.009, OR (95%CI) = 1.66 (1.13 – 2.43)] in case of rs1200108. 10,000 permutation test indicated that, this association remains significant (P = 0.008) with a higher sample size. 31.0% of the FECD patients have one copy of risk allele 'G' and 1.0% of the FECD cases have two copies of allele 'G'. Also, genotypic association was found in the dominant model [AA versus GG + AG: P = 0.001, OR (95%CI) = 1.98 (1.29 – 3.02)] and the additive model [AA versus AG: P = 0.0004, OR (95%CI) = 2.15 (1.39 – 3.31)] **(Table 4.6).** Based on the minor allele frequency in both the controls and FECD cases, the statistical power of rs1200108 genetic association analysis is 46.5%.

Table 4.6: Genetic association of rs4656175 and rs1200108 with FECD in the Indian population in replicative set population

SNP	Type Allele/ Geno	Control Count (freq.)	FECD Count (freq.)	Model	χ2	P value	OR (95%CI)
rs4656175	C	638(0.90)	207(0.86)		2.03	0.21	1.37 (0.89 - 2.13)
	G	74(0.10)	33(0.14)				
	CC	287(0.81)	88(0.73)	DOM	2.85	0.91	1.51 (0.93 – 2.45)
	CG	64(0.18)	31(0.26)	REC	0.24	0.63	0.59 (0.07 – 5.10)
	GG	5(0.01)	1(0.01)	ADD	3.37	0.77	1.58 (0.98 – 2.58)
					0.15	0.60	0.65 (0.08 – 5.66)
rs1200108	A	681 (0.90)	260 (0.84)		6.83	**0.009**	**1.66 (1.13-2.43)**
	G	79 (0.10)	50 (0.16)				
	AA	308 (0.81)	106 (0.68)	DOM	10.09	**0.001**	**1.98 (1.29–3.02)**
	AG	65 (0.17)	48 (0.31)	REC	1.07	0.30	0.35 (0.04–2.84)
	GG	7 (0.02)	1 (0.01)	ADD	12.22	**0.0004**	**2.15 (1.39–3.31)**
					0.71	0.40	0.42 (0.50–3.41)

Statistical test = Pearson Chi-Square (χ^2, df1), **Geno** = Genotype, **freq.** = frequency, **DOM** = Dominant, **REC** = Recessive, **ADD** = Additive

Next, we calculated the haplotype association of rs4656175-rs1200108-rs1200114 based on the replicative set sample size. We found that haplotype 'C-A-A' is present significantly in

higher frequency in the control population (0.87) compared with the cases (0.81, P = 0.01), suggesting it is a protective haplotype **(Table 4.7)**. The LD plot of rs4656175-rs1200108-rs1200114 is shown in **Fig. 4.5A.** Since rs1200108 is only 2.5 kb apart from the reference SNP rs1200114, we also performed haplotype analysis of rs1200108-rs1200114 and found that protective haplotype 'A-A' (rs1200108 – rs1200114) is significantly more common in controls (0.87) in contrast to cases (0.80, P = 0.004); whereas the risk haplotype 'G-G' was more frequently present in FECD cases (0.13, P = 0.04) **(Table 4.7).** The LD plot of rs1200108 - rs1200114 is presented in **Fig. 4.5B**.

Table 4.7: Haplotype association of rs46456175, rs1200108 and rs1200114 with FECD in the Indian population

Haplotype (rs4656175-rs1200108-rs1200114)	**Haplotype frequency**		χ^2	**P value**	**OR (95%CI)**
	Control	**Case**			
C-A-A	0.87	0.81	6.02	**0.01**	**0.63 (0.44-0.92)**
G-G-G	0.09	0.12	2.63	0.12	1.42 (0.91-2.22)
G-G-A	0.02	0.02	0.00	0.98	1.00 (0.34-2.95)
C-A-G	0.01	0.02	1.33	0.25	2.02 (0.58-7.02)
Haplotype (rs1200108-rs1200114)	**Haplotype frequency**		χ^2	**P value**	**OR (95%CI)**
	Control	**Case**			
A-A	0.87	0.80	8.30	**0.004**	**0.60 (0.42-0.86)**
G-G	0.09	0.13	4.43	**0.04**	**1.56 (1.04-2.35)**
G-A	0.02	0.03	1.44	0.22	1.55 (0.70-3.45)
A-G	0.02	0.02	2.02	0.15	1.80 (0.72-4.52)

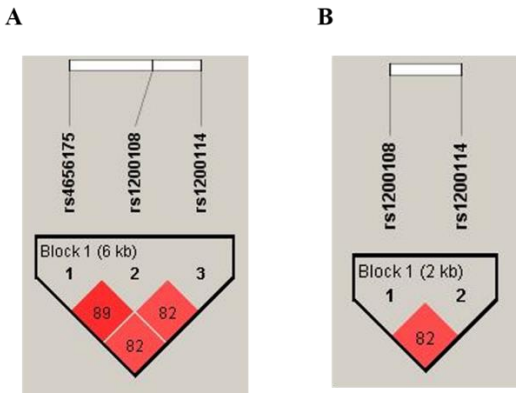

Fig. 4.5: Linkage disequilibrium (LD) plot of the tag SNPs with reference SNP rs1200114. **(A)** LD plot of the intergenic SNPs rs4656175, rs1200108, and rs1200114 based on the total sample size (380 controls and 155 FECD cases) used for the study, depicting high linkage disequilibrium manifested between these three SNPs in the Indian population. **(B)** LD plot of the intergenic SNP rs1200108 and rs1200114 to evaluate the combined effect of these two variants on genetic predisposition with FECD, signifying high linkage disequilibrium existed between these two SNPs in the Indian population. The diamond shaped red box indicates the D′ value.

4.3.5 rs1200108: G>A displayed allele specific regulatory activity:

As SNP rs1200108 falls within the acetylation of histone H3 (H3K27ac) region, we speculated that this variant might display regulatory activity. To check this hypothesis, we performed a luciferase reporter assay using the pGL4.23 minimal promoter vector, containing a 26 bp region, encompassing allele ‘G’ or allele ‘A’. An empty pGL4.23 vector was considered the baseline control. The result suggested an approximately 40.0% reduction of luciferase activity, with a change from the rs1200108 allele ‘G’ (0.98 ± 0.10) to rs1200108 ‘A’ (0.58 ± 0.08, P = 0.014). Also, 42.0% diminution of reporter activity was noticed between the empty vector (1.00 ± 0.12) and the rs1200108 allele ‘A’ (0.58 ± 0.08, P = 0.018). On the contrary, no change in the regulatory activity was observed between the empty vector (1.00 ± 0.12) and rs1200108 allele ‘G’ (0.98 ± 0.10, P = 0.93) **(Fig. 4.6).**

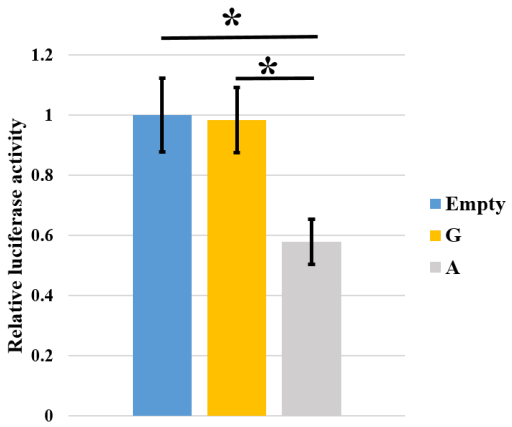

Fig. 4.6: Allele specific reporter activity in rs1200108. Each construct (Empty pGL4.23, rs1200108 'G' and rs1200108 'A') was co-transfected in the HEK-293 cell line with the renilla reporter vector and luciferase activities were measured 24 hours after transfection. Significant difference in reporter activity was observed between rs1200108 allele 'G', and rs1200108 allele 'A'. The diminution of reporter activity was also detected between the empty vector and the rs1200108 allele 'A'. Each group was transfected for three separate individuals on a single day, and the total experiment was repeated six different times. Data is represented as mean ± SEM after normalization with renilla reporter activity and statistical significance was calculated using student's t-test. * $P < 0.05$.

4.4 Discussion:

Intergenic SNPs are key factors for regulating long range gene expression because of altered transcription factor binding sites and their interaction with neighbouring SNPs.[210] In this present investigation, we found a genetic association between the intergenic variant rs1200114, present in chromosome1:169091251, and FECD in the Indian cohort. Risk allele 'G' confers an increased risk of disease compared to protective allele 'A' of rs1200114. This report on the Indian population replicates the previous GWAS's findings in the European population.[64] We found that the 'AG' genotype is present at an increased frequency in FECD individuals in comparison to controls. As a result, the inheritance pattern of the disease was observed significantly in the dominant model and the additive model. Besides the South Asian population (0.89), the protective and major allele 'A' of this variant has a higher frequency in European (0.67), African (0.96), American (0.80), and East Asian (0.97) populations than the

risk allele ‘G'. On the other hand, in comparison to the South Asian population (0.11), the risk allele shows higher frequency in the European (0.33) and American (0.20) populations only (http://www.ensembl.org/Homo_sapiens/Variation/Population?db=core;r=1:169090751-169091751;v=rs1200114;vdb=variation;vf=885997). ENCODE data reflects that rs1200114 falls within an active chromatin site with the epigenetic signatures of acetylation of histone H3 (H3K27ac) and methylation of histone H3 (H3K4me1). Various transcription factors bind in this region and regulate surrounding gene expression. Since we did not find any allele specific transcription factors for rs1200114, therefore, we hypothesized that this variant could interact with its neighbouring variants via long range interaction to regulate the *ATP1B1* and other adjoining gene’s expression. For genetic association analysis and to check their contributing role of *ATP1B1* and other gene expression, we selected six tag SNPs that are in LD with rs1200114 based on the minor allele frequency, r^2, and D′ value. Only one of them, rs1200108 showed a positive genetic association with 1.66 times increased risk of disease. Also, the dominant and the additive modes of inheritance advance the risk of disease penetrance in the population. Previously, researchers noticed that this variant was highly associated with the factors linked to corneal biomechanics.[211] Also variant rs1200108 is genetically associated with yet another corneal dystrophy, keratoconus in the UK population. [212] Haplotype analysis indicated that protective allele ‘A’ of rs1200114 and protective allele ‘A’ of rs1200108 (‘A-A’ haplotype) is seen at a higher frequency in the control population, implying that individuals carrying this particular combination of alleles have a lower chance of disease causation. Moreover, the frequency of rs1200108 - rs1200114 risk haplotype ‘G-G’ was figured out to be more common in FECD cases, inferring its relation to disease causation. *In vitro* reporter assay also implied that certain regulatory factors might bind to the protective allele ‘A’ of rs1200108 and regulate its activity. Based on these results, we hypothesized further that any particular or combination of a group of transcription factors that are highly expressed in disease conditions

might bind to the allele 'A' and curtail its activity. *In silico* data indicated that transcription factors (TFs) Neurofibromin 1 (NF1), Mesoderm forkhead 3 (MF3), YY1 transcription factor (YY1) might bind to the protective allele 'A' of rs1200108 but not to the risk allele 'G'. NF1 and YY1 are transcriptional repressor proteins. Although reporter assay could indirectly reveal the regulatory effect of the transition of allele 'G' to allele 'A', it cannot directly disclose the functional role of the variant rs1200108 for regulating *ATP1B1* and the surrounding gene's expression. This is one of the major limitations of this study. So, in the future, additional experiments will need to be performed by CRISPR-Cas9 based genome editing technique to show the functional role of individual variants, if any. There remains a high possibility that the haplotype containing the associated SNPs, rs1200114 and rs1200118 together confers a greater association role than individual SNPs themselves. So, it needs to be checked if rs1200108 alone or the haplotype containing rs1200114 and rs1200108 affects ATP1B1 expression and its underlying gene regulation

Na,K-ATPase pump is a ubiquitously present oligomeric protein P-type pump, comprising a catalytic α subunit, a structural N-glycosylated β subunit, and an optional γ (FXYD protein family) subunit. [213] In the presence of ATP and magnesium, it pumps 3 Na^+ out and 2 K^+ across the plasma membrane throughout every cycle, creating the ion concentration gradient across the membrane.[214–217] These concentration gradients are essential for retaining resting membrane potential, driving many facilitated transporters, and a variety of cellular processes such as cell proliferation, differentiation, migration, and volume regulation, among others.[214,218–223] Also, the expression level of Na,K-ATPase is significantly downregulated in the case of FECD, compared with the control corneal endothelium.[180]

Four isoforms of α and three of β are present in Na,K-ATPase, but the majority of the isoforms present in the cells are α1 and β1 subunits.[224,225] The α subunit is the catalytic one, whereas the β subunit is crucial for the proper folding of the α subunit in the endoplasmic reticulum and trafficking and insertion into the plasma membrane.[221,226–229] The β1 subunit is encoded by the *ATP1B1* gene and it also functions as a cell to cell adhesion molecule.[230–236] Downregulation of β1 in FECD could be the possible reason for the failure of endothelial pump function which, ultimately leads to corneal edema.[127] We found almost 82.0% low expression of *ATP1B1* expression, similar to the Caucasian population.[64] This suboptimal expression may be due to the genetic and epigenetic changes in the diseased tissue. The *ATP1B1* gene has been previously reported to be silenced by hypermethylation at its promoter region in renal cell carcinoma.[237] It opens up new avenues to explore in future and remains to be seen whether this diminished expression of the beta subunit leads to corneal edema formation in FECD individuals.

In conclusion, we observed a significant genetic association of rs1200114 present in the intergenic region between *LINC00970* and *ATP1B1* with FECD in the Indian population. Moreover, genetic association study of other SNPs, present in linkage disequilibrium with the reference SNP rs1200114 showed an association of rs1200108 with FECD. We also identified that protective haplotype 'A-A' (rs1200108 - rs1200114) is more prevalent in the control individuals than in the FECD population. Expression analysis established decreased expression of *ATP1B1* in the FECD endothelium compared to the control corneal endothelium. Altogether, our study not only replicated the genetic association of the intergenic variant rs1200114 but also revealed the role of a new SNP, rs1200108 with FECD in the Indian population.

CHAPTER 5

Role of CASP8AP2 in FECD pathogenesis

5.0 Role of CASP8AP2 in FECD pathogenesis

5.1 Introduction:

Corneal endothelial cells maintain the transparency of the cornea through a well-established pump and leak mechanism.[238] These cells are terminally differentiated, but they have the migration capability to cover the wound created by any type of injury. Endothelium cells change shape and acquire the ability to migrate by reorganising actin filaments and forming lamellipodia and filopodia. They also secrete extracellular matrix proteins such as collagen subtypes I, III, and XVI; fibronectin; and agrin, which in turn act as signalling molecules for this wound healing process.[239–242] These entire mechanism by which the endothelial cells lose contact with the neighbouring cells and transform into fibroblast type is also known as endothelial to mesenchymal transition (EndoMT).[243] The major hallmarks of EndoMT are the increased expression of different cytoskeletal organization proteins like vimentin, α-SMA as well as enhanced expression of extracellular matrix proteins such as fibronectin, COL1A1, COL1A2, and others.[244] The repression of the endothelial phenotypes and activation of the mesenchymal features are also induced by the transcription factors ZEB1, SNAIL, and TWIST, which are the key regulators of this EndoMT process.[245]

In FECD, the number of functionally active corneal endothelial cells slowly declines due to apoptosis. The viable cells change their shape, size and secrete aberrant extracellular matrix proteins, which deposit in the DM. Although the reason for improper aggregation of ECM on DM is questionable, researchers suggested that EndoMT-inducing genes may be responsible.[9,208,246,247] Previously, it was hypothesized that because TCF4 is a regulator of ZEB1 expression, variants of TCF4 could be the cause of FECD due to their ability to regulate ZEB1 expression.[20] EndoMT-inducing genes, ZEB1 and SNAIL, were found to be

overexpressed in FECD-affected corneal endothelial cells, and these genes are actively involved in the deregulated synthesis of ECM proteins and the transformation of endothelial cells into fibroblastic cells via various signalling pathways. Knockdown of ZEB1 and SNAIL reduces the production of various ECM proteins in the FECD cell line but not in the healthy corneal endothelium line. ZEB1 and SNAIL expression levels were also reduced after treatment with TGF-β type I ALK receptor inhibitor SB431542 accompanied by decreased ECM deposition.[137] Most TGFBIp types were significantly overexpressed in the FECD endothelium compared with normal subjects.[120] Treatment of the corneal endothelial cells with UVA induced expression of EMT responsible genes SNAIL2 and α-SMA, resulting in cell elongation, and disruption of cell-to-cell junctions, phenotypes similar to those seen in FECD. Increased SNAIL2 and α-SMA expression was found in the mouse corneal endothelial cells two weeks after post-UVA irradiation.[248] Menadione (MN) treatment resulted in elongation of the hexagonal corneal endothelial cells and rosette formation due to disruption of cell-to-cell junctions, which are the major characteristics of the primary FECD corneal endothelial cells and ex vivo FECD tissue samples. MN treatment also increased the expression of α-SMA, SNAIL, and ZEB1, all of which are the major markers of EndoMT.[248] Upregulation of the EndoMT proteins in FECD endothelial cells boosts their migration capacity compared with normal corneal endothelial cells.[208]

FECD is genetically associated with various variants and mutations found in the exonic and intronic regions of the EndoMT aggravating transcription factor ZEB1.[108,109]In this objective, we tried to find out the genetic association of different variants present in the intronic and exonic regions of *ZEB1*, with FECD in our Indian population and their functional role in the pathogenesis of FECD.

5.2 Materials and Methods:

The methods implemented to execute the specific aims of this chapter are discussed in chapter 2 in detail. These include RNA isolation from tissue samples, quantitative real-time PCR, deletional plasmid construction, PCR amplification, Sanger sequencing, site-directed mutagenesis, cell culture, *in silico* analysis, ultracompetent bacterial cell preparation, colony PCR, luciferase reporter assay, western blotting, knockdown by shRNA, and overexpression of the protein.

5.3 Results:

5.3.1 Intronic variants rs220057 and rs220060 of *ZEB1* are not genetically associated with FECD in the Indian population:

A total of two hundred and five (205) controls and eighty-eight (88) FECD patients were sorted from the samples collected at LV Prasad Eye Hospital after receiving their written consent for involvement in this study. The demographic data of the samples is presented below.

Table 5.1: Demographics of samples used for rs220057 and rs220060 analysis

Group	Sample size	Mean age ± SD (years)	P value	Sex		P value
				Male	Female	
Control	205	63.80 ± 6.94	0.53	82	123	0.82
Case	88	61.70 ± 7.00		34	54	

Previously, we performed a gene scan of the entire *ZEB1* to find the genetic association of the variants in our population. In the discovery set (40 controls and 30 FECD cases), variant rs220057 and rs220060 showed genetic association with FECD (Nanda *et al*., unpublished).

The genetic association study of rs220057 and rs220060 with FECD was re-evaluated with higher sample size as presented in **Table 5.2.** 38.0% of the FECD affected individuals have a single copy of the minor allele 'C' for rs220057, whereas 2.0% have double copies of the minor allele 'C'. We found that the minor allele 'C' of rs220057 is not genetically associated with the risk of FECD in the Indian population [P = 0.60; OR (95%CI) = 0.90 (0.58-1.4)]. The genotypic association study also failed to show any significant association with FECD. We also did not notice any significant allelic association after performing the 10,000 permutation test (P = 0.65). The statistical power of this genetic association study is only 5.3%. In the case of rs220060, 6.0% of the FECD population has single copy of the major allele 'A' and 94.0% has double copies of the major allele 'A'. Like rs220057, we did not observe any significant genetic association of rs220060 with FECD in the Indian population (P = 0.50; OR (95%CI) = 1.18 (0.38-3.64)]. Additionally, after performing a 10,000 permutation test, the genetic association of rs220060 with FECD remained same (P = 0.56). The statistical power of this genetic association was 4.7%.

Table 5.2: Genetic association of rs220057 and rs220060 with FECD in the Indian population

SNP	**Type Allele/ Geno**	**Control Count (freq.)**	**FECD Count (freq.)**	**Model**	**$\chi 2$**	**P value**	**OR (95%CI)**
rs220057	C	79 (0.19)	37 (0.21)		0.24	0.60	0.90 (0.58-1.4)
	T	331 (0.81)	139 (0.79)				
	CC	11 (0.05)	2 (0.02)	DOM	1.18	0.28	0.75 (0.45-1.26)
	CT	57 (0.28)	33 (0.38)	REC	1.39	0.24	2.44 (0.53-11.24)
	TT	137 (0.67)	53 (0.60)	ADD	1.05	0.23	1.54 (0.67-8.77)
					1.09	0.25	2.34 (0.78-9.65)

rs220060	A	381 (0.93)	170 (0.97)		0.30	0.50	1.18 (0.38-3.64)
	G	29 (0.07)	6 (0.03)				
	AA	176 (0.86)	82 (0.94)	DOM	0.95	0.70	0.86 (0.34-2.20)
	AG	29 (0.14)	6 (0.06)	REC	0.94	0.80	0.87 (0.43-2.24)
	GG	0 (0.00)	0 (0.00)	ADD	0.89	0.76	0.34 (0.44-1.65)
					0.65	0.45	0.90 (0.23-1.78)

Statistical test = Pearson Chi-Square (χ^2, df1), **Geno** = Genotype, **freq.** = frequency, **DOM** = Dominant, **REC** = Recessive, **ADD** = Additive

5.3.1 CASP8AP2 is overexpressed in the FECD endothelium:

A previous report suggested that ZEB1 is overexpressed in the FECD patient derived corneal endothelium cells compared with the respective control.[137] Because we did not find any variant of *ZEB1* genetically associated with FECD in our population, we hypothesized that this overexpression may be due to any transcriptional or post-transcriptional regulatory protein that upregulates its expression in the FECD endothelium. Abshire *et al.* identified that the new post-transcriptional regulatory protein CASP8AP2 prevents ZEB1 degradation by SIAH1 and FBXO45 in multiple cell lines.CASP8AP2 is overexpressed in the malignant gastric epithelial cells and activates Fas-mediated apoptosis.[169,249]. Overexpression of the apoptotic markers caspase 3 and caspase 7 was also found in FECD corneal endothelium tissues.[250] Therefore, we intended to check the expression status of *CASP8AP2* in the FECD corneal endothelium. mRNA expression of *CASP8AP2* indicated a 1.68-fold upregulation of *CASP8AP2* expression (P = 0.01) in the corneal endothelium of FECD patients (n = 17) compared with the control ones (n = 20) **(Fig. 5.1)**.

P.T.O

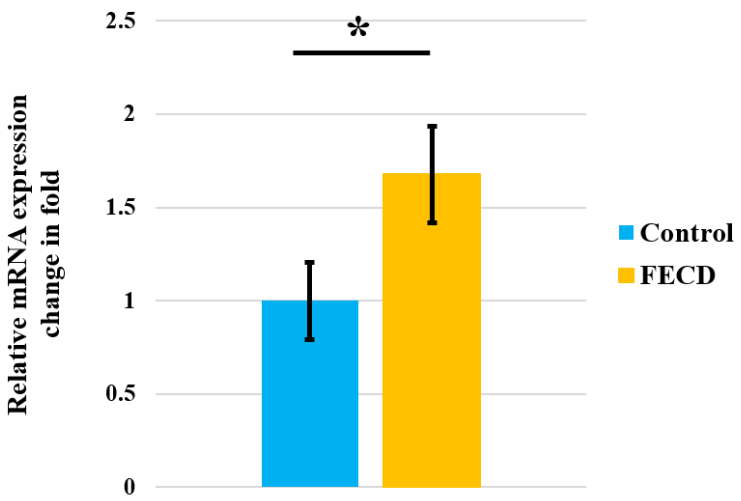

Fig. 5.1: *CASP8AP2* is upregulated in the FECD-affected corneal endothelium compared to age and sex-matched control. (A) qRT-PCR was used to compare the relative mRNA expression between the control (n = 20) and FECD (n = 17) groups, and the data is represented as mean ± SEM. Student's t-test was applied to calculate the statistical significance between the two groups (* $P < 0.05$).

5.3.2. Identification of the strongest transcriptional regulatory fragment of the *CASP8AP2* promoter:

To determine the most important transcriptional regulatory region of the *CASP8AP2* promoter, we first recovered the promoter region using the MatInspector Promoter 2 database. The nucleotide sequence of the *CASP8AP2* promoter region from -1336 to +68 of the transcription start site is presented in **Fig. 5.2.**

P.T.O

-1336 **GGTTGATATGGCAGTTAAGAC**TAAATGGGGTCAGGTGCAGTGACTCACACCTGTA
-1281 ATCCCAGCACTTTGGGAGACTGAGGTGGGAGGATTGTTTGAGCCCAGAAGTTCGT
-1226 GACCAGCCTGGGCAACATAGCAAGACCCCATCTCTACAAAAATTTTAAAAAATTA
-1171 GCCAGGGGTGGCCGG**GCGTGGGTGGCTCAC**GCCTTTAATCCCAGCACTTTGGGAG
-1116 GCCAAGCTGGGCAGATCACCTGAGGACAGGAGTTCAAGACCAGCCTGGTCAACAT
-1061 GGCGAAACCCTGTCTCTACTAAAAATACAAAAATTAGGTTGGCGTGGTAACACAT
-1006 GCCTGCAATCCCAGCTACTCGGGAGACTGAGGCAGGAGAATCACTTGAACCCCGG
-951 AGGCGGAGGTTGTAGTGGGTCGAGATCGCGCCATTGCACTCCAGCCTGGGCAACA
-896 AGAGTGAAACTCCATCTCAGAAACAAAACGAAACAAAACAGCCAGGGGTGGTGGT
-841 **CGCTCGCGTCTATGGT**CCCAGCTACTCTGGAGGCAGAGGTGGGAGGATCTCTCGA
-786 GCCTTGGAGGTGGAGGTTGCAGGGAGCCGAAATCGCTCCACTGCGCTCCAGCCTG
-731 AGCGACAAAGCGATACCCTGTCTGAAAGCAAAAAGAAAAAAAAAAGCTAAGTGGA
-676 CAAACGAGGAAATGGGTAGGGATGAATATAGGCAGACTATAAGTAGCCGAGGAAG
-621 GTGGCCTTATTTTCGCACCTATCAATGCTCAGGCTGAGCTCCTGAGGC**TAGACCT**
-566 **ACCGGCAC**CCCCCATTCCTACAGGTTCTATAAGGCAAGTCAGGTATTCCACCCTG
-511 TAAAAAGCTCTTCTCTCTCCTGCCCCGCTAGACTAGTATCCCCTCCTTAAGGCTC
-456 CCAACATCCGAAGCTAAGTTGTTTGTCTGCCTATCATCCAGGAACGCGTCTGAGG
-401 GCAGGGAACAAATTTATTCA**TCGTAATCGAGCCCA**GCACTTTGTCTCGCACGCAG
-346 CTGACAGCAGAATTTTAAGATAAAGTATTAAATAAATGACAGACCTCTCAAGGCT
-291 TCCTGTCTTTCACTAAAAAGCTTCTCTCAGGCCACGCCCCTACCTCCACTCAGGT
-236 CAGCCCCTTCCTATTGAAGCCCCGCCCCATCGCCTTCCCCGCCACCTTACACCCC
-181 **GCCCCTCTCTCTTAAAGCC**CTAGGAAGATTACTGGAGTTTGGCGCCAACCGTGTT
-126 TTTTTTTTTCCCTTCCAAAGGCGGGAACTAGTTGTGGGCGCTGCGACGTGCTTTG
-71 CGTCTGATATGATTGGCCGTAGGCACTCAGTCCCGCCTCCATACCCTGATAGCGC
-16 TCTGGTATTGGTGGAG**ATG**CCAGGGAGACCTCGGTGGGCAGAAAGGAACCGGGT
+40 TGTCTTGGGCCGGGCAGGGCGGGTAAGTTG

Fig. 5.2: Identification of the *CASP8AP2* promoter. Nucleotide sequence of the human *CASP8AP2* promoter. The start codon (ATG) is highlighted in bold, and all the primer sequences used for promoter analysis are highlighted in different colours.

Next, we designed PCR primers to chop the entire fragment of the 5′ region of 1404 bases (-1336/+68) of the *CASP8AP2* gene into different overlapping PCR segments (-181/+68, -381/+68, -573/+68, -841/+68, -1156/+68, and -1336/+68). The deletional fragments are presented in **Fig. 5.3**.

P.T.O

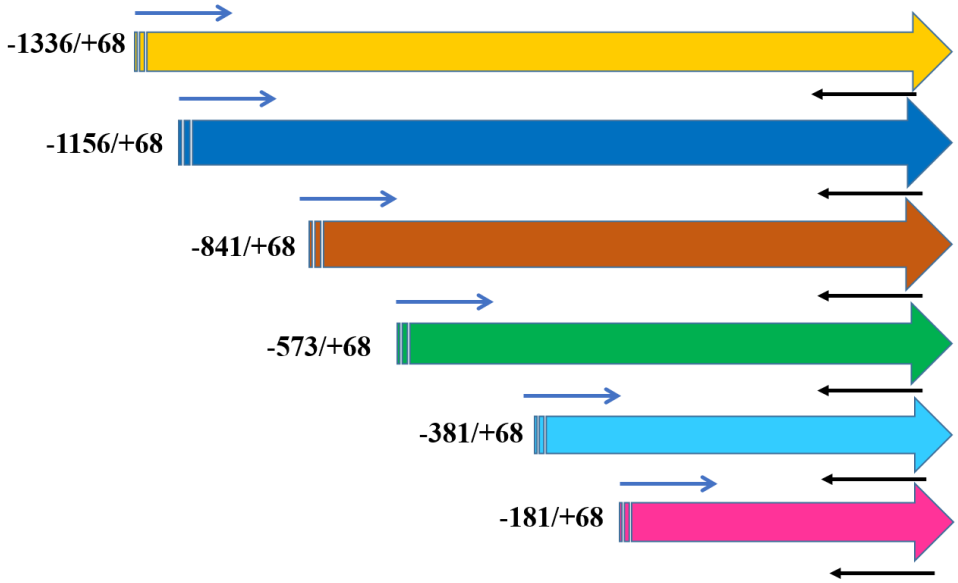

Fig. 5.3: Characterization of the *CASP8AP2* promoter. Different promoter fragments were cloned in frame with the luciferase gene of pGL3 basic vector for functional analysis. The numbers indicate the length of each fragment. The arrows denote the primer start sites.

All the 5′ deletional fragments, cloned into the pGL3 basic luciferase vector, were transfected along with the pGL4.74 [hRluc/TK] renilla vector (100:1) in the HEK-293 cell line, and luciferase activities were measured 48 hours after transfection. The result suggested that all overlapping segments of the promoter exhibited increased luciferase activity as opposed to the negative control pGL3 basic empty vector, but the comparatively smaller region -381/+68 displayed the most significant luciferase activity (3.72 ± 0.06, $P = 5.42 \times 10^{-6}$) compared to the other regions, which indicates that this region bears the strongest regulatory activity, which might be due to its sequence specificity, binding probability of different transcription factors and mediator complex, and other epigenetic changes **(Fig. 5.4)**. *In silico* analysis by the Lasagna 2.0 database showed that this -381/+68 region has four GC- rich motifs, which are the potent binding sites of SP1 family transcription factors. The luciferase activity is comparable between the -381/+68 and the -573/+68 regions, but it falls when the promoter fragment length increases beyond the -573 to -1336 bp region, indicating any silencer element in these regions. For further study, we selected the -381/+68 region to analyse its functional elements.

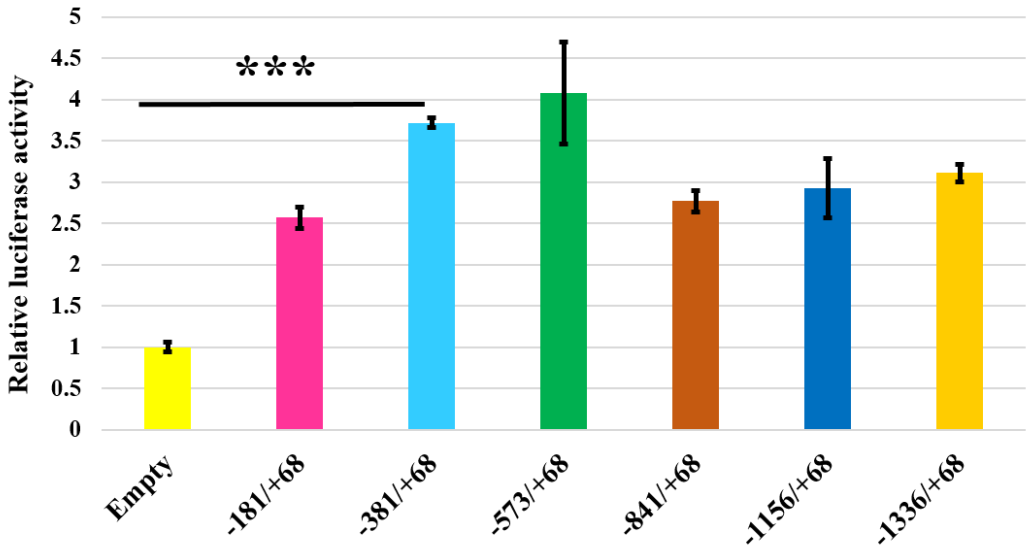

Fig. 5.4: Relative luciferase activity of the overlapping promoter fragments of the *CASP8AP2* promoter. The luciferase activities of all fragments were first normalized with co-transfected, constitutive pGL4.74 [hRluc/TK] renilla luciferase activity, and data is represented with respect to the empty vector. In comparison to the empty pGL3 basic vector, the most significant increase in luciferase activity was found in the -381/+68 region. Although the -573/+68 region showed the highest activity, there was no significant difference in luciferase activity between the -381+68 and -573/+68 regions. The result is depicted as mean ± SEM with at least three individual replications in triplicate, and statistical significance was calculated between the fragments using Student's t test (* $P < 0.5$, ** $P < 0.01$, and *** $P < 0.001$).

5.3.3. Specificity protein 1 (SP1) binding sites in a GC rich area of the *CASP8AP2* promoter support *CASP8AP2* transcription:

To identify the most potent transcription factor binding sites between the -381/+68 bp region of the *CASP8AP2* promoter, we preferred the LASAGNA 2.0 database as a motif search tool. Bioinformatics analysis revealed that there are four potent SP1 transcription factor binding GC-rich motifs present in this region, and the probability of binding is also very high ($P < 0.001$). To prove that, each individual binding site, SP1.1 (-42 to -31 bp), SP1.2 (-187 to -176 bp), SP1.3 (-221 to -205 bp), and SP1.4 (-261 to -251 bp), was mutated by site-directed mutagenesis and cloned into pGL3 basic vectors, which are named 'SDM1', 'SDM2', 'SDM3', and 'SDM4' respectively. One additional construct was also prepared where all the binding sites were

mutated and no SP1 binding sites were available, which is named 'SDM-All'. In the case of the wild-type construct, none of the SP1 binding sites were mutated **(Fig. 5.5)**.

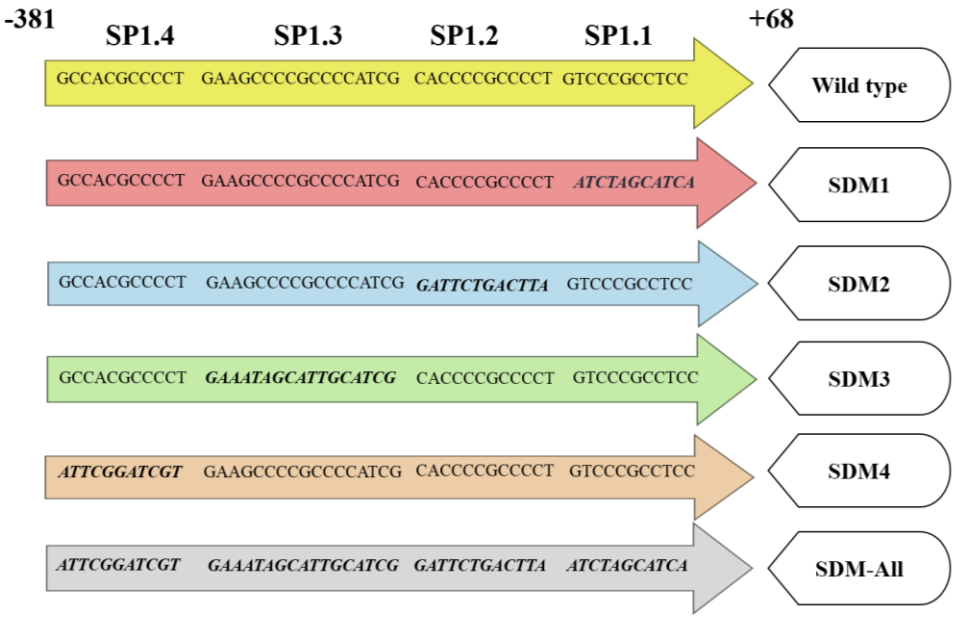

Fig. 5.5: Bioinformatic analysis of SP1 binding sites in the *CASP8AP2* promoter. SP1 binding sites in -381/+68 region of *CASP8AP2* promoter. Four SP1 binding sites (SP1.1, SP1.2, SP1.3, and SP1.4), located between -381 to +68 sequences, were mutated separately (named 'SDM1', 'SDM2', 'SDM3', and 'SDM4') and cloned into the pGL3 basic vector. An extra clone was also designed with four mutated binding sites ('SDM-All'). The wild-type construct acted as a positive control, where none of the sites were mutated. The mutated motifs are indicated in bold and italics.

All the clones were co-transfected with the renilla vector (100:1) into the HEK-293 cell line, and 48 hours after transfection, luciferase activities were estimated. The result showed that except for SDM4, there is significant downregulation of the luciferase activities of all the constructs in comparison to the wild type, and the most promising reduction of luciferase activity is observed in 'SDM1' (1.73 ± 0.36, $P = 5 \times 10^{-4}$) and 'SDM-All' (0.80 ± 0.20, $P = 4.2 \times 10^{-6}$) constructs in comparison to the wild type (4.34 ± 0.24) **(Fig. 5.6)**. So, from this result, we concluded that transcription factor SP1 has a significant binding probability to the most

potent, active sites of the *CASP8AP2* promoter region. Even though four regions could interact with SP1, the luciferase result confirmed that out of the four SP1 binding regions, SP1.1 is the most effective one.

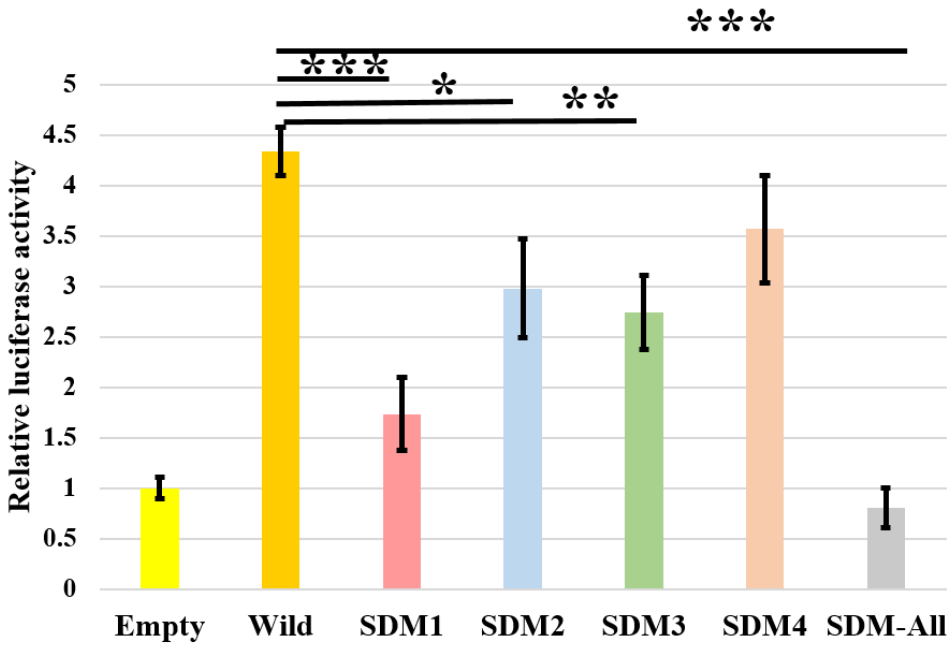

Fig. 5.6: Functional analysis of SP1 binding sites in the *CASP8AP2* promoter. Differential luciferase activities of mutated SP1 binding sites compared to wild type. After normalization with the co-transfected renilla vector, the relative luciferase activities of all constructs (Wild type and the mutated) were calculated and the data is represented as mean ± SEM. Significant changes in the luciferase activities were observed in the mutated constructs compared to the wild-type. The entire experiment was repeated three times in triplicate, and Student's t-test was used to calculate the statistical significance between the wild and the other groups (* $P < 0.05$, ** $P < 0.01$, and *** $P < 0.001$).

We also performed EMSA using biotin-labeled oligos and nuclear extract from the HEK-293 cell line. Four different double-stranded biotin-labeled oligos were designed with wild-type SP1 binding motifs (SP1.1 wild, SP1.2 wild, SP1.3 wild, and SP1.4 wild). Furthermore, another four biotin-labeled oligos were also prepared, carrying mutated SP1 binding motifs (SP1.1 mut,

SP1.2 mut, SP1.3 mut, and SP1.4 mut). In the case of SP1.1, two specific shifts appeared after incubation of nuclear extract with the wild-type oligos, not with the mutated ones **(Fig. 5.7A)**. The addition of 200 fold unlabeled excess wild-type oligos decreased the intensity of the shifts, suggesting that these specific shifts were formed due to the DNA-protein complex formation. The shifts reappeared even after preincubation of the nuclear extract with excess mutant unlabeled oligos, indicating the specificity of the shifts for the wild-type binding motif **(Fig. 5.7A)**. In the case of SP1.2, three shifts appeared after mixing the nuclear extract with the labeled wild-type oligos. These shifts were not visible in the case of the mutant oligos, suggesting the specificities of the shifts **(Fig. 5.7B)**. Preincubation of the nuclear extract with 200-fold excess unlabeled wild-type oligos abolished the intensity of the shifts, indicating that these shifts were formed due to the binding of nuclear protein with the wild-type oligos. However, the shifts came back even after preincubation of the nuclear extract with excess unlabeled mutant oligos, inferring that the protein can bind only the wild-type motif and not the mutated one **(Fig. 5.7B)**.

P.T.O

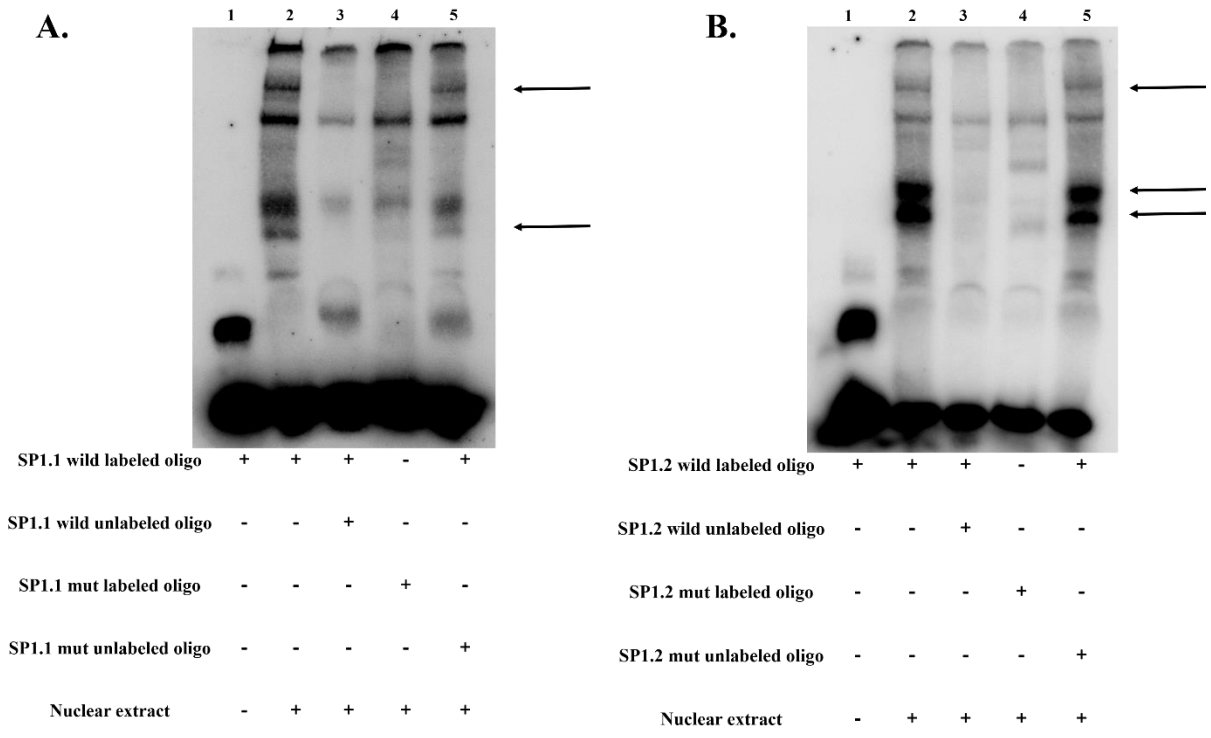

Fig. 5.7: Differential transcription factor binding probability between wild type and mutant oligos. (A) EMSA was carried out to determine the binding affinity of the transcription factor for the wild-type oligos compared with the mutant. Shifts were visible in two different positions (lane 2, indicated by arrow marks) after incubation of nuclear extract with wild-type oligos; the intensities of the shifts declined due to the preincubation of unlabeled excess wild-type oligos with the nuclear extract (lane 3). The mutant oligos did not show any specific shifts (lane 4), but they came back even after preincubation of the nuclear extract with unlabelled excess mutated oligos (lane 5). **(B)** DNA-protein binding assay with SP1.2 oligos. In three individual positions, shifts appeared (lane 2), and those vanished in the presence of unlabeled excess wild-type oligos (lane 3). The specific shifts reappeared even in the presence of unlabelled excess mutant oligos (lane 5).

The DNA-protein binding assay was also accomplished using SP1.3 and SP1.4 oligos. The combination of wild-type SP1.3 oligos with the nuclear extract produced three shifts that were not present in the case of the mutant oligos. The intensity of these shifts decreased when the nuclear extract was preincubated with excess unlabeled oligos **(Fig. 5.8A)**. The shifts became visible even after the addition of excess unlabeled mutant oligos to the nuclear extract before the incubation with the labeled oligos, indicating the selective binding of the protein with the

wild-type binding motif and not with the mutated one **(Fig. 5.8A)**. Like SP1.3, combining the SP1.4 labeled oligos with the nuclear extract resulted in three shifts; the mutant oligos failed to show these three shifts **(Fig. 5.8B)**. When excess unlabeled oligos were pre-incubated with the nuclear extract, the intensity of these shifts was reduced. Also, we added excess unlabeled mutant oligos to the nuclear extract before incubating them with the labeled oligos, and in that case, the shifts were still noticeable, indicating that the protein only binds to the wild-type binding motif **(Fig. 5.8B)**.

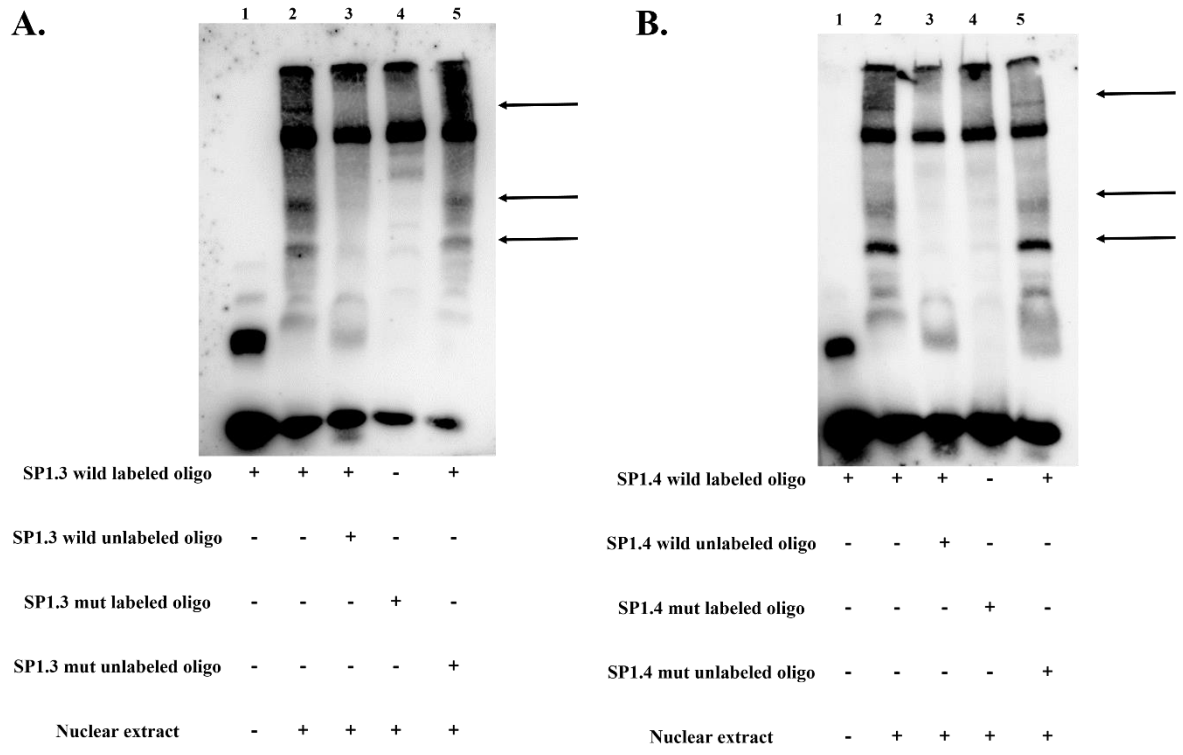

Fig. 5.8: Variability of the DNA-protein complex formation between wild-type and mutant oligos. (A) The combination of the wild-type SP1.3 oligos with the nuclear extract led to the formation of DNA-protein complexes, noted as shifts in three different positions (lane 2). These shifts did not appear in the presence of mutant oligos (lane 4) or after preincubation with wild-type excess unlabelled oligos, indicating the specificity of the shifts (lane 3). **(B)** DNA-protein complexes appeared when wild-type SP1.4 oligos were mixed with the nuclear extract (lane 2); preincubation of the nuclear extract with the excess unlabeled wild-type SP1.4 oligos caused the disappearance of the shifts,

implying their specificity (lane 3). Regardless of the presence of unlabelled excess mutant oligos, the specific shifts persisted (lane 5).

5.3.4. SP1 binding in the -381/+68 region of the *CASP8AP2* promoter enhances its transcription:

After finding the GC-rich motif regions, we wanted to prove that the binding of SP1 in these regions facilitates *CASP8AP2* transcription. Co-transfection of the *CASP8AP2* -381/+68 plasmid with SP1 specific shRNA (SP1 shRNA) significantly decreased its luciferase activity (1.06 ± 0.09) compared to the scramble shRNA (Sc shRNA) (4.19 ± 0.42, P = 0.01). The 'SDM-All' mutant -381/+68 plasmid was selected as a negative control **(Fig. 5.9)**.

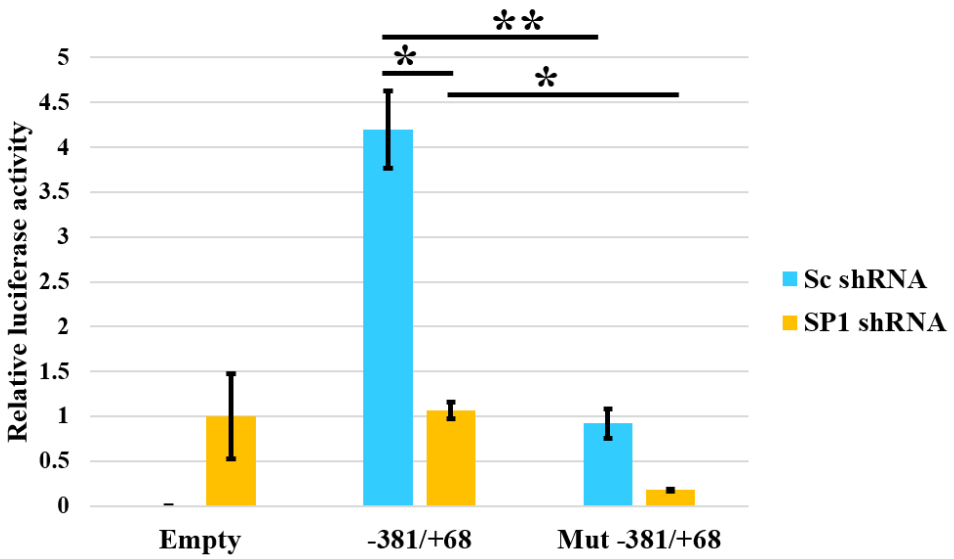

Fig. 5.9: Binding of SP1 increases transcriptional activity in the -381/+68 region of the *CASP8AP2* promoter. (A) Luciferase activity of the -381/+68 region in the presence of scramble shRNA (Sc shRNA) and SP1 specific shRNA (SP1 shRNA). A reduction of luciferase activity was found in the presence of SP1 shRNA compared with Sc shRNA. The bar graph was plotted relative to empty (* P < 0.05, ** P < 0.01).

Western blotting was carried out to validate the knockdown efficiency of SP1 shRNA, and we noticed that, compared with the Sc shRNA, there is a decrease in SP1 expression in the presence of SP1-specific shRNA **(Fig. 5.10A)**. Densitometry analysis demonstrated 60% reduction of SP1 expression in the presence of SP1 shRNA compared with Sc shRNA (P = 0.03) (**Fig. 5.10B).**

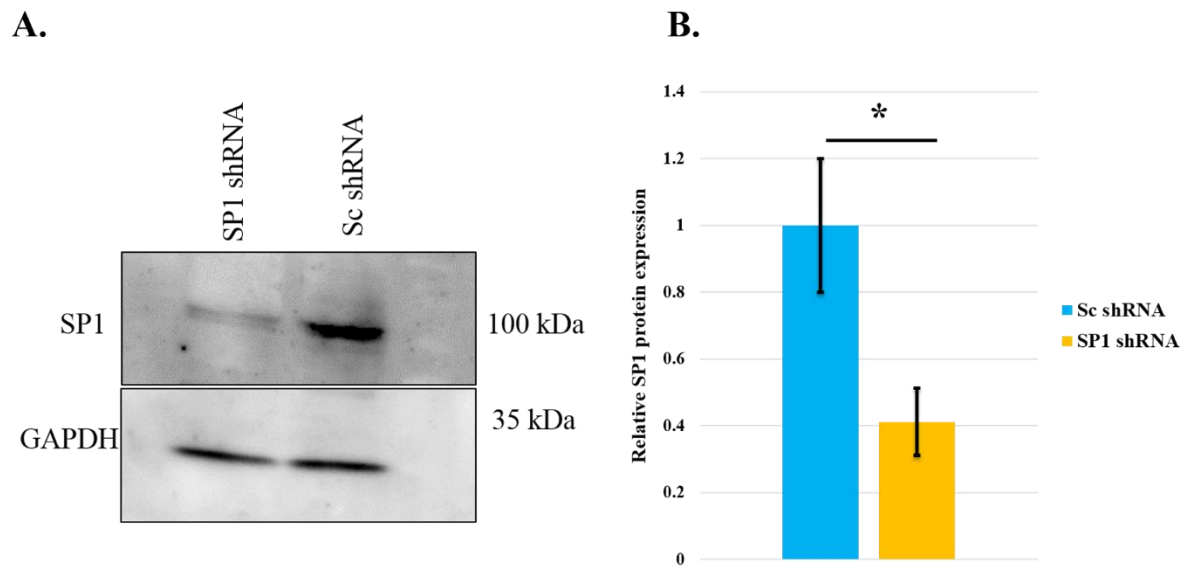

Fig. 5.10: Diminution of SP1 expression in the presence of SP1 shRNA. **(A)** Western blot was performed to verify the knockdown efficiency of SP1 shRNA. Decreased SP1 expression was visible in the presence of SP1 shRNA compared to Sc shRNA. GAPDH was used as a loading control. **(B)** Quantification of the immunoblot. SP1 expression was normalized to GAPDH, and the data is plotted relative to the control. There is 0.41 fold decrease in the expression of SP1 in the presence of SP1 shRNA with respect to Sc shRNA. (* $P < 0.05$).

Furthermore, to confirm the shRNA co-transfection result, we transfected the -381/+68 plasmid along with the renilla plasmid (100:1) in cells, and after 8 hours of transfection, 0.1 µM of SP1-specific inhibitor Mithramycin A was added to the cell culture medium for another 40 hours. Finally, after 48 hours of the experiment, we extracted the total cell proteins and performed the luciferase assay. 100% ethanol was considered the vehicle control. Luciferase assay results suggested that, compared with the vehicle control (4.46 ± 0.81), there was a significant

deduction of luciferase activity of the -381/+68 plasmid (1.53 ± 0.34, P = 0.03) in the presence of Mithramycin A **(Fig. 5.11)**. The 'SDM-All' mutant -381/+68 plasmid was transfected separately to ensure the efficacy of the binding sites. There was also a significant reduction in reporter activity in the presence of vehicle between the -381/+68 plasmid (4.46 ± 0.81) and 'SDM-All' mutant -381/+68 plasmid (0.91 ± 0.18, P = 0.02).

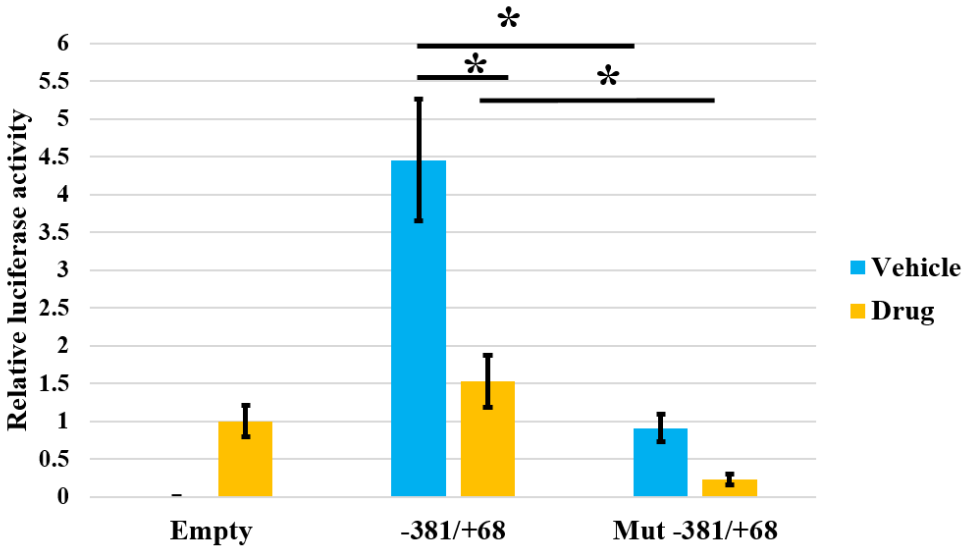

Fig. 5.11: Luciferase activity of the -381/+68 region in the presence of vehicle and drug (Mithramycin A). A reduction in luciferase activity was visible in the presence of the drug. The luciferase activity was normalized with renilla luciferase activity, and the data is represented relative to the empty vector (* P < 0.05).

Western blotting was carried out to check the efficacy of the drug. We observed that the presence of the drug reduce the endogenous SP1 level compared to the vehicle control **(Fig. 5.12A)**. The densitometry calculation indicated a 65% reduction in SP1 expression in the presence of the drug, as opposed to vehicle control. (P = 0.03) **(Fig. 5.12B)**.

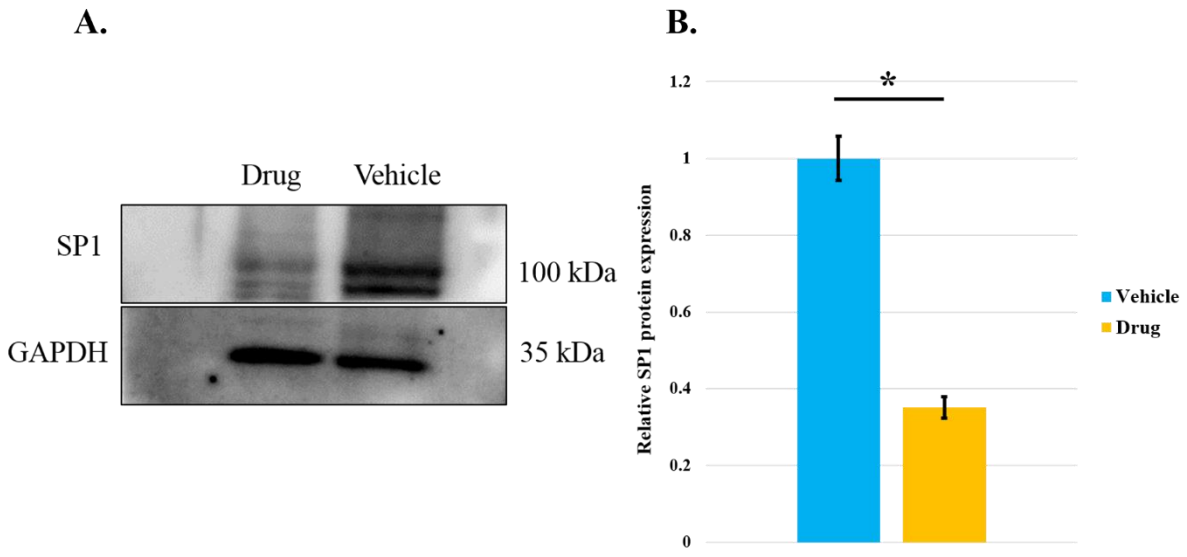

Fig. 5.12: SP1 expression differences between vehicle and drug (Mithramycin A) treatment. **(A)** Decreased expression of SP1 was visible in the presence of the drug. GAPDH was used as a loading control. **(B)** Quantitative analysis of SP1 expression after normalization with GAPDH. The densitometry graph demonstrated 0.35 fold reduced expression of SP1 in the presence of the drug compared with the control. Each experiment was repeated at least three times, and the data is represented as mean ± SEM. Student's t-test was applied to evaluate the statistical significance between the groups (* $P < 0.05$ and ** $P < 0.01$).

5.3.5. No differential expression of *SP1* was detected between control and FECD endothelium tissues:

Next, we also wanted to check the expression pattern of *SP1* between control and FECD endothelium tissues. We hypothesized either that differences in the *SP1* binding or expression between control and FECD endothelium could be one of the major factors, causing CASP8AP2 upregulation in the FECD endothelium. qRT-PCR was performed with eight (8) controls and nine (9) FECD endothelium tissues, and it was found that there is no significant difference in *SP1* expression between them **(Fig. 5.13)**. This highlights that the binding of SP1 might increase the transcriptional activity in the -381/+68 region of the *CASP8AP2* promoter and thus bring out a differential regulation between the FECD patients and healthy controls.

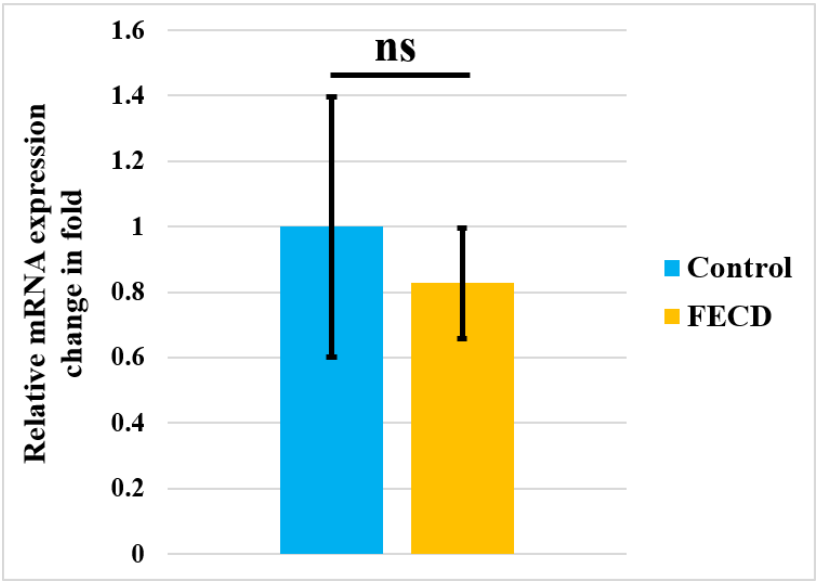

Fig. 5.13: Characteristics of *SP1* expression between the control and FECD endothelium. qRT-PCR was implemented to assess the relative mRNA expression between control (n = 8) and FECD (n = 9) tissues, and the data is depicted as mean ± SEM. Student's t-test was applied to evaluate the statistical significance. No significant difference in *SP1* expression was observed (ns = non-significant).

5.4 Discussion:

CASP8AP2 (or FLASH), a 1,962-amino-acid protein with both a nuclear export signal (NES) and a nuclear localization signal (NLS), is involved in many cellular functions such as mRNA processing, cell cycle progression, apoptosis, histone gene transcription, transcriptional regulation, etc.[169,251–257] Immunogold labelling found a co-localization signal of CASP8AP2 with coilin and p220/NPAT in different cell lines. The downregulation of CASP8AP2 resulted in the disappearance of large Cajal bodies and diffuse localization of Collin.[258] Recent research revealed that CASP8AP2 does not just exist in Cajal bodies. Cajal bodies were found in a small percentage of CASP8AP2-containing nuclear entities. Studies showed that CASP8AP2 and NPAT are specific nuclear body indicators that play a role in controlling histone gene transcription. CASP8AP2 and NPAT co-localize at histone gene bodies that are distinct from Cajal bodies.[259] These two proteins help in histone gene transcription and cell cycle

progression. Also, UV irradiation causes the normal structure of Histone locus bodies (HLBs) to be disrupted, as well as the mislocalization and degradation of two key HLB components, CASP8AP2 and NPAT. The disruption of HLBs causes a halt in the cell cycle's S phase.[260] CASP8AP2 was also discovered as a part of the proapoptosis pathway and a component of the death-inducing signalling complex (DISC), which is implicated in Fas and TNF-alpha-mediated apoptosis. It works by binding to the death effector domains (DED) of procaspase-8, which activate caspase-8, and its downstream caspases, such as caspase-3.[169,252,257].

In this study, we found an upregulation of *CASP8AP2* in the FECD endothelium compared with the control. Previous reports suggested that CASP8AP2 protects the EMT-related transcriptional factors from proteasomal degradation, and overexpression of this protein is also well correlated with apoptosis. We hypothesized that this upregulation could be due to the increased activity of any promoter segments. To ascertain this hypothesis, we chopped the promoter region and tried to find the maximum potential regulatory region of the entire promoter segment. Reporter assays revealed an increase in regulatory activity from -181/+68 to -537/+68 promoter segments, indicating the presence of prominent positive regulatory transcription factor binding motifs in these regions. The activity decreases beyond the -537/+68 region, proving that repressor transcription factor binding sites are present in this region. The -381/+68 region showed the statistically most significant regulatory activity, and there was no significant difference in the regulatory activity between the -381/+68 and -537/+68 segments. Overall, our findings indicate that the 381/+68 promoter region contains the most promising regulatory region of the *CASP8AP2* promoter and that it positively regulates *CASP8AP2* promoter activity.

Next, we intended to identify the specific transcription factors that might be able to bind in this region. It is possible that any particular transcription factor or a group of transcription factors from the same family could bind and regulate the activity of the -381/+68 promoter segment. *In silico* analysis by the LASAGNA2.0 database suggested that this region harbours four GC-rich sites, and the SP1 transcription factor has the highest probability of binding these motifs. Out of the four SP1 binding motifs, the first one, SP1.1 resides in the -181/+68 region. The SP1.2 is located at the intersection of the -381 and -181 bp regions, while the other two, SP1.3 and SP1.4, are located between the -381 and -181 bp regions. Therefore, SP1.2, SP1.3, and SP1.4 are located very near the -381/+68 region, and they could together increase the chance of binding any regulatory protein due to the presence of multiple sites of the binding motifs. To determine the potency of these motifs to regulate *CASP8AP2* expression, we mutated the motifs individually and performed the reporter assay. Out of the four motifs, mutated SP1.1 ('SDM1') showed the most significant decrease in reporter activity compared with the wild type. Mutated SP1.2 ('SDM2') and SP1.3 ('SDM3') also showed a prominent reduction in regulatory activity, but not as much as 'SDM1'. However, mutated SP1.4 ('SDM4') failed to show a significant reduction in regulatory activity. This suggests that this motif is not very active in binding the SP1 transcription factor like the other motifs. In the case of the 'SDM-All' mutant also, there was a significant reduction in luciferase activity compared to the wild type. But the reporter activity never reached zero, which indicates that there are also other transcription factor binding motifs present in this region that also play an important role in *CASP8AP2* transcriptional regulation. To validate the reporter assay, we performed EMSA using biotin-labeled oligos carrying SP1 binding sites in all different positions of the -381/+68 region. The results showed that transcription factor SP1 forms the DNA-protein complexes with the GC-rich motifs in all four positions. We also detected multiple shifts in all EMSA blots. We hypothesized that these multiple shifts are formed by the interactions between SP1

and other family member proteins like SP2, SP3. Mutated oligos failed to show any specific shifts because of the lack of binding sites. Apart from these specific shifts, there were also some DNA-protein complexes, found in all four oligos; these complexes were formed in the wild type and in the mutated oligos in the presence of the nuclear extract. This is because of those transcription factors, which bind to the oligos outside the SP1 binding sites.

The -381/+68 region of the *CASP8AP2* promoter has four SP1 binding motifs, and we suspected that the binding of SP1 in these four motifs enhances the transcriptional activity of the *CASP8AP2* promoter. We found that SP1 binding in these four motifs augments the reporter activity of the -381/+68 region of *CASP8AP2*. The reporter activity was decreased in the presence of SP1 shRNA, which indicated that a threshold level of endogenous SP1 protein is necessary for its action. SP1 shRNA specifically targets the mRNA of SP1 and eventually degrades it, which ultimately lowers the SP1 protein level inside the cells. As a result, the reporter activity was reduced. In the case of the 'SDM-All' mutant construct, the reporter activity was significantly less than the wild type because no binding sites were remaining for this protein, although there was no variation of endogenous SP1. Therefore, both the abundance of the SP1 protein and its binding motifs are required for its action to upregulate the expression of CASP8AP2. We also noticed a significant decline in the reporter activity of the SDM-All mutant construct in the presence of SP1 shRNA compared with Sc shRNA. This reduction in reporter activity may be due to the unavailability of other transcription factors, that have binding motifs in the -381/+68 region. SP1 binding motifs are present in the promoter and intronic regions of many transcription factors, and as a result, knockdown of SP1 eventually decreases the protein level of most of those regulatory proteins. Due to the decreased level of these transcription factors, the luciferase activity of the -381/+68 region was less, although there was no alteration of their binding sites. We also observed a significant decrease in

luciferase activity between -381/+68 transfected cells with SP1 shRNA and SDM-All transfected cells treated with SP1 shRNA. This reflects the fact that in the case of SDM-All mutant, the combination of mutated motifs and low SP1 levels reduces the reporter activity. To validate this experiment, we also treated the transfected cells with the antibiotic Mithramycin A and checked the reported activity. It was well established that this drug has the probability of binding GC-rich region of the DNA and displaces SP1 from its binding sites.[261] Treatment of -381/+68 transfected cells with Mithramycin A decreased the reporter activity compared to the vehicle alone. It hinted that in the presence of the drug, SP1 could not bind to the GC-rich motifs, and as a result, the reporter activity was decreased compared with the vehicle-treated cells, although there was no impairment of the SP1 binding at its target sites in the vehicle-treated cells. A significant decline in reporter activity was also observed in SDM-All mutant transfected drug-treated cells versus only vehicle-treated cells, indicating the global effect of reduced SP1 expression on its target genes.

SP1 binding in the promoter region of many genes affects their transcription. This transcription factor activates the transcriptional rate of many genes, but it could also function as a negative regulator also.[262–266]. We wanted to compare the SP1 expression in control and FECD endothelium tissues because it was possible that enhanced SP1 expression is one of the causes of increased CASP8AP2 expression in the FECD endothelium. But we did not find any dissimilar expression of SP1 between the control and FECD endothelium. Therefore, neither over- nor under-expression but only the binding of SP1 in the -381/+68 region of the *CASP8AP2* promoter is responsible for its increased expression in the FECD endothelium.

In this study, we found that the post-transcriptional regulatory protein of ZEB1, *CASP8AP2* is overexpressed in the FECD endothelium. Furthermore, both bioinformatics and functional assays confirmed that the key regulatory protein of the TGF-β pathway, SP1 regulates *CASP8AP2* transcription and is responsible for its overexpression in the FECD corneal endothelium.

CHAPTER 6

Discussion

6.0 Discussion

6.1 Genetic and functional association of *LAMC1* rs3768617 with FECD in the Indian population:

Previously, rs3768617 present in the intronic region of *LAMC1*, was found to be significantly associated with FECD in the Caucasian population.[64] Researchers also identified the female-specific increased risk of the major allele 'C' of rs3768617 compared with male. Apart from that, no report has validated this genetic association with FECD in different ethnicities. In the present study, we found that rs3768617 is significantly associated with FECD in our Indian population with an odds ratio of 2.73 (95% CI = 1.90 - 3.93). It implies that the persons carrying the risk allele 'C' have 2.73 fold increased chance of disease compared with the persons carrying the protective allele 'T'. The frequency of the 'CC' genotype was very high in FECD patients (0.71) compared with controls (0.42), but the frequency of 'CT' genotype was lower in FECD cases (0.21). We performed a genotypic association study in the context of the dominant, recessive models and found significant associations with the FECD based on these two genetic models. But, a further study based on the additive model indicated that people with a single copy of risk allele 'C' [OR (95%CI) = 1.18 (0.52 – 2.67] have a lower risk of FECD than people with a double copy of 'C' [OR (95%CI) = 3.86 (1.83 - 8.16)]. Therefore, the risk of the disease is increased with the copy number of the major allele 'C' and heterozygote 'CT' has a decreased risk of FECD compared with homozygote 'CC'. After segregating the total sample size into male and female groups, we also calculated the genetic association separately for both groups. We noticed that females have an increased risk of the disease [OR (95%CI) = 3.13 (1.99 - 4.93)] compared with males [OR (95%CI) = 2.09 (1.14 - 3.85)]. Although both the dominant, recessive, and additive models showed significant association in the case of females, for males except for the recessive model, others failed to show any significant association with FECD in our population. So, both the allelic and genotypic there is a significant increased risk

of disease associated with the female group. Also, in females the presence of both copies of the risk allele 'C' (homozygote 'CC') showed an increased risk of the disease [OR (95%CI) = 5.96 (2.26 – 15.72)] compared to the single copy of 'C' [heterozygote 'CT', OR (95%CI) = 1.61 (0.60 – 4.64)], whereas for males, only the double copy of the risk allele 'C' (homozygote 'CC') could increase the chance of the disease [OR (95%CI) = 2.11 (0.64 – 6.93)]. It also partially reveals that FECD affects women more frequently than men. rs3768617 resides in an open chromatin region, and DNA-protein binding assay suggested that transcription factor GFI1B binds only to the risk allele 'C', not the protective allele 'T'. It binds to the risk allele 'C' and increases the luciferase activity. As the frequency of the risk allele 'C' was very high in FECD cases, it is possible that GFI1B binds to the risk allele 'C' in FECD corneal endothelium and upregulates LAMC1 expression. Upregulation of LAMC1 is not possible whenever the protective allele 'T' is present as GFI1B loses its binding sites, and thus the basal level of LAMC1 expression is maintained in the corneal endothelium. Overexpression of LAMC1 was also found in other studies. Based on our findings, we proposed that the GFI1B binding to the risk allele 'C' regulates LAMC1 expression in the FECD endothelium. LAMC1 in conjunction with extracellular matrix proteins (FN1, COL4A1, and COL1A1) accumulates in the DM and eventually leads to guttae formation. Increased thickness in the DM enhances central corneal thickness, upregulation of EndoMT inducing genes, and apoptosis of corneal endothelial cells.[267]

6.2 Genetic association of rs1200114 and its neighbouring SNP rs1200108, with reduced *ATP1B1* expression confers a high risk of FECD pathogenesis:

Intergenic variant rs1200114 is located between *LINC00970* and *ATP1B1*. This polymorphism was identified as being significantly associated with FECD in the Caucasian population. But

like rs3768617, the genetic association of rs1200114 with FECD in other populations has not been studied to date. In our present study, we noticed a significant association of rs1200114 with FECD in our population, and the minor allele 'G' confers 1.64 fold increased chance of disease. The genetic model analysis presented a significant association in the dominant and additive models (AA versus AG) only. The recessive and additive models (AA versus GG) failed to show any association because the frequency of the 'GG' genotype was almost similar in both controls and cases. However, we did not find any functional significance for rs1200114 in the HEK-293 cell line. Expression analysis indicated that *ATP1B1* is less expressed in the FECD endothelium compared with the control endothelium. It is possible that this variant, in conjunction with its neighbouring variants, may contribute a significant role in *ATP1B1* and other gene expression. To check that, we picked six tag SNPs that are in high LD with rs1200114 and first performed a case-control study of the individual tag SNPs with 100 controls and 100 FECD cases (discovery set). Out of six tag SNPs, one of them rs1200108, appeared as a significantly associated variant with FECD in both the discovery and replicative sets in our population. This particular SNP was reported to be associated with keratoconus in the UK population.[212] But, the genetic association of this variant with other corneal dystrophies and its functional role have not been thoroughly studied. In the case of FECD, we found a significant genetic association of this variant for the first time in our population at both the allelic and genotypic level. Also, the haplotype association study noticed that the risk haplotype 'G-G' of rs1200108-1200104 was present at a higher frequency in the FECD cases in comparison to the control. This risk haplotype also exhibited 1.56 fold increased risk of disease. We suspected that people with the 'G-G' risk haplotype might have decreased *ATP1B1* expression, which ultimately leads to disruption in corneal barrier function, high IOP, and corneal edema formation. Decreased *ATP1B1* expression is also linked with the EndoMT transition.[268] So, it is quite reasonable that individuals having this 'G-G' risk haplotype might

have the chance of EndoMT transition of corneal endothelial cells to recover the cell loss. In contrast, the haplotype 'A-A' gives a protective effect from FECD causation [OR (95%CI) = 0.60 (0.42 – 0.86)]. Reporter assay manifested that transcription factor binds to the protective allele 'A' of rs1200108 and decreases the luciferase activity. Bioinformatic analysis suggested that different repressor transcription factors (NF1, YY1) have the probability of binding only to the protective allele 'A' but not to the risk allele 'G'. So, any of them that overexpress in FECD endothelium might bind to the allele 'A' and decrease its activity, which eventually may drive to less ATP1B1 expression. So, this information also conveys that, it is not just the risk allele but other negative regulators may also be responsible for decreased *ATP1B1* expression in the FECD endothelium. Further study needs to be performed to prove this hypothesis. Altogether, this chapter represents the genetic association of two SNPs, rs1200114 and rs1200108, with their probable effects on *ATP1B1* expression.

6.3 The binding of SP1 to the *CASP8AP2* promoter regulates its expression in a positive way:

The upsurge of corneal endothelial cell apoptosis is one of the primary causes of FECD pathogenesis. It was noticed that, corneal endothelium cells turn fibroblastic shaped and migrate into the central cornea from the periphery to fill up the vacant spaces. Due to this reason, the cell size and shape both change. Previous study found that CASP8AP2 protects ZEB1 from proteosomal degradation and, by upregulating EMT-related transcription factors like ZEB1 and SNAIL, enhances cancer cell metastasis. We hypothesized that, in the case of FECD condition, CASP8AP2 may play a major role in the fibroblastic transformation of the corneal endothelial cells. To know that, we first checked the expression of CASP8AP2 and found that it is upregulated in FECD tissue samples compared with controls. There might be

various reasons for the upregulation of a specific protein in a specific condition, but we suspected that it is the interaction between the transcription factor and the promoter region of *CASP8AP2* that helps to upregulate its expression. Promoter analysis indicated that the -381/+68 region of the *CASP8AP2* promoter has the strongest transcriptional regulatory activity, and DNA-protein binding assays showed that transcription factor SP1 binds to the -381/+68 region of the *CASP8AP2* promoter and upregulates its expression. Decreased level of intracellular SP1 downregulates the promoter activity. Also, mutated SP1 binding sites hamper the binding of SP1 to the *CASP8AP2* promoter, which eventually decreases promoter activity. So, we could come to the conclusion that SP1 is a key transcription factor that regulates CASP8AP2 expression. .

6.4 Conclusion:

This study correlates the genetic and functional associations of different polymorphisms with the molecular mechanisms of the transcriptional regulation of one EndoMT-causing gene, *CASP8AP2,* in the pathogenesis of FECD. Our study reported that variants rs3768717 and rs1200114 are genetically associated with FECD in the Indian population. In addition, we noticed that females are more susceptible than males to the rs3768617-induced higher risk of FECD. Transcription factor GFI1B specifically binds to the risk allele ‘C’ of rs3768617 and upregulates its regulatory activity, which could drive increased expression of LAMC1 in FECD endothelium. Overexpression of LAMC1 is one of the factors responsible for guttae formation, which could upregulate different EndoMT-inducing genes in the FECD endothelium. Expression analysis indicated lower expression of GFI1B in the FECD corneal endothelium relative to the control endothelium. Although we did not find any regulatory activity of rs1200114, we noticed the reduced expression of *ATP1B1* in FECD corneal endothelium

compared with control. Decreased expression of *ATP1B1* is well related to cellular migration. Furthermore, to find out the possible causes, we performed a genetic association analysis of the tag SNPs, which are in strong LD with rs1200114, and the result showed that SNP rs1200108 is significantly associated with FECD in our population. Haplotype analysis implied that the risk haplotype 'G-G' of rs1200108-rs1200114 is present at a significantly higher frequency in FECD cases compared to controls and contributes to an increased risk of the disease's pathogenesis. The functional analysis proposed that various repressor transcription factors could bind to the protective allele 'A' of rs1200108 and downregulate the regulatory activity, suggesting its effect on *ATP1B1* and surrounding other gene's expression.

Besides the genetic association study, we also identified overexpression of CASP8AP2 in the FECD corneal endothelium relative to control. Transcription factor SP1 binds to the promoter region of *CASP8AP2* and upregulates its expression. In summary, our study highlighted three major mechanisms that together assist in the endothelial to mesenchymal transition of corneal endothelium cells in FECD.

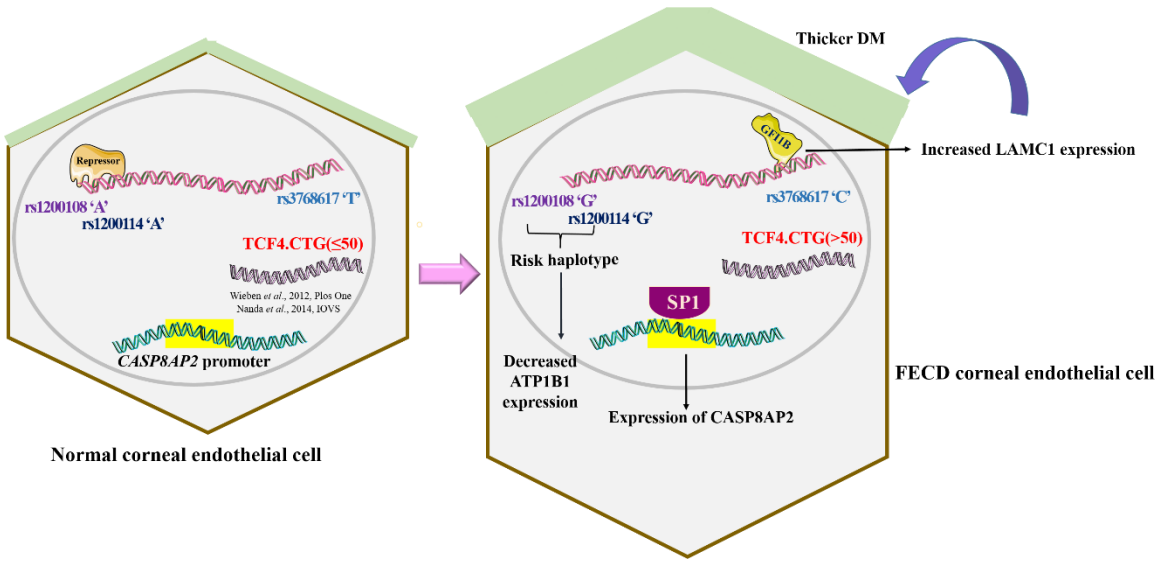

Fig. 6.1: Summary of the different risk factors involved in the progression of a healthy corneal endothelium cell to a FECD corneal endothelium cell. In comparison to the control, the FECD corneal endothelium has more no. of CTG repeats (> 50), present in the third intron of *TCF4*. rs3768617 allele 'C' is significantly present at a higher frequency in FECD corneal endothelium and GFI1B binds to the risk allele 'C', leading to the upregulation of LAMC1 expression and subsequently thickening of DM. GFI1B cannot bind to the protective allele 'T' of rs3768617, and that maintains the normal thickness of DM. The risk haplotype 'G-G' of rs1200108-rs1200114 is significantly associated with FECD, and that might be responsible for the decreased *ATP1B1* expression in the FECD corneal endothelium compared with the control. Transcription factor SP1 binds to the promoter region of *CASP8AP2* and regulates its expression.

6.5 Key findings from this study:

- Variant rs3768617 present in the intronic region of *LAMC1* is genetically and functionally associated with FECD in the Indian population.
- Females are more affected by the rs3768617-induced increased risk of FECD relative to males.
- Transcription factor GFI1B binds to the risk allele 'C' of rs3768617, not the protective allele 'T'.
- Decreased expression of GFI1B was found in the FECD endothelium compared with control.
- Intergenic polymorphism rs1200114, present between *LINC00970* and *ATP1B1*, is genetically associated with FECD in the Indian population.
- Decreased expression of *ATP1B1* was detected in the FECD corneal endothelium compared to the control endothelium.
- Novel SNP rs1200108, present in high LD with rs1200114, is genetically associated with FECD in the Indian cohort.

- Haplotype ‘G-G’ of rs1200108-rs1200114 is significantly more prevalent at a higher frequency in the FECD cases.
- Haplotype ‘A-A’ of rs1200108-rs1200114 is more frequent in the control population, implying its protective effect from the disease.
- Repressor transcription factors bind to the protective allele ‘A’ of rs1200108 and suppress its regulatory activity.
- CASP8AP2 is overexpressed in FECD corneal endothelium compared with the control endothelium.
- -381/+68 region of the *CASP8AP2* promoter displayed the most significant transcriptional regulatory activity.
- SP1 binds to the four GC-rich motifs in -381/+68 and regulates CASP8AP2 expression.
- Downregulation of SP1 significantly hampers *CASP8AP2* transcription.

6.6 Protocols standardization during the course of the study:

- Ultracompetent cell preparation for the transformation of different plasmids.
- Site-directed mutagenesis for the preparation of mutant constructs.
- Whole-cell protein extraction for western blotting.
- Standardization and optimization of the chromatin immunoprecipitation assay to study transcription factor binding in gene’s regulatory regions.

6.7 Future directions:

- To evaluate the genome-wide differential binding sites of GFI1B in control versus FECD endothelium tissues by ChIP-sequencing.

- To understand the interactions of different co-factors with GFI1B by immunoprecipitation and mass-spectrometry.
- To find out the effects of rs1200114 and rs1200108 in *ATP1B1* and surrounding other gene expression by a CRISPR-Cas9 gene editing approach.
- To identify the binding of different co-factors with SP1 for regulation of CASP8AP2 expression by TF-ChIP and SILAC.

CHAPTER 7

References

7.0 References

1. Weiss, J. S. *et al.* The IC3D Classification of the Corneal Dystrophies. *Cornea* **27**, S1 (2008).

2. Fuchs, E. Dystrophia epithelialis corneae. *Albr. von Græfe's Arch. für Ophthalmol.* **76**, 478–508 (1910).

3. Graves, B. REPORT TO THE LANG CLINICAL RESEARCH COMMITTEE, ROYAL LONDON OPHTHALMIC HOSPITAL: A BILATERAL CHRONIC AFFECTION OF THE ENDOTHELIAL FACE OF THE CORNEA OF ELDERLY PERSONS WITH AN ACCOUNT OF THE TECHNICAL AND CLINICAL PRINCIPLES OF ITS SLIT-LAMP OBSERVATION. *Br. J. Ophthalmol.* **8**, 502–544 (1924).

4. Adamis, A. P., Filatov, V., Tripathi, B. J. & Tripathi, R. A. mes. C. Fuchs' endothelial dystrophy of the cornea. *Survey of Ophthalmology* vol. 38 149–168 (1993).

5. Waring, G. O., Bourne, W. M., Edelhauser, H. F. & Kenyon, K. R. The Corneal Endothelium: Normal and Pathologic Structure and Function. *Ophthalmology* **89**, 531–590 (1982).

6. Bigar, F., Schimmelpfennig, B. & Hürzeler, R. Cornea Guttata in Donor Material. *Arch. Ophthalmol.* **96**, 653–655 (1978).

7. Laing, R. A. *et al.* Endothelial Mosaic in Fuchs' Dystrophy: A Qualitative Evaluation With the Specular Microscope. *Arch. Ophthalmol.* **99**, 80–83 (1981).

8. Elhalis, H., Azizi, B. & Jurkunas, U. V. Fuchs Endothelial Corneal Dystrophy. *Ocul. Surf.* **8**, 173 (2010).

9. Krachmer, J. H., Purcell, J. J., Young, C. W. & Bucher, K. D. Corneal endothelial dystrophy. A study of 64 families. *Arch. Ophthalmol. (Chicago, Ill. 1960)* **96**, 2036–2039 (1978).

10. Cross, H. E., Maumenee, A. E. & Cantolino, S. J. Inheritance of Fuchs' endothelial dystrophy. *Arch. Ophthalmol. (Chicago, Ill. 1960)* **85**, 268–272 (1971).

11. Biswas, S. *et al.* Missense mutations in COL8A2, the gene encoding the alpha2 chain of type VIII collagen, cause two forms of corneal endothelial dystrophy. *Hum. Mol. Genet.* **10**, 2415–2423 (2001).

12. Gottsch, J. D. *et al.* Inheritance of a novel COL8A2 mutation defines a distinct early-onset subtype of fuchs corneal dystrophy. *Invest. Ophthalmol. Vis. Sci.* **46**, 1934–1939 (2005).

13. Magovern, M., Beauchamp, G. R., McTigue, J. W., Fine, B. S. & Baumiller, R. C. Inheritance of Fuchs' combined dystrophy. *Ophthalmology* **86**, 1897–1920 (1979).

14. Rosenblum, P., Stark, W. J. & Maumenee, I. H. Hereditary Fuchs' Dystrophy. *Am. J. Ophthalmol.* **90**, 455–462 (1980).

15. Levy, S. G., Moss, J., Sawada, H., Dopping-Hepenstal, P. J. C. & McCartney, A. C. E. The composition of wide-spaced collagen in normal and diseased Descemet's membrane. *Curr. Eye Res.* **15**, 45–52 (1996).

16. SAGE, H. & IRUELA-ARISPE, M. -L. Type VIII collagen in murine development.

Association with capillary formation in vitro. *Ann. N. Y. Acad. Sci.* **580**, 17–31 (1990).

17. Park, M., Li, Q., Shcheynikov, N., Zeng, W. & Muallem, S. NaBC1 Is a Ubiquitous Electrogenic Na+-Coupled Borate Transporter Essential for Cellular Boron Homeostasis and Cell Growth and Proliferation. *Mol. Cell* **16**, 331–341 (2004).

18. Riazuddin, S. A. *et al.* Missense mutations in the sodium borate cotransporter SLC4A11 cause late-onset Fuchs corneal dystrophy. *Hum. Mutat.* **31**, 1261–1268 (2010).

19. Vithana, E. N. *et al.* SLC4A11 mutations in Fuchs endothelial corneal dystrophy. *Hum. Mol. Genet.* **17**, 656–666 (2008).

20. Baratz, K. H. *et al.* E2-2 Protein and Fuchs's Corneal Dystrophy. *N. Engl. J. Med.* **363**, 1016–1024 (2010).

21. Sánchez-Tilló, E. *et al.* β-catenin/TCF4 complex induces the epithelial-to-mesenchymal transition (EMT)-activator ZEB1 to regulate tumor invasiveness. *Proc. Natl. Acad. Sci. U. S. A.* **108**, 19204–19209 (2011).

22. Riazuddin, S. A. *et al.* Missense mutations in TCF8 cause late-onset Fuchs corneal dystrophy and interact with FCD4 on chromosome 9p. *Am. J. Hum. Genet.* **86**, 45–53 (2010).

23. Eger, A. *et al.* DeltaEF1 is a transcriptional repressor of E-cadherin and regulates epithelial plasticity in breast cancer cells. *Oncogene* **24**, 2375–2385 (2005).

24. Sobrado, V. R. *et al.* The class I bHLH factors E2-2A and E2-2B regulate EMT. *J. Cell Sci.* **122**, 1014–1024 (2009).

25. Riazuddin, S. A. *et al.* Replication of the TCF4 intronic variant in late-onset Fuchs corneal dystrophy and evidence of independence from the FCD2 locus. *Invest. Ophthalmol. Vis. Sci.* **52**, 2825–2829 (2011).

26. Thalamuthu, A. *et al.* Association of TCF4 gene polymorphisms with Fuchs' corneal dystrophy in the Chinese. *Invest. Ophthalmol. Vis. Sci.* **52**, 5573–5578 (2011).

27. Gain, P. *et al.* Global Survey of Corneal Transplantation and Eye Banking. *JAMA Ophthalmol.* **134**, 167–173 (2016).

28. Eghrari, A. O. *et al.* Prevalence and Severity of Fuchs Corneal Dystrophy in Tangier Island. *Am. J. Ophthalmol.* **153**, 1067 (2012).

29. Zoega, G. M. *et al.* Prevalence and risk factors for cornea guttata in the Reykjavik Eye Study. *Ophthalmology* **113**, 565–569 (2006).

30. A, H. *et al.* Prevalence of and risk factors for cornea guttata in a population-based study in a southwestern island of Japan: the Kumejima study. *Arch. Ophthalmol. (Chicago, Ill. 1960)* **129**, 332–336 (2011).

31. Kitagawa, K. *et al.* Prevalence of Primary Cornea guttata and Morphology of Corneal Endothelium in Aging Japanese and Singaporean Subjects. *Ophthalmic Res.* **34**, 135–138 (2002).

32. Pandrowala, H., Bansal, A., Vemuganti, G. K. & Rao, G. N. Frequency, distribution, and outcome of keratoplasty for corneal dystrophies at a tertiary eye care center in South India. *Cornea* **23**, 541–546 (2004).

33. Chaurasia, S. & Vanathi, M. Specular microscopy in clinical practice. *Indian J. Ophthalmol.* **69**, 517 (2021).

34. Nanda, G. G., Padhy, B., Samal, S., Das, S. & Alone, D. P. Genetic Association of TCF4 Intronic Polymorphisms, CTG18.1 and rs17089887, With Fuchs' Endothelial Corneal Dystrophy in an Indian Population. *Invest. Ophthalmol. Vis. Sci.* **55**, 7674–7680 (2014).

35. Buxton, J. N., Preston, R. W., Riechers, R. & Guilbault, N. Tonography in cornea guttata. A preliminary report. *Arch. Ophthalmol. (Chicago, Ill. 1960)* **77**, 602–603 (1967).

36. del Buey, M. A., Cristóbal, J. A., Ascaso, F. J., Lavilla, L. & Lanchares, E. Biomechanical Properties of the Cornea in Fuchs' Corneal Dystrophy. *Invest. Ophthalmol. Vis. Sci.* **50**, 3199–3202 (2009).

37. Jackson, A. J., Robinson, F. O., Frazer, D. G. & Archer, D. B. Corneal guttata: A comparative clinical and specular micrographic study. *Eye 1999 136* **13**, 737–743 (1999).

38. Terry, M. A. *et al.* Endothelial keratoplasty for Fuchs' dystrophy with cataract: complications and clinical results with the new triple procedure. *Ophthalmology* **116**, 631–639 (2009).

39. Lipman, R. M., Rubenstein, J. B. & Torczynski, E. Keratoconus and Fuchs' corneal endothelial dystrophy in a patient and her family. *Arch. Ophthalmol. (Chicago, Ill. 1960)* **108**, 993–994 (1990).

40. Rao, G. P., Kaye, S. B. & Agius-Fernandez, A. Central corneal endothelial guttae and age-related macular degeneration : is there an association? *Indian J. Ophthalmol.* **46**, 145 (1998).

41. Olsen, T. Is there an association between Fuchs' endothelial dystrophy and cardiovascular disease? *Graefes Arch. Clin. Exp. Ophthalmol.* **221**, 239–240 (1984).

42. Lyslo, A., Kvernes, S. & Kjelstrup Ratkje, S. Ionic and water transference numbers of Descemet's membrane of the bovine cornea. *Exp. Eye Res.* **32**, 673–679 (1981).

43. Bourne, W. M. Corneal endothelium--past, present, and future. *Eye Contact Lens* **36**, 310–314 (2010).

44. Johnson, D. H., Bourne, W. M. & Campbell, R. J. The ultrastructure of Descemet's membrane. I. Changes with age in normal corneas. *Arch. Ophthalmol. (Chicago, Ill. 1960)* **100**, 1942–1947 (1982).

45. Yuen, H. K. L. *et al.* A morphologic study of Fuchs dystrophy and bullous keratopathy. *Cornea* **24**, 319–327 (2005).

46. Jurkunas, U. V., Bitar, M. S., Funaki, T. & Azizi, B. Evidence of Oxidative Stress in the Pathogenesis of Fuchs Endothelial Corneal Dystrophy. *Am. J. Pathol.* **177**, 2278–2289 (2010).

47. Zhang, J. & Patel, D. V. The pathophysiology of Fuchs' endothelial dystrophy - A review of molecular and cellular insights. *Exp. Eye Res.* **130**, 97–105 (2015).

48. Bergmanson, J. P. G., Sheldon, T. M. & Goosey, J. D. Fuchs' endothelial dystrophy: a fresh look at an aging disease. *Ophthalmic Physiol. Opt.* **19**, 210–222 (1999).

49. Alomar, T. S., Al-Aqaba, M., Gray, T., Lowe, J. & Dua, H. S. Histological and Confocal Microscopy Changes in Chronic Corneal Edema: Implications for Endothelial Transplantation. *Invest. Ophthalmol. Vis. Sci.* **52**, 8193–8207 (2011).

50. Hernández-Quintela, E. *et al.* Confocal microscopy of cystic disorders of the corneal epithelium. *Ophthalmology* **105**, 631–636 (1998).

51. Mustonen, R. K. *et al.* In vivo confocal microscopy of Fuchs' endothelial dystrophy. *Cornea* **17**, 493–503 (1998).

52. Naumann, G. O. H. & Schlötzer-Schrehardt, U. Keratopathy in pseudoexfoliation syndrome as a cause of corneal endothelial decompensation: a clinicopathologic study. *Ophthalmology* **107**, 1111–1124 (2000).

53. Engler, C. *et al.* Unfolded Protein Response in Fuchs Endothelial Corneal Dystrophy: A Unifying Pathogenic Pathway? *Am. J. Ophthalmol.* **149**, 194-202.e2 (2010).

54. Hidayat, A. A. & Cockerham, G. C. Epithelial metaplasia of the corneal endothelium in fuchs endothelial dystrophy. *Cornea* **25**, 956–959 (2006).

55. Burns, R. R., Bourne, W. M. & Brubaker, R. F. Endothelial function in patients with cornea guttata. *Investig. Ophthalmol. Vis. Sci.* **20**, 77–85 (1981).

56. Geroski, D. H., Matsuda, M., Yee, R. W. & Edelhauser, H. F. Pump function of the human corneal endothelium. Effects of age and cornea guttata. *Ophthalmology* **92**, 759–763 (1985).

57. McCartney, M. D., Wood, T. O. & McLaughlin, B. J. Moderate Fuchs' endothelial dystrophy ATPase pump site density. *Investig. Ophthalmol. Vis. Sci.* **30**, 1560–1564 (1989).

58. McCartney, M. D., Robertson, D. P., Wood, T. O. & McLaughlin, B. J. ATPase pump site density in human dysfunctional corneal endothelium. *Invest. Ophthalmol. Vis. Sci.* **28**, 1955–1962 (1987).

59. Mccartney, M. D., Robertson, D. P. & Wood, T. O. ATPase Pump Site Density in Human Dysfunctional Corneal Endothelium. 1955–1962 (1987).

60. Ljubimov, A. V. *et al.* Extracellular matrix and Na+,K+-ATPase in human corneas following cataract surgery: comparison with bullous keratopathy and Fuchs' dystrophy corneas. *Cornea* **21**, 74–80 (2002).

61. Kenney, M. C. *et al.* Altered Expression of Aquaporins in Bullous Keratopathy and Fuchs' Dystrophy Corneas. *J. Histochem. Cytochem.* doi:10.1369/jhc.4A6385.2004.

62. Macnamara, Mol Vis 2004; 10:51-56. http://www.molvis.org/molvis/v10/a7/.

63. Kolko, M., Prause, J. U., Bazan, N. G. & Heegaard, S. Human secretory phospholipase A2, group IB in normal eyes and in eye diseases. *Acta Ophthalmol. Scand.* **85**, 317–323 (2007).

64. Afshari, N. A. *et al.* Genome-wide association study identifies three novel loci in Fuchs endothelial corneal dystrophy. *Nat. Commun.* **8**, 1–8 (2017).

65. Patel, D. V. & McGhee, C. N. J. Contemporary in vivo confocal microscopy of the living human cornea using white light and laser scanning techniques: a major review. *Clin. Experiment. Ophthalmol.* **35**, 71–88 (2007).

66. Davies, Y. *et al.* Keratan sulphate in the trabecular meshwork and cornea. *Curr. Eye Res.* **16**, 677–686 (1997).

67. Polack, F. M. Contributions of electron microscopy to the study of corneal pathology. *Surv. Ophthalmol.* **20**, 375–414 (1976).

68. Kelliher, C. *et al.* A cellular model for the investigation of Fuchs' endothelial corneal dystrophy. *Exp. Eye Res.* **93**, 880–888 (2011).

69. Weller, J. M. *et al.* Extracellular matrix alterations in late-onset Fuchs' corneal dystrophy. *Invest. Ophthalmol. Vis. Sci.* **55**, 3700–3708 (2014).

70. Okumura, N. *et al.* Feasibility of cell-based therapy combined with descemetorhexis for treating Fuchs endothelial corneal dystrophy in rabbit model. *PLoS One* **13**, 1–14 (2018).

71. Hecker, L. A., McLaren, J. W., Bachman, L. A. & Patel, S. V. Anterior Keratocyte Depletion in Fuchs' Endothelial Dystrophy. *Arch. Ophthalmol.* **129**, 555 (2011).

72. Matthaei, M. *et al.* Endothelial Cell MicroRNA Expression in Human Late-Onset Fuchs' Dystrophy. *Invest. Ophthalmol. Vis. Sci.* **55**, 216–225 (2014).

73. Schrems-Hoesl, L. M. *et al.* Cellular and subbasal nerve alterations in early stage Fuchs' endothelial corneal dystrophy: an in vivo confocal microscopy study. *Eye* **27**, 42 (2013).

74. Ahuja, Y., Baratz, K. H., McLaren, J. W., Bourne, W. M. & Patel, S. V. Decreased Corneal Sensitivity and Abnormal Corneal Nerves in Fuchs Endothelial Dystrophy. *Cornea* **31**, 1257 (2012).

75. Bucher, F. *et al.* Corneal nerve alterations in different stages of Fuchs' endothelial corneal dystrophy: An in vivo confocal microscopy study. *Graefe's Arch. Clin. Exp. Ophthalmol.* **252**, 1119–1126 (2014).

76. Baratz, K. H., McLaren, J. W., Maguire, L. J. & Patel, S. V. Corneal haze determined by confocal microscopy 2 years after Descemet stripping with endothelial keratoplasty for Fuchs corneal dystrophy. *Arch. Ophthalmol. (Chicago, Ill. 1960)* **130**, 868–874 (2012).

77. Klintworth, G. K. Corneal dystrophies. *Orphanet J. Rare Dis.* **4**, 1–38 (2009).

78. Liskova, P., Prescott, Q., Bhattacharya, S. S. & Tuft, S. J. British family with early-onset Fuchs' endothelial corneal dystrophy associated with p.L450W mutation in the COL8A2 gene. *Br. J. Ophthalmol.* **91**, 1717–1718 (2007).

79. Gottsch, J. D. *et al.* Fuchs corneal dystrophy: Aberrant collagen distribution in an L450W Mutant of the COL8A2 gene. *Investig. Ophthalmol. Vis. Sci.* **46**, 4504–4511 (2005).

80. Zhang, C. *et al.* IMMUNOHISTOCHEMISTRY AND ELECTRON MICROSCOPY OF EARLY-ONSET FUCHS CORNEAL DYSTROPHY IN THREE CASES WITH THE SAME L450W COL8A2 MUTATION. *Trans. Am. Ophthalmol. Soc.* **104**, 85 (2006).

81. Jun, A. S. *et al.* An alpha 2 collagen VIII transgenic knock-in mouse model of Fuchs endothelial corneal dystrophy shows early endothelial cell unfolded protein response and apoptosis. *Hum. Mol. Genet.* **21**, 384–393 (2012).

82. Meng, H. *et al.* L450W and Q455K Col8a2 knock-in mouse models of Fuchs endothelial

corneal dystrophy show distinct phenotypes and evidence for altered autophagy. *Invest. Ophthalmol. Vis. Sci.* **54**, 1887–1897 (2013).

83. Kuot, A., Mills, R., Craig, J. E., Sharma, S. & Burdon, K. P. Screening of the COL8A2 gene in an Australian family with early-onset Fuchs' endothelial corneal dystrophy. *Clin. Experiment. Ophthalmol.* **42**, 198–200 (2014).

84. Mok, J. W., Kim, H. S. & Joo, C. K. Q455V mutation in COL8A2 is associated with Fuchs' corneal dystrophy in Korean patients. *Eye (Lond).* **23**, 895–903 (2009).

85. Hemadevi, B., Srinivasan, M., Arunkumar, J., Prajna, N. V. & Sundaresan, P. Genetic analysis of patients with Fuchs endothelial corneal dystrophy in India. *BMC Ophthalmol.* **10**, 1–6 (2010).

86. Forrest, M. P., Hill, M. J., Quantock, A. J., Martin-Rendon, E. & Blake, D. J. The emerging roles of TCF4 in disease and development. *Trends Mol. Med.* **20**, 322–331 (2014).

87. Wedel, M. *et al.* Transcription factor Tcf4 is the preferred heterodimerization partner for Olig2 in oligodendrocytes and required for differentiation. *Nucleic Acids Res.* **48**, 4839–4857 (2020).

88. Verzi, M. P. *et al.* TCF4 and CDX2, major transcription factors for intestinal function, converge on the same cis-regulatory regions. *Proc. Natl. Acad. Sci. U. S. A.* **107**, 15157–15162 (2010).

89. Forrest, M. P., Waite, A. J., Martin-Rendon, E. & Blake, D. J. Knockdown of Human TCF4 Affects Multiple Signaling Pathways Involved in Cell Survival, Epithelial to Mesenchymal Transition and Neuronal Differentiation. *PLoS One* **8**, e73169 (2013).

90. Wieben, E. D. *et al.* A Common Trinucleotide Repeat Expansion within the Transcription Factor 4 (TCF4, E2-2) Gene Predicts Fuchs Corneal Dystrophy. *PLoS One* **7**, e49083 (2012).

91. Kuot, A. *et al.* TGC repeat expansion in the TCF4 gene increases the risk of Fuchs' endothelial corneal dystrophy in Australian cases. *PLoS One* **12**, e0183719 (2017).

92. Zarouchlioti, C. *et al.* Antisense Therapy for a Common Corneal Dystrophy Ameliorates TCF4 Repeat Expansion-Mediated Toxicity. *Am. J. Hum. Genet.* **102**, 528 (2018).

93. Soh, Y. Q. *et al.* Trinucleotide repeat expansion length as a predictor of the clinical progression of Fuchs' Endothelial Corneal Dystrophy. *PLoS One* **14**, (2019).

94. Vasanth, S. *et al.* Expansion of CTG18.1 Trinucleotide Repeat in TCF4 Is a Potent Driver of Fuchs' Corneal Dystrophy. *Invest. Ophthalmol. Vis. Sci.* **56**, 4531–4536 (2015).

95. Mootha, V. V. *et al.* TCF4 Triplet Repeat Expansion and Nuclear RNA Foci in Fuchs' Endothelial Corneal Dystrophy. *Invest. Ophthalmol. Vis. Sci.* **56**, 2003–2011 (2015).

96. Hu, J. *et al.* Oligonucleotides targeting TCF4 triplet repeat expansion inhibit RNA foci and mis-splicing in Fuchs' dystrophy. *Hum. Mol. Genet.* **27**, 1015–1026 (2018).

97. Kuot, A. *et al.* Association of TCF4 and CLU polymorphisms with Fuchs' endothelial dystrophy and implication of CLU and TGFBI proteins in the disease process. *Eur. J. Hum. Genet.* **20**, 632–638 (2012).

98. Stamler, J. F. *et al.* Confirmation of the association between the TCF4 risk allele and Fuchs endothelial corneal dystrophy in patients from the Midwestern United States. *Ophthalmic Genet.* **34**, 32–34 (2013).

99. Rao, B., Tharigopala, A., Rachapalli, S., Rajagopal, R. & Soumittra, N. Association of polymorphisms in the intron of TCF4 gene to late-onset Fuchs endothelial corneal dystrophy: An Indian cohort study. *Indian J. Ophthalmol.* **65**, 931–935 (2017).

100. Jalimarada, S. S., Ogando, D. G., Vithana, E. N. & Bonanno, J. A. Ion transport function of SLC4A11 in corneal endothelium. *Invest. Ophthalmol. Vis. Sci.* **54**, 4330–4340 (2013).

101. Vilas, G. L. *et al.* Transmembrane water-flux through SLC4A11: a route defective in genetic corneal diseases. *Hum. Mol. Genet.* **22**, 4579–4590 (2013).

102. Vithana, E. N. *et al.* SLC4A11 mutations in Fuchs endothelial corneal dystrophy. *Hum. Mol. Genet.* **17**, 656–666 (2008).

103. Minear, M. A. *et al.* Genetic screen of African Americans with Fuchs endothelial corneal dystrophy. *Mol. Vis.* **19**, 2508 (2013).

104. Soumittra, N. *et al.* Biosynthetic and functional defects in newly identified SLC4A11 mutants and absence of COL8A2 mutations in Fuchs endothelial corneal dystrophy. *J. Hum. Genet.* **59**, 444–453 (2014).

105. Kim, J. H., Ko, J. M. & Tchah, H. Fuchs Endothelial Corneal Dystrophy in a Heterozygous Carrier of Congenital Hereditary Endothelial Dystrophy Type 2 with a Novel Mutation in SLC4A11. *http://dx.doi.org/10.3109/13816810.2014.881510* **36**, 284–286 (2014).

106. Zhang, W. *et al.* Conditionally Immortal Slc4a11−/− Mouse Corneal Endothelial Cell Line Recapitulates Disrupted Glutaminolysis Seen in Slc4a11−/− Mouse Model. *Invest. Ophthalmol. Vis. Sci.* **58**, 3723–3731 (2017).

107. Gröger, N. *et al.* SLC4A11 prevents osmotic imbalance leading to corneal endothelial dystrophy, deafness, and polyuria. *J. Biol. Chem.* **285**, 14467–14474 (2010).

108. Mehta, J. S. *et al.* Analysis of the posterior polymorphous corneal dystrophy 3 gene, TCF8, in late-onset Fuchs endothelial corneal dystrophy. *Invest. Ophthalmol. Vis. Sci.* **49**, 184–188 (2008).

109. Gupta, R. *et al.* Association of ZEB1 and TCF4 rs613872 changes with late onset Fuchs endothelial corneal dystrophy in patients from northern India. *Mol. Vis.* **21**, 1252–1260 (2015).

110. Chung, D. W. D., Frausto, R. F., Ann, L. B., Jang, M. S. & Aldave, A. J. Functional impact of ZEB1 mutations associated with posterior polymorphous and Fuchs' endothelial corneal dystrophies. *Invest. Ophthalmol. Vis. Sci.* **55**, 6159–6166 (2014).

111. Riazuddin, S. A. *et al.* Mutations in LOXHD1, a recessive-deafness locus, cause dominant late-onset Fuchs corneal dystrophy. *Am. J. Hum. Genet.* **90**, 533–539 (2012).

112. Tang, H. *et al.* Analysis of SLC4A11, ZEB1, LOXHD1, COL8A2 and TCF4 gene sequences in a multi-generational family with late-onset Fuchs corneal dystrophy. *Int. J. Mol. Med.* **37**, 1487–1500 (2016).

113. Rao, B. S. *et al.* Analysis of candidate genes ZEB1 and LOXHD1 in late-onset Fuchs' endothelial corneal dystrophy in an Indian cohort. *https://doi.org/10.1080/13816810.2018.1474367* **39**, 443–449 (2018).

114. Riazuddin, S. A., Vasanth, S., Katsanis, N. & Gottsch, J. D. Mutations in AGBL1 cause dominant late-onset Fuchs corneal dystrophy and alter protein-protein interaction with TCF4. *Am. J. Hum. Genet.* **93**, 758–764 (2013).

115. Jurkunas, U. V. *et al.* Increased clusterin expression in Fuchs' endothelial dystrophy. *Invest. Ophthalmol. Vis. Sci.* **49**, 2946–2955 (2008).

116. Synowiec, E. *et al.* Polymorphisms of the homologous recombination gene RAD51 in keratoconus and Fuchs endothelial corneal dystrophy. *Dis. Markers* **35**, 353–362 (2013).

117. Synowiec, E. *et al.* Polymorphisms of the apoptosis-related FAS and FAS ligand genes in keratoconus and Fuchs endothelial corneal dystrophy. *Tohoku J. Exp. Med.* **234**, 17–27 (2014).

118. Wójcik, K. A. *et al.* Variation in DNA Base Excision Repair Genes in Fuchs Endothelial Corneal Dystrophy. *Med. Sci. Monit.* **21**, 2809 (2015).

119. Kniestedt, C. *et al.* A novel PITX2 mutation and a polymorphism in a 5-generation family with Axenfeld-Rieger anomaly and coexisting Fuchs' endothelial dystrophy. *Ophthalmology* **113**, (2006).

120. Jurkunas, U. V., Bitar, M. & Rawe, I. Colocalization of increased transforming growth factor-beta-induced protein (TGFBIp) and Clusterin in Fuchs endothelial corneal dystrophy. *Invest. Ophthalmol. Vis. Sci.* **50**, 1129–1136 (2009).

121. Zoega, G. M. *et al.* Prevalence and Risk Factors for Cornea Guttata in the Reykjavik Eye Study. *Ophthalmology* **113**, 565–569 (2006).

122. X, Z. *et al.* Association of smoking and other risk factors with Fuchs' endothelial corneal dystrophy severity and corneal thickness. *Invest. Ophthalmol. Vis. Sci.* **54**, 5829–5835 (2013).

123. Pan, P. *et al.* Aberrant DNA methylation of miRNAs in Fuchs endothelial corneal dystrophy. *Sci. Reports 2019 91* **9**, 1–13 (2019).

124. Khuc, E. *et al.* Comprehensive characterization of DNA methylation changes in Fuchs endothelial corneal dystrophy. *PLoS One* **12**, e0175112 (2017).

125. Wilson, S. E., Bourne, W. M., O'Brien, P. C. & Brubaker, R. F. Endothelial function and aqueous humor flow rate in patients with Fuchs' dystrophy. *Am. J. Ophthalmol.* **106**, 270–278 (1988).

126. Zhang, W., Ogando, D. G., Bonanno, J. A. & Obukhov, A. G. Human SLC4A11 Is a Novel NH3/H+ Co-transporter. *J. Biol. Chem.* **290**, 16894–16905 (2015).

127. Jalimarada, S. S., Ogando, D. G. & Bonanno, J. A. Loss of ion transporters and increased unfolded protein response in Fuchs' dystrophy. *Mol. Vis.* **20**, 1668–1679 (2014).

128. Runager, K., Enghild, J. J. & Klintworth, G. K. Focus on molecules: Transforming growth factor beta induced protein (TGFBIp). *Exp. Eye Res.* **87**, 298 (2008).

129. Hashimoto, K. *et al.* Characterization of a cartilage-derived 66-kDa protein (RGD-CAP/beta ig-h3) that binds to collagen. *Biochim. Biophys. Acta* **1355**, 303–314 (1997).

130. Kim, J. E. *et al.* Identification of Motifs for Cell Adhesion within the Repeated Domains of Transforming Growth Factor-β-induced Gene,βig-h3. *J. Biol. Chem.* **275**, 30907–30915 (2000).

131. Gottsch, J. D. *et al.* Serial Analysis of Gene Expression in the Corneal Endothelium of Fuchs' Dystrophy. *Invest. Ophthalmol. Vis. Sci.* **44**, 594–599 (2003).

132. Benischke, A. S. *et al.* Activation of mitophagy leads to decline in Mfn2 and loss of mitochondrial mass in Fuchs endothelial corneal dystrophy. *Sci. Rep.* **7**, (2017).

133. Li, Y. J. *et al.* Mitochondrial Polymorphism A10398G and Haplogroup I Are Associated With Fuchs' Endothelial Corneal Dystrophy. *Invest. Ophthalmol. Vis. Sci.* **55**, 4577–4584 (2014).

134. Okumura, N. *et al.* Sustained Activation of the Unfolded Protein Response Induces Cell Death in Fuchs' Endothelial Corneal Dystrophy. *Invest. Ophthalmol. Vis. Sci.* **58**, 3697–3707 (2017).

135. Okumura, N. *et al.* Activation of TGF-β signaling induces cell death via the unfolded protein response in Fuchs endothelial corneal dystrophy. *Sci. Rep.* **7**, (2017).

136. Goyer, B. *et al.* Extracellular Matrix and Integrin Expression Profiles in Fuchs Endothelial Corneal Dystrophy Cells and Tissue Model. *Tissue Eng. Part A* **24**, 607–615 (2018).

137. Okumura, N. *et al.* Involvement of ZEB1 and Snail1 in excessive production of extracellular matrix in Fuchs endothelial corneal dystrophy. *Lab. Investig.* **95**, 1291–1304 (2015).

138. Buddi, R. *et al.* Evidence of oxidative stress in human corneal diseases. *J. Histochem. Cytochem.* **50**, 341–351 (2002).

139. Jurkunas, U. V. *et al.* Decreased Expression of Peroxiredoxins in Fuchs' Endothelial Dystrophy. *Invest. Ophthalmol. Vis. Sci.* **49**, 2956–2963 (2008).

140. Lee, J. M., Calkins, M. J., Chan, K., Kan, Y. W. & Johnson, J. A. Identification of the NF-E2-related Factor-2-dependent Genes Conferring Protection against Oxidative Stress in Primary Cortical Astrocytes Using Oligonucleotide Microarray Analysis. *J. Biol. Chem.* **278**, 12029–12038 (2003).

141. Ishii, T. *et al.* Transcription factor Nrf2 coordinately regulates a group of oxidative stress-inducible genes in macrophages. *J. Biol. Chem.* **275**, 16023–16029 (2000).

142. Bitar, M. S. *et al.* Decline in DJ-1 and decreased nuclear translocation of Nrf2 in Fuchs endothelial corneal dystrophy. *Invest. Ophthalmol. Vis. Sci.* **53**, 5806–5813 (2012).

143. Wang, Z. *et al.* Advanced glycation end products and receptors in Fuchs' dystrophy corneas undergoing Descemet's stripping with endothelial keratoplasty. *Ophthalmology* **114**, 1453–1460 (2007).

144. Borderie, V. M. *et al.* Corneal endothelial cell apoptosis in patients with Fuchs' dystrophy. *Investig. Ophthalmol. Vis. Sci.* **41**, 2501–2505 (2000).

145. Li, Q. J. *et al.* The role of apoptosis in the pathogenesis of Fuchs endothelial dystrophy of the cornea. *Arch. Ophthalmol. (Chicago, Ill. 1960)* **119**, 1597–1604 (2001).

146. Szentmáry, N., Szende, B. & Süveges, I. Epithelial cell, keratocyte, and endothelial cell

apoptosis in Fuchs' dystrophy and in pseudophakic bullous keratopathy. *Eur. J. Ophthalmol.* **15**, 17–22 (2005).

147. Matthaei, M. *et al.* Endothelial cell whole genome expression analysis in a mouse model of early-onset Fuchs' endothelial corneal dystrophy. *Invest. Ophthalmol. Vis. Sci.* **54**, 1931–1940 (2013).

148. Matthaei, M. *et al.* Tissue microarray analysis of cyclin-dependent kinase inhibitors p21 and p16 in Fuchs dystrophy. *Cornea* **32**, 473–478 (2013).

149. Krishnamurthy, J. *et al.* Ink4a/Arf expression is a biomarker of aging. *J. Clin. Invest.* **114**, 1299–1307 (2004).

150. Ohtani, N. *et al.* Opposing effects of Ets and Id proteins on p16INK4a expression during cellular senescence. *Nature* **409**, 1067–1070 (2001).

151. Matthaei, M. *et al.* Transcript profile of cellular senescence-related genes in Fuchs endothelial corneal dystrophy. *Exp. Eye Res.* **129**, 13–17 (2014).

152. Bahar, I., Kaiserman, I., McAllum, P., Slomovic, A. & Rootman, D. Comparison of Posterior Lamellar Keratoplasty Techniques to Penetrating Keratoplasty. *Ophthalmology* **115**, 1525–1533 (2008).

153. Price, F. W. & Price, M. O. Descemet's stripping with endothelial keratoplasty in 200 eyes. Early challenges and techniques to enhance donor adherence. *J. Cataract Refract. Surg.* **32**, 411–418 (2006).

154. Koenig, S. B. & Covert, D. J. Early results of small-incision Descemet's stripping and automated endothelial keratoplasty. *Ophthalmology* **114**, (2007).

155. Price, M. O., Giebel, A. W., Fairchild, K. M. & Price, F. W. Descemet's Membrane Endothelial Keratoplasty: Prospective Multicenter Study of Visual and Refractive Outcomes and Endothelial Survival. *Ophthalmology* **116**, 2361–2368 (2009).

156. Guerra, F. P., Anshu, A., Price, M. O., Giebel, A. W. & Price, F. W. Descemet's membrane endothelial keratoplasty: prospective study of 1-year visual outcomes, graft survival, and endothelial cell loss. *Ophthalmology* **118**, 2368–2373 (2011).

157. Dapena, I., Ham, L., Netuková, M., Van Der Wees, J. & Melles, G. R. J. Incidence of early allograft rejection after Descemet membrane endothelial keratoplasty. *Cornea* **30**, 1341–1345 (2011).

158. Guerra, F. P., Anshu, A., Price, M. O. & Price, F. W. Endothelial keratoplasty: fellow eyes comparison of Descemet stripping automated endothelial keratoplasty and Descemet membrane endothelial keratoplasty. *Cornea* **30**, 1382–1386 (2011).

159. Goldich, Y. *et al.* Contralateral eye comparison of descemet membrane endothelial keratoplasty and descemet stripping automated endothelial keratoplasty. *Am. J. Ophthalmol.* **159**, 155-159.e1 (2015).

160. Okumura, N. *et al.* The ROCK inhibitor eye drop accelerates corneal endothelium wound healing. *Invest. Ophthalmol. Vis. Sci.* **54**, 2439–2502 (2013).

161. Koizumi, N., Okumura, N., Ueno, M. & Kinoshita, S. New therapeutic modality for corneal endothelial disease using Rho-associated kinase inhibitor eye drops. *Cornea* **33 Suppl 11**, S25–S31 (2014).

162. Kinoshita, S. *et al.* Injection of Cultured Cells with a ROCK Inhibitor for Bullous Keratopathy. *N. Engl. J. Med.* **378**, 995–1003 (2018).

163. Kim, E. C., Meng, H. & Jun, A. S. Lithium treatment increases endothelial cell survival and autophagy in a mouse model of Fuchs endothelial corneal dystrophy. *Br. J. Ophthalmol.* **97**, 1068–1073 (2013).

164. Kim, E. C., Meng, H. & Jun, A. S. N-Acetylcysteine increases corneal endothelial cell survival in a mouse model of Fuchs endothelial corneal dystrophy. *Exp. Eye Res.* **127**, 20–25 (2014).

165. Chiu, A. M., Mandziuk, J. J., Loganathan, S. K., Alka, K. & Casey, J. R. High Throughput Assay Identifies Glafenine as a Corrector for the Folding Defect in Corneal Dystrophy-Causing Mutants of SLC4A11. *Invest. Ophthalmol. Vis. Sci.* **56**, 7739–7753 (2015).

166. Alka, K. & Casey, J. R. Ophthalmic Nonsteroidal Anti-Inflammatory Drugs as a Therapy for Corneal Dystrophies Caused by SLC4A11 Mutation. *Invest. Ophthalmol. Vis. Sci.* **59**, 4258–4267 (2018).

167. Thériault, M., Gendron, S. P., Brunette, I., Rochette, P. J. & Proulx, S. MOLECULAR PATHOGENESIS OF GENETIC AND INHERITED DISEASES Function-Related Protein Expression in Fuchs Endothelial Corneal Dystrophy Cells and Tissue Models. *Am. J. Pathol.* **188**, (2018).

168. Abshire, C. F., Carroll, J. L. & Dragoi, A. M. FLASH protects ZEB1 from degradation and supports cancer cells' epithelial-to-mesenchymal transition. *Oncog. 2016 58* **5**, e254–e254 (2016).

169. Imai, Y. *et al.* The CED-4-homologous protein FLASH is involved in Fas-mediated activation of caspase-8 during apoptosis. *Nature* **398**, 777–785 (1999).

170. Hogan, M. J., Wood, I. & Fine, M. Fuchs' endothelial dystrophy of the cornea. 29th Sanford Gifford Memorial Lecture. *Am. J. Ophthalmol.* **78**, 363–383 (1974).

171. Vogt, A. Weitere Ergebnisse der Spaltlampenmikroskopie des vordern Bulbusabschnittes - II. Abschnitt: Vorderkammer. *Albr. von Graæes Arch. für Ophthalmol.* **106**, 104–113 (1921).

172. Scholar], J. M. A. F. observations on the fine structure of the cornea. I. O. 1962;1:202–225. [Abstract] [Google. Further Observations on the Fine Structure of the Cornea | IOVS | ARVO Journals. https://iovs.arvojournals.org/article.aspx?articleid=2159099.

173. Iwamoto, T., and DeVoe, IOVS, 1971. Electron Microscopic Studies on Fuchs' Combined Dystrophy :II. Anterior Portion of the Cornea | IOVS | ARVO Journals. https://iovs.arvojournals.org/article.aspx?articleid=2158207.

174. Waring, G. O., Rodrigues, M. M. & Laibson, P. R. Corneal dystrophies. II. Endothelial dystrophies. *Survey of Ophthalmology* vol. 23 147–168 (1978).

175. Goar, E. L. Dystrophy of the corneal endothelium. (Cornea guttata) with report of a histological examination. *Am. J. Ophthalmol.* **17**, 215–221 (1934).

176. Lorenzetti, D. W. C., Uotila, M. H., Parikh, N. & Kaufman, H. E. Central Cornea Guttata: Incidence in the General Population. *Am. J. Ophthalmol.* **64**, 1155–1158 (1967).

177. Shimazaki, J., Amano, S., Uno, T. & Maeda, N. National Survey on Bullous Keratopathy in Japan. **26**, 274–278 (2007).

178. Higa, A. *et al.* Prevalence of and Risk Factors for Cornea Guttata in a Population-Based Study in a Southwestern Island of Japan: The Kumejima Study. *Arch. Ophthalmol.* **129**, 332–336 (2011).

179. H, P., A, B., GK, V. & GN, R. Frequency, distribution, and outcome of keratoplasty for corneal dystrophies at a tertiary eye care center in South India. *Cornea* **23**, 541–546 (2004).

180. Mohamed, A. *et al.* Endothelial Keratoplasty : A Review of Indications at a Tertiary Eye Care Centre in South India. **3**, 207–210 (2014).

181. Afshari, N. A., Pittard, A. B., Siddiqui, A. & Klintworth, G. K. Clinical Study of Fuchs Corneal Endothelial Dystrophy Leading to Penetrating Keratoplasty: A 30-Year Experience. *Arch. Ophthalmol.* **124**, 777–780 (2006).

182. Zhang, X. *et al.* Association of smoking and other risk factors with Fuchs' endothelial corneal dystrophy severity and corneal thickness. *Investig. Ophthalmol. Vis. Sci.* **54**, 5829–5835 (2013).

183. Chan, S. W. S., Yucel, Y. & Gupta, N. New trends in corneal transplants at the University of Toronto. *Can. J. Ophthalmol.* **53**, 580–587 (2018).

184. V, C., S, M., P, P., K, L. & P, J. Incidence and Risk Factors of Corneal Endothelial Failure after Phacoemulsification in Patients with Fuchs Endothelial Corneal Dystrophy: A 13-Year Retrospective Cohort. *Clin. Ophthalmol.* **15**, 2367–2373 (2021).

185. Aumailley, M. The laminin family. *Cell Adhesion and Migration* vol. 7 48–55 (2013).

186. Domogatskaya, A., Rodin, S. & Tryggvason, K. Functional diversity of laminins. *Annual Review of Cell and Developmental Biology* vol. 28 523–553 (2012).

187. Aumailley, M. *et al.* A simplified laminin nomenclature. *Matrix Biology* vol. 24 326–332 (2005).

188. Tunggal. Laminins: structure and genetic regulation - PubMed. https://pubmed.ncbi.nlm.nih.gov/11054872/.

189. Simon-Assmann, P. The laminin family: Founding members of the basement membrane. *Cell Adhes. Migr.* **7**, 44–47 (2013).

190. Givant-Horwitz, V., Davidson, B. & Reich, R. Laminin-induced signaling in tumor cells. *Cancer Letters* vol. 223 1–10 (2005).

191. Patarroyo, M., Tryggvason, K. & Virtanen, I. Laminin isoforms in tumor invasion, angiogenesis and metastasis. *Semin. Cancer Biol.* **12**, 197–207 (2002).

192. Kuratomi, Y. *et al.* Laminin γ1 chain peptide, C-16 (KAFDITYVRLKF), promotes migration, MMP-9 secretion, and pulmonary metastasis of B16-F10 mouse melanoma cells. *Br. J. Cancer* **86**, 1169–1173 (2002).

193. Smyth, N. *et al.* The targeted deletion of the LAMC1 gene. in *Annals of the New York Academy of Sciences* vol. 857 283–286 (New York Academy of Sciences, 1998).

194. Ke, J. *et al.* Identification of a functional polymorphism affecting microRNA binding in

the susceptibility locus 1q25.3 for colorectal cancer. *Mol. Carcinog.* **56**, 2014–2021 (2017).

195. Pyun, J. A., Cha, D. H. & Kwack, K. LAMC1 gene is associated with premature ovarian failure. *Maturitas* **71**, 402–406 (2012).

196. Chen, J., Li, L., Lang, J. & Zhu, L. Common variants in LAMC1 confer risk for pelvic organ prolapse in Chinese population. *Hereditas* **157**, 1–6 (2020).

197. Nikolova, G. *et al.* Sequence variant in the laminin γ1 (LAMC1) gene associated with familial pelvic organ prolapse. *Hum. Genet.* **120**, 847–856 (2007).

198. Wu, J. M. *et al.* Comprehensive analysis of LAMC1 genetic variants in advanced pelvic organ prolapse. *Am. J. Obstet. Gynecol.* **206**, 447.e1-447.e6 (2012).

199. Zweidler-Mckay, P. A., Grimes, H. L., Flubacher, M. M. & Tsichlis, P. N. Gfi-1 encodes a nuclear zinc finger protein that binds DNA and functions as a transcriptional repressor. *Mol. Cell. Biol.* **16**, 4024–4034 (1996).

200. Tong, B. *et al.* The Gfi-1B Proto-Oncoprotein Represses p21 WAF1 and Inhibits Myeloid Cell Differentiation . *Mol. Cell. Biol.* **18**, 2462–2473 (1998).

201. Lee, S. *et al.* Solution structure of Gfi-1 zinc domain bound to consensus DNA. *J. Mol. Biol.* **397**, 1055–1066 (2010).

202. Lin, Y. *et al.* The SNAG domain of snail1 functions as a molecular hook for recruiting lysine-specific demethylase 1. *EMBO J.* **29**, 1803–1816 (2010).

203. Shi, Y. *et al.* Histone demethylation mediated by the nuclear amine oxidase homolog LSD1. *Cell* **119**, 941–953 (2004).

204. Metzger, E. *et al.* LSD1 demethylates repressive histone marks to promote androgen-receptor- dependent transcription. *Nature* **437**, 436–439 (2005).

205. Eghrari, A. O. & Gottsch, J. D. Fuchs' corneal dystrophy. *Expert Rev. Ophthalmol.* **5**, 147–159 (2010).

206. Nanda, G. G. & Alone, D. P. Mv-V25-295. 295–310 (2019).

207. Cui, Z. *et al.* Pathological molecular mechanism of symptomatic late-onset Fuchs endothelial corneal dystrophy by bioinformatic analysis. *PLoS One* **13**, (2018).

208. Ong Tone, S. *et al.* Fuchs endothelial corneal dystrophy: The vicious cycle of Fuchs pathogenesis. *Prog. Retin. Eye Res.* **80**, 100863 (2021).

209. Chakraborty, M., Das, R. K., Samal, S., Das, S. & Alone, D. P. Fuchs Endothelial Corneal Dystrophy associated risk variant, rs3768617 in LAMC1 shows allele specific binding of GFI1B. *Gene* **817**, (2022).

210. Schierding, W., Antony, J., Cutfield, W. S., Horsfield, J. A. & O'Sullivan, J. M. Intergenic GWAS SNPs are key components of the spatial and regulatory network for human growth. *Hum. Mol. Genet.* **25**, 3372–3382 (2016).

211. Simcoe, M. J., Khawaja, A. P., Hysi, P. G. & Hammond, C. J. Genome-wide association study of corneal biomechanical properties identifies over 200 loci providing insight into the genetic etiology of ocular diseases. *Hum. Mol. Genet.* **29**, 3154–3164 (2020).

212. Hardcastle, A. J. *et al.* A multi-ethnic genome-wide association study implicates

collagen matrix integrity and cell differentiation pathways in keratoconus. *Commun. Biol.* **4**, 36 (2021).

213. Li, C., Capendeguy, O., Geering, K. & Horisberger, J. D. A third Na+-binding site in the sodium pump. *Proc. Natl. Acad. Sci.* **102**, 12706–12711 (2005).

214. Kaplan, J. H. Biochemistry of Na,K-ATPase. *Annu. Rev. Biochem.* **71**, 511–535 (2002).

215. Skou, J. C. & Esmann, M. The Na,K-ATPase. *J. Bioenerg. Biomembr.* **24**, 249–261 (1992).

216. Clausen, M. J. V. & Poulsen, H. Sodium/Potassium homeostasis in the cell. *Met. Ions Life Sci.* **12**, 41–67 (2013).

217. Skou, J. C. The influence of some cations on an adenosine triphosphatase from peripheral nerves. *Biochim. Biophys. Acta* **23**, 394–401 (1957).

218. Glynn, I. M. A hundred years of sodium pumping. *Annu. Rev. Physiol.* **64**, 1–18 (2002).

219. Clausen, M. V., Hilbers, F. & Poulsen, H. The structure and function of the Na,K-ATPase isoforms in health and disease. *Front. Physiol.* **8**, 371 (2017).

220. Blaustein, M. P. Endogenous ouabain: role in the pathogenesis of hypertension. *Kidney Int.* **49**, 1748–1753 (1996).

221. Geering, K. Functional roles of Na,K-ATPase subunits. *Curr. Opin. Nephrol. Hypertens.* **17**, 526–532 (2008).

222. Li, Z. & Langhans, S. A. Transcriptional regulators of Na,K-ATPase subunits. *Front. Cell Dev. Biol.* **3**, 66 (2015).

223. Sweadner, K. J. Isozymes of the Na+/K+-ATPase. *Biochim. Biophys. Acta* **988**, 185–220 (1989).

224. Blanco, G. & Mercer, R. W. Isozymes of the Na-K-ATPase: Heterogeneity in structure, diversity in function. *Am. J. Physiol. - Ren. Physiol.* **275**, 633–650 (1998).

225. Crambert, G. *et al.* Transport and pharmacological properties of nine different human Na, K-ATPase isozymes. *J. Biol. Chem.* **275**, 1976–1986 (2000).

226. Barwe, S. P. *et al.* Novel role for Na,K-ATPase in phosphatidylinositol 3-kinase signaling and suppression of cell motility. *Mol. Biol. Cell* **16**, 1082–1094 (2005).

227. Chow, D. C. & Forte, J. G. Functional significance of the beta-subunit for heterodimeric P-type ATPases. *J. Exp. Biol.* **198**, 1–17 (1995).

228. Ackermann, U. & Geering, K. Mutual dependence of Na,K-ATPase alpha- and beta-subunits for correct posttranslational processing and intracellular transport. *FEBS Lett.* **269**, 105–108 (1990).

229. McDonough, A. A., Geering, K. & Farley, R. A. The sodium pump needs its beta subunit. *FASEB J.* **4**, 1598–1605 (1990).

230. Bab-Dinitz, E. *et al.* A C-terminal lobe of the beta subunit of Na,K-ATPase and H,K-ATPase resembles cell adhesion molecules. *Biochemistry* **48**, 8684–8691 (2009).

231. Barwe, S. P., Kim, S., Rajasekaran, S. A., Bowie, J. U. & Rajasekaran, A. K. Janus model of the Na,K-ATPase beta-subunit transmembrane domain: distinct faces mediate

alpha/beta assembly and beta-beta homo-oligomerization. *J. Mol. Biol.* **365**, 706–714 (2007).

232. Inge, L. J. *et al.* Evidence for a potential tumor suppressor role for the Na,K-ATPase beta1-subunit. *Histol. Histopathol.* **23**, 459–467 (2008).

233. Kitamura, N. *et al.* Mouse Na+/K+-ATPase beta1-subunit has a K+-dependent cell adhesion activity for beta-GlcNAc-terminating glycans. *Proc. Natl. Acad. Sci. U. S. A.* **102**, 2796–2801 (2005).

234. Rajasekaran, S. A. *et al.* Na,K-ATPase activity is required for formation of tight junctions, desmosomes, and induction of polarity in epithelial cells. *Mol. Biol. Cell* **12**, 3717–3732 (2001).

235. Shoshani, L. *et al.* The polarized expression of Na+,K+-ATPase in epithelia depends on the association between β-subunits located in neighboring cells. *Mol. Biol. Cell* **16**, 1071–1081 (2005).

236. Vagin, O., Tokhtaeva, E. & Sachs, G. The role of the beta1 subunit of the Na,K-ATPase and its glycosylation in cell-cell adhesion. *J. Biol. Chem.* **281**, 39573–39587 (2006).

237. Selvakumar, P. *et al.* Epigenetic silencing of Na,K-ATPase β1 subunit gene ATP1B1 by methylation in clear cell renal cell carcinoma. *Epigenetics* **9**, 579–586 (2014).

238. DelMonte, D. W. & Kim, T. Anatomy and physiology of the cornea. *J. Cataract Refract. Surg.* **37**, 588–598 (2011).

239. Gordon, S. R. & Staley, C. A. Role of the cytoskeleton during injury-induced cell migration in corneal endothelium. *Cell Motil. Cytoskeleton* **16**, 47–57 (1990).

240. Gordon, S. R. & Buxar, R. M. Inhibition of cytoskeletal reorganization stimulates actin and tubulin syntheses during injury-induced cell migration in the corneal endothelium. *J. Cell. Biochem.* **67**, 409–421 (1997).

241. Sabet, M. D. & Gordon, S. R. Ultrastructural immunocytochemical localization of fibronectin deposition during corneal endothelial wound repair. Evidence for cytoskeletal involvement. *Biol. cell* **65**, 171–179 (1989).

242. Berzat, A. & Hall, A. Cellular responses to extracellular guidance cues. *EMBO J.* **29**, 2734–2745 (2010).

243. Liu, J., Wen, Y., Luo, W., Liu, Y. & Sha, X. Human Amniotic Epithelial Cells Promote the Proliferation of Human Corneal Endothelial Cells by Regulating Telomerase Activity via the Wnt/β-catenin Pathway. *Curr. Eye Res.* **46**, 159–167 (2021).

244. Lamouille, S., Xu, J. & Derynck, R. Molecular mechanisms of epithelial-mesenchymal transition. *Nat. Rev. Mol. Cell Biol.* **15**, 178–196 (2014).

245. Lee, J. G., Jung, E. & Heur, M. Fibroblast growth factor 2 induces proliferation and fibrosis via SNAI1-mediated activation of CDK2 and ZEB1 in corneal endothelium. *J. Biol. Chem.* **293**, 3758–3769 (2018).

246. Vedana, G., Villarreal, G. & Jun, A. S. Fuchs endothelial corneal dystrophy: current perspectives. *Clin. Ophthalmol.* **10**, 321–330 (2016).

247. Jun, A. S. One hundred years of Fuchs' dystrophy. *Ophthalmology* **117**, (2010).

248. Katikireddy, K. R., White, T. L., Miyajima, T. & Vasanth, S. HHS Public Access. 19–30 (2019) doi:10.1016/j.freeradbiomed.2017.12.036.NQO1.

249. Jeong, E. G. *et al.* Immunohistochemical and mutational analysis of FLASH in gastric carcinomas. *APMIS* **115**, 900–905 (2007).

250. Méthot, S. J., Proulx, S., Brunette, I. & Rochette, P. J. Chronology of cellular events related to mitochondrial burnout leading to cell death in Fuchs endothelial corneal dystrophy. *Sci. Reports 2020 101* **10**, 1–10 (2020).

251. Barcaroli, D. *et al.* FLASH is required for histone transcription and S-phase progression. *Proc. Natl. Acad. Sci. U. S. A.* **103**, 14808–14812 (2006).

252. Yang, X. cui, Burch, B. D., Yan, Y., Marzluff, W. F. & Dominski, Z. FLASH, a proapoptotic protein involved in activation of caspase-8, is essential for 3' end processing of histone pre-mRNAs. *Mol. Cell* **36**, 267–278 (2009).

253. Yang, X. *et al.* FLASH is required for the endonucleolytic cleavage of histone pre-mRNAs but is dispensable for the 5' exonucleolytic degradation of the downstream cleavage product. *Mol. Cell. Biol.* **31**, 1492–1502 (2011).

254. Kino, T. & Chrousos, G. P. Tumor necrosis factor alpha receptor- and Fas-associated FLASH inhibit transcriptional activity of the glucocorticoid receptor by binding to and interfering with its interaction with p160 type nuclear receptor coactivators. *J. Biol. Chem.* **278**, 3023–3029 (2003).

255. Alm-Kristiansen, A. H. *et al.* FLASH acts as a co-activator of the transcription factor c-Myb and localizes to active RNA polymerase II foci. *Oncogene* **27**, 4644–4656 (2008).

256. Chen, S., Evans, H. G. & Evans, D. R. FLASH knockdown sensitizes cells to Fas-mediated apoptosis via down-regulation of the anti-apoptotic proteins, MCL-1 and Cflip short. *PLoS One* **7**, (2012).

257. Krieghoff, E., Milovic-Holm, K. & Hofmann, T. G. FLASH Meets Nuclear Bodies: CD95 Receptor Signals via a Nuclear Pathway. *http://dx.doi.org/10.4161/cc.6.7.4046* **6**, 771–775 (2007).

258. Barcaroli, D. *et al.* FLASH is an essential component of Cajal bodies. *Proc. Natl. Acad. Sci. U. S. A.* **103**, 14802–14807 (2006).

259. Bongiorno-Borbone, L. *et al.* FLASH and NPAT positive but not Coilin positive Cajal Bodies correlate with cell ploidy. *Cell Cycle* **7**, 2357–2367 (2008).

260. Bongiorno-Borbone, L. *et al.* FLASH degradation in response to UV-C results in histone locus bodies disruption and cell-cycle arrest. *Oncogene 2010 296* **29**, 802–810 (2009).

261. Sleiman, S. F. *et al.* Mithramycin Is a Gene-Selective Sp1 Inhibitor That Identifies a Biological Intersection between Cancer and Neurodegeneration. *J. Neurosci.* **31**, 6858 (2011).

262. Ji, C., Casinghino, S., Mccarthy, T. L. & Centrella, M. Multiple and Essential Sp1 Binding Sites in the Promoter for Transforming Growth Factor-Î² Type I Receptor*. (1997) doi:10.1074/jbc.272.34.21260.

263. Dufour, S., Broders-Bondon, F. & Bondurand, N. β1-Integrin Function and Interplay during Enteric Nervous System Development. *Neural Surf. Antigens From Basic Biol.*

Towar. Biomed. Appl. 153–166 (2015) doi:10.1016/B978-0-12-800781-5.00013-X.

264. Deniaud, E. *et al.* Overexpression of Transcription Factor Sp1 Leads to Gene Expression Perturbations and Cell Cycle Inhibition. *PLoS One* **4**, (2009).

265. Mansilla, S., Priebe, W. & Portugal, J. Changes in gene expression induced by Sp1 knockdown differ from those caused by challenging Sp1 binding to gene promoters. *Biochim. Biophys. Acta - Gene Regul. Mech.* **1809**, 327–336 (2011).

266. Zhang, R. *et al.* Transcription Factor Sp1 Promotes the Expression of Porcine ROCK1 Gene. *Int. J. Mol. Sci. 2016, Vol. 17, Page 112* **17**, 112 (2016).

267. Kocaba, V. *et al.* Association of the gutta-induced microenvironment with corneal endothelial cell behavior and demise in fuchs endothelial corneal dystrophy. *JAMA Ophthalmol.* **136**, 886–892 (2018).

268. Mony, S., Lee, S. J., Harper, J. F., Barwe, S. P. & Langhans, S. A. Regulation of Na,K-ATPase β1-subunit in TGF-β2-mediated epithelial-to-mesenchymal transition in human retinal pigmented epithelial cells. *Exp. Eye Res.* **115**, 113–122 (2013).